LUT UNIVERSITY
LUT School of Energy Systems
Energy Technology
BH10A2000 Master's Thesis

Juho Kivelä

WATER CIRCULATION MODELING OF A RECOVERY BOILER UNDERGOING A POWER BLACKOUT

Examiners: Associate Professor, D.Sc. (Tech.) Jouni Ritvanen
Instructors: M.Sc. (Tech.) Antti Sirainen
M.Sc. (Tech.) Jukka Röppänen

TIIVISTELMÄ

LUT-Yliopisto
School of Energy Systems
Energiatekniikka

Juho Kivelä

Water Circulation Modeling Of A Recovery Boiler Undergoing A Power Blackout

Diplomityö

2019

96 sivua, 76 kuvaa, 15 taulukkoa ja 4 liitettä

Tarkastaja: TkT Jouni Ritvanen

Ohjaajat: DI Antti Sirainen
DI Jukka Röppänen

Hakusanat: soodakattila, dynaaminen simulaatio, mallinnus, sähkökatkos, Apros, herkkyystarkastelu, vesikierto, kuona, kuonaantuminen

Työssä on tarkoitus esittää yhdenmukainen tapa simuloida soodakattilan sähkökatkosta. Yhdenmukaisuus parantaa tulosten luotettavuutta ja tekee tutkimuksista vertailukelpoisia. Sähkökatkoksia soodakattiloissa tapahtuu harvoin, mutta niissä on potentiaalinen vaara putkirikoille, jotka voivat johtaa sula-vesi räjähdykseen kattilan sisällä. Apros-mallinnusohjelmaa käytetään simuloimaan kahta simulointitapausta, joille määritellään erilaiset kuonakerrosten paksuudet tulipesän ylä- ja alaosiin. Putkimateriaalien lämpötiloja ja kattilaputkien kuivumista tarkastellaan kokeen ajan. Toinen tutkimuskohde työssä on tutkia kuonakerroksen paksuuden vaikutusta tuloksiin herkkyystarkastelun avulla.

Tässä työssä esitetään yhdenmukainen tapa simuloida soodakattilan sähkökatkosta. Malli on skaalattavissa eri kokoisille kattiloille. Simulaatioiden tuloksien todenperäisyyttä on vaikea arvioida, sillä kokeellista dataa sähkökatkoksista ei juuri ole. Käytetty kuonamalli on hyvin konservatiivinen, ja muutamaa metodia esitetään approksimoimaan kuonan paksuutta tarkemmin.

Kriittisen korkeita lämpötiloja havaitaan ensimmäisen simulaation kattialan ala-osassa ja lattiaputkissa. Korkeimmat lämpötilat havaitaan tulipesän nurkissa, missä kuonan alkulämpötila on korkeampi verrattuna keskiseinään. Epätasainen kuonakerros tulipesän seinillä vaikuttaa merkittävästi lattiaputkien kuivumisjärjestykseen ja ajoitukseen.

ABSTRACT

LUT University
School of Energy Systems
Energy Technology

Juho Kivelä

Water Circulation Modeling Of A Recovery Boiler Undergoing A Power Blackout

Master's Thesis

2019

96 pages, 76 figures, 15 tables and 4 appendixes

Examiner: D.Sc. (Tech.) Jouni Ritvanen

Instructors: M.Sc. (Tech.) Antti Sirainen
M.Sc. (Tech.) Jukka Röppänen

Keywords: recovery boiler, dynamic simulation, simulation, power blackout, Apros, sensitivity analysis, deposit, slagging, water circulation

The main objective of this work is to present a standard way to simulate a power blackout in a recovery boiler. A standard procedure leads to more reliable case studies which are comparable with each other. Power blackout of the boiler happens seldom, but has the potential of damaging boiler tubes, which might lead to a smelt-water explosion inside the furnace. Apros modeling software is used to simulate two base cases, which are given different deposit accumulation on the lower furnace. Material temperatures and boiler tube drying are observed during the simulation. A secondary objective of the work is to find the main effects of deposit thickness variation on the furnace walls. We conduct a sensitivity analysis to find the effects.

This work presents successfully a standard way to perform a power blackout simulation. The model can be scaled to simulate different sized boilers. Accuracy of the simulation results is hard to determine, since no experimental data was available. The used deposit model is very conservative. New methods to approximate the wall deposit mass are suggested to replace the old model, to attain more accuracy in the results.

Critically high temperatures are observed in the lower furnace and floor tubes of the first case. Highest temperatures originate in the wall corners, where the initial deposit temperature is the highest. Uneven deposit thickness strongly affects the timing and order of floor tube drying.

LIST OF SYMBOLS

A	Area	[m^2]
c_p	Specific heat capacity	[J kg^{-1} K^{-1}]
D, d	Diameter	[m]
g	Gravitational acceleration	[m s^{-2}]
H	Height	[m]
h	Heat transfer coefficient	[W m^{-2} K^{-1}]
k	Thermal conductivity	[W m^{-1} K^{-1}]
L, l	Length	[m]
Nu	Nusselt number	[-]
P	Pressure	[Pa]
Q	Heat energy	[J]
q	Heat transfer rate	[W]
q''	Heat flux	[W m^{-2}]
R	Heat resistance	[K W^{-1}]
Re	Reynolds number	[-]
T	Temperature	[K, °C]
t	Time	[s]
V	Volume	[m^3]

Greek

α	Thermal diffusivity	[m^2 s]
ϵ	Friction loss coefficient	[-]
ω	Flow velocity	[m s^{-1}]
μ	Dynamic viscosity	[kg m^{-1} s^{-1}]
ρ	Density	[kg m^{-3}]
ζ	Pressure loss coefficient	[-]

Abbreviations

BFB	Bubbling fluidized bed
CFD	Computational fluid dynamics
CHF	Critical heat flux
CS	Carbon steel
DS	Dry solids

DWO	Density wave oscillation
IC	Information and control
NCG	Non-condensable gases
PDO	Pressure drop oscillation
TRS	Total reduced sulfur gas

FOREWORD

While this thesis is the end of my master's thesis studies, I hope that it will also be a beginning for something new. I wholeheartedly enjoyed being a student at LUT. Big thanks goes to my friends from LUT, with whom I could share the journey to become an engineer. In addition, huge thanks for my family for supporting me in everything I do. Because of you, I am where I am right now.

Special thanks to Jukka Röppänen and Antti Sirainen, who gave me expert advice on recovery boilers and guided me to the right direction throughout the writing process. Thank you Jouni Ritvanen, without your help this work would lack the clarity and structure required of a good scientific paper.

"*Patsaaksi ei muutu seisomalla paikoillaan, yrittäneille vain niitä laitetaan.*"
– Some appropriate lyrics by the male choir Seminaarimäen mieslaulajat

TABLE OF CONTENTS

1 INTRODUCTION

A kraft recovery boiler is a component of the pulping process of a pulping plant. Its most important tasks include recycling pulping chemicals, producing high pressure steam and minimizing the pulping process emissions (Vakkilainen 2005, p. 2-1). Recovery boiler operation is dependent on the needs of the pulping process, which dictate the size of the recovery boiler. In essence, the need for recovery boilers ultimately reflects the demand for paper and paperboard. In Pöyry's World Fibre Outlook report the global demand for paper and paperboard is growing at a rate of 1% (67 million tons) per year (Pöyry 2015, p. 16). In addition for providing steam for other processes, the recovery boiler produces generally more electricity and steam that the pulping plant requires. This energy can be sold to local district heating and electricity networks for additional profit. According to International Energy Agency, the global energy demand will grow more than 25% to the year 2040, while the overall consumption of coal will slightly decrease. (IEA 2018, p. 1)

Recovery boiler size can be described with its rate of black liquor consumption. During the 1980s the maximum black liquor consumption of a recovery boiler was considered approximately a quarter of what it is today (Vakkilainen et al. 2014, p. 95). Eventually, plant size could be scaled up because of the increase of dry solids in black liquor, even black liquor spraying as well as better automation and control technologies (Gullichsen & Fogelholm 1999, p. 96). By adapting certain features from power boiler designs, the recovery boiler can be harnessed to produce electricity even more efficiently. (Vakkilainen et al. 2014, p. 95)

The key design parameter having the largest effect on boiler size is the black liquor dry solids consumption rate, measured in tons of dry solids per day (tds/d) units. (Vakkilainen 2017, p. 247). Largest boilers of their time are presented in figure 1.

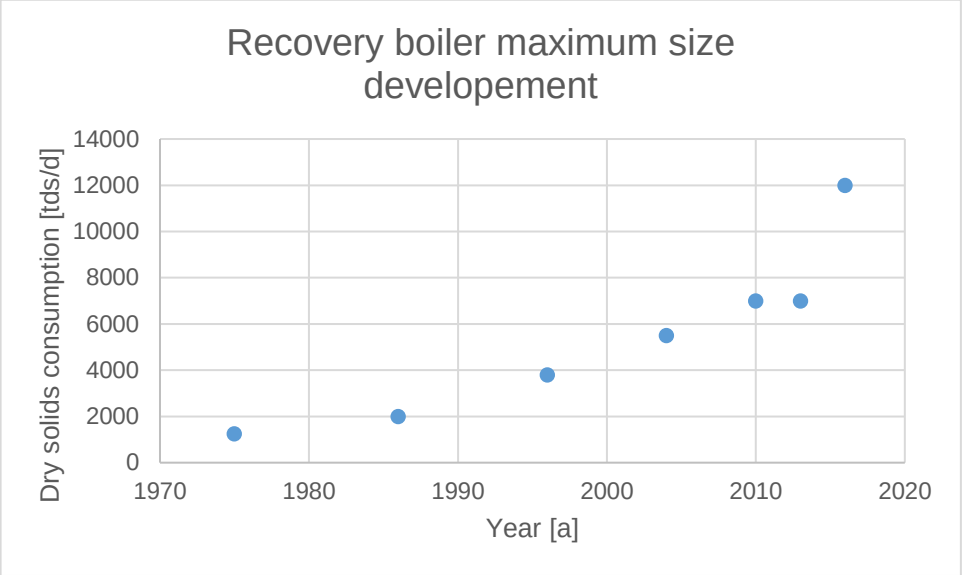

Figure 1. The highest capacity boilers during their time. (Vakkilainen et al. 2014, pp. 96-97; Andritz Oy 2016a)

The maximum boiler size has increased a lot during past few decades. Designing a boiler above 10 000 tds/d is challenging because of missing experience; Current design rules might not be applicable to the design or might work poorly. Larger boilers require larger water circulation systems and the total amount of heat stored in the furnace volume will be larger. These problems create a need for new studies to develop the most efficient designs regarding large boiler size.

1.1 Literature

The recovery boiler uses a specific type of fuel called black liquor. Black liquor is a concentrated mixture of spent pulping chemicals and organic material (Adams et al. 1997, p. 249). During fuel combustion, some or all of the organics combust, while the rest ends up in the char bed or as a deposit on the evaporative surfaces. The bed enables efficient recycling of pulping chemicals and is therefore essential part of the recovery boiler (Vakkilainen 2005, p. 5-4). Furnace side deposits are a mixture of organic and inorganic material that accumulates on furnace inside surfaces. Accumulation rate, chemical composition and thermal properties of the deposit vary depending on fuel composition, combustion dynamics and deposit location inside the furnace (Adams et al. 1997, p. 256; Baxter et al. 2001, p. 135). Combustion of black liquor provides the heat needed to boil water in the boiler tubing. The heat transfers from the furnace volume, through the deposit and steel tube walls to the boiler water. Heat is stored in the deposits and the furnace bed, which

gradually transfers to the water circulation when the boiler shuts down, or when a blackout happens.

A blackout is an off-design operation event for the boiler. During a blackout, all external power to the boiler is lost. Many of the systems that work in the normal and the back-up electrical network are lost. Therefore, problems caused by blackout are commonly sudden stop of vital processes keeping up normal boiler operations like black liquor pumps, feed water pumps and combustion air blowers (Finnish recovery boiler committee 2013, p. 4).

The water circulation system of a boiler contains a steam drum, which is located at the top of the boiler. The drum contains boiler water and the nominal water level, which is the highest point of water in the boiler. Steam is separated in the drum from the boiler water, and directed out of the water circulation through a steam valve. The drum receives feed water to replace the evaporating steam through a feed water valve. Feed water is mixed with the circulation in the drum, and directed to downcomers, which supply the water to the evaporative components. The circulation of water is driven by a density difference between the water inside downcomers and the boiling steam/water-mixture in the evaporative components. A modern recovery boiler by Andritz is presented in figure 2. The key parts are numbered in the picture.

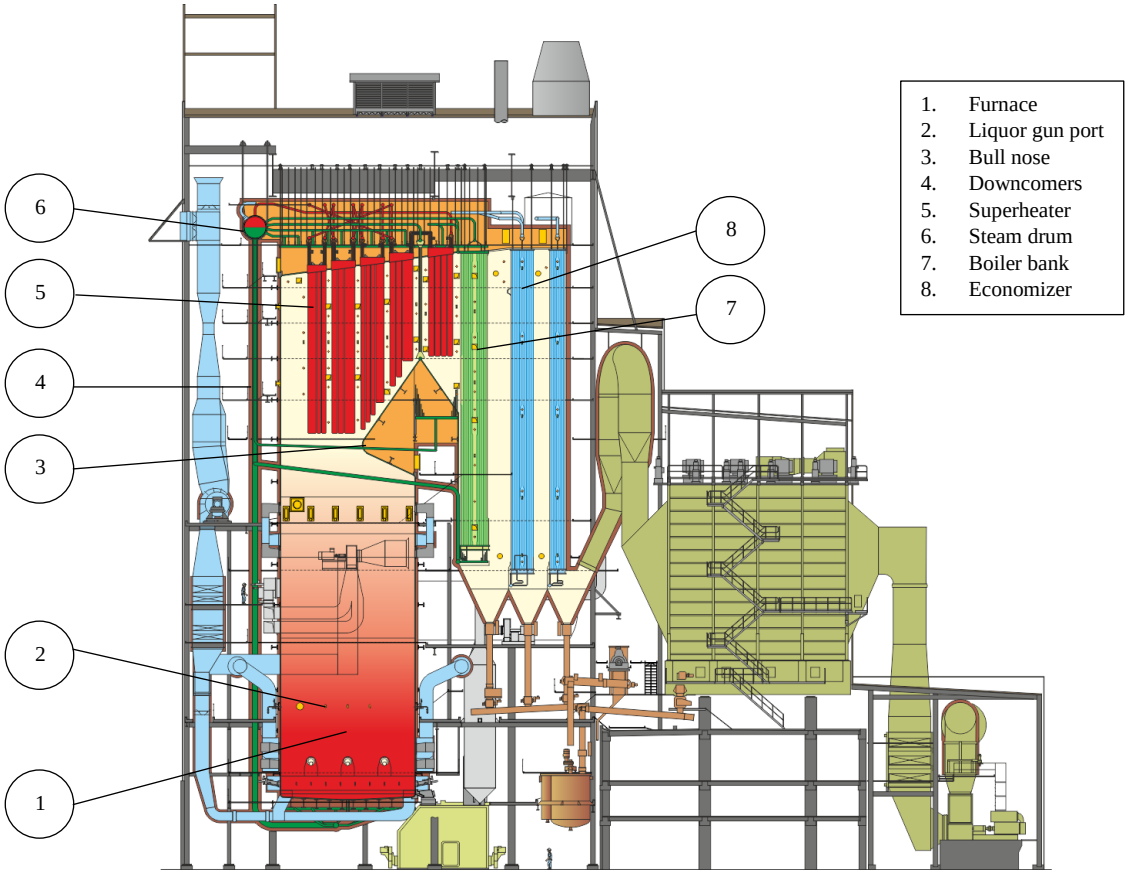

Figure 2. A single-drum recovery boiler. Located at Iggesund and presented from the right side. (Andritz Oy 2016b)

When feed water flow to the boiler stops, the water level inside the boiler starts to sink. When the water level decreases below the steam drum the normal circulation of water in the boiler stops, which exposes the boiler tubing to dryout. Dryout occurs, when the tube inner walls are exposed to a constant steam flow (Baehr & Stephan 2006, p. 493). Steam flow cools the tube walls worse than boiling water flow, because of latent heat that is captured in the boiling event. Poor heat absorption of steam causes immediate rising of the tube wall temperature. Allowable stress limit of the wall material is dependent of temperature (Vakkilainen 2017, p. 176). Since the tube material strength is dependent of temperature, dryout might ultimately cause cracking of the tube wall.

It is essential to keep the tubes intact, so that no water escapes in to the furnace. If water interacts with the hot char bed in the boiler, there is a chance of a steam explosion. Steam explosions in North America have been recorded by Black Liquor Recovery Boiler Association Committee (BLRBAC):

Table 1. Smelt-water explosions in North America recoded by BLRBAC. (The black liquor recovery boiler advisory committee, 2018, p. 30)

	1960s	1970s	1980s	1990s	2000s	2010s
Pressure Part Failure	9	19	10	2	1	2
Black Liquor System						
wash water	1	2		1		
black liquor	10	5	2	1		
Spout Leaks		2	2	2		
Wash Water	2	4				
Miscellaneous	3				1	
Pyrolysis Gas			4	2		
Auxiliary Fuel	10	6	2	1	1	
TOTAL	35	38	20	8	3	2

The amount of explosions have been drastically reduced from the 60s, but occasional accidents still happen. Majority of these accidents happen from wall, screen or floor tube leaks (The black liquor recovery boiler advisory committee, 2018, p. 32). Steam explosion is a rapid evaporation of water that raises the pressure inside the boiler (Finnish recovery boiler committee, 2009, p. 11). Steam explosions have been recorded to bend furnace walls out of shape (Vakkilainen 2005, p. 5-8). Since it is important to keep the tubes cool as long as possible, the boiler water must be conserved by keeping the nominal boiler pressure during the blackout. Boiler pressure is adjusted with the steam valve.

1.2 Methods

A blackout study is carried out to understand how the evaporative components of the boiler water circulation react to the event. A simulation study is necessary, since the modelled phenomena are very time dependent. The model is constructed according to dimensions of a real recovery boiler. Furnace walls, screen, ash hopper wall, boiler bank platens and walls, rear wall screen and the steam drum are included in the model, as well as other non-heated tubes and headers. Apros modeling software is used to create and simulate the study. Apros modeling software has been validated against real plant data and test facility experiments (Ylijoki *et al.*, 2015). No previous blackout studies have been done before at this scale that can be found in the public research databases. However, a study was found where the complete boiler circulation is simulated. Albrecht (2002) conducted a study regarding water circulation simulation of a recovery boiler, and concluded that the combustion model utilized

in the study plays an important role when accurate characterization of the circulation is required.

The thermodynamic properties and total mass of deposits on evaporative surfaces determine the amount of heat transferred to the circulation, and is therefore strongly connected to the evaporation inside the boiler. In this work, the deposit is modelled as a homogeneous material with constant thermodynamic properties. Heat from combustion determines the steady-state temperature on each evaporative surface at the start of the experiment, which also has an effect on evaporation. To acquire an accurate combustion heat model, the heat load is determined partly with the help of CFD calculation. Generic heat flux data from another furnace simulation is scaled according to current furnace geometry. The intensity of the heat is adjusted by an iterative process.

1.3 Objective

This work presents a standard way of power blackout simulation on Apros regarding kraft recovery boilers. Occasionally, a blackout study is required from a customer of Andritz. Creating a standard procedure to follow makes the case studies more reliable, comparable between each other and prevents human errors.

To simulate the blackout, we use a 1-D dynamic model, which simulates the water-steam flow in the boiler tubes as well as the thermodynamic changes in the deposit and tube materials. Deposit thickness is determined for two base cases based on observations from inside the furnace, and represent the most likely deposit accumulation in the furnace. The cases have difference in lower furnace deposit thickness. The boiler tube drying phenomena and material temperatures are studied in each case. The main objective is to find out if allowable temperature limits of the tube material are crossed. The results are also compared with previous blackout modelling cases.

Another objective of the thesis is to find the main effects of deposit thickness and drum pressure variation. There can be great variance in the deposit thickness during normal operation, which makes it important to understand how sensitive water circulation is of the thickness change. The sensitivity of results is analyzed with a sensitivity study of deposit thickness and drum pressure. Deposit thickness is varied only on the furnace walls and the

analysis is done by comparing the results from four sensitivity cases to the reference case. Boiler pressure variation is studied with two cases of lower boiler pressure, which are then compared with the reference case.

2 RECOVERY BOILER

A recovery boiler is a component of pulp making process. There are a few different types of pulp making processes, but the most commonly used is the kraft process, which utilizes the kraft recovery boiler. This thesis focuses only on the mentioned type and is referred to as just recovery boiler. The key decisions in recovery boiler design are screen utilization, stem drum count, tubing material on the lower furnace, boiler bank orientation, economizer arrangement and utilization of air levels (Vakkilainen 2017, p. 246). This thesis focuses mostly on the operation of evaporative surfaces and tubing, combustion in the furnace including char bed behavior and furnace-side deposit accumulation on the heat transfer surfaces.

2.1 Function

Adams et al. (1997) suggests there are two main functions for a recovery boiler: Recovery of the inorganic chemicals and making use of the chemical energy in the organic portion of the liquor (Adams et al. 1997, p. 3). Vakkilainen (2005) elaborates these functions by specifying three functions of a recovery boiler as follows:

1. To generate high pressure steam by combustion of black liquor,
2. To recycle and regenerate pulping chemicals,
3. To minimize waste streams. (Vakkilainen 2005, p. 2-1)

2.1.1 Flue gas heat recovery

Black liquor burning creates heat with which the recovery boiler produces steam. The steam can be consumed by a turbine to produce electricity or can be used in other processes as heat. Primary steam circuit pressure and temperature should be high enough for running the turbine efficiently, which generally means temperatures of around 490°C and pressures of 90bar for a 3000tds/d capacity boiler. (Gullichsen & Fogelholm 1999, p. 106) Modern recovery boilers such as OKI in Indonesia can achieve temperatures and pressures as high as 515°C and 110bar (Andritz Oy 2016a). Sub-processes in the recovery boiler such as soot blowing, air pre-heating and black liquor drying require some of the produced steam.

Integrated pulp and paper factories can utilize all the leftover steam efficiently. (KnowPulp 2016)

2.1.2 Chemical re-circulation

After the black liquor combustion, the inorganic part of the fuel remains. Most of these chemicals end up in the char bed of the furnace and exit as liquid smelt while some parts exit the furnace with flue gases. The smelt flowing out of the furnaces smelt spout contains mostly Na_2SO_4 (sodium sulfate), Na_2S (sodium sulfide), $Na_2S_2O_3$ (sodium thiosulfate) and Na_2CO_3 (sodium carbonate) (Vakkilainen 2005, p. 5-10). Na_2SO_4, which is a sulfur compound of black liquor, reduces in the char bed to Na_2S forming CO_2 (carbon dioxide) in the process. Na_2CO_3 is utilized in the re-causticizing process as shown in figure 3.

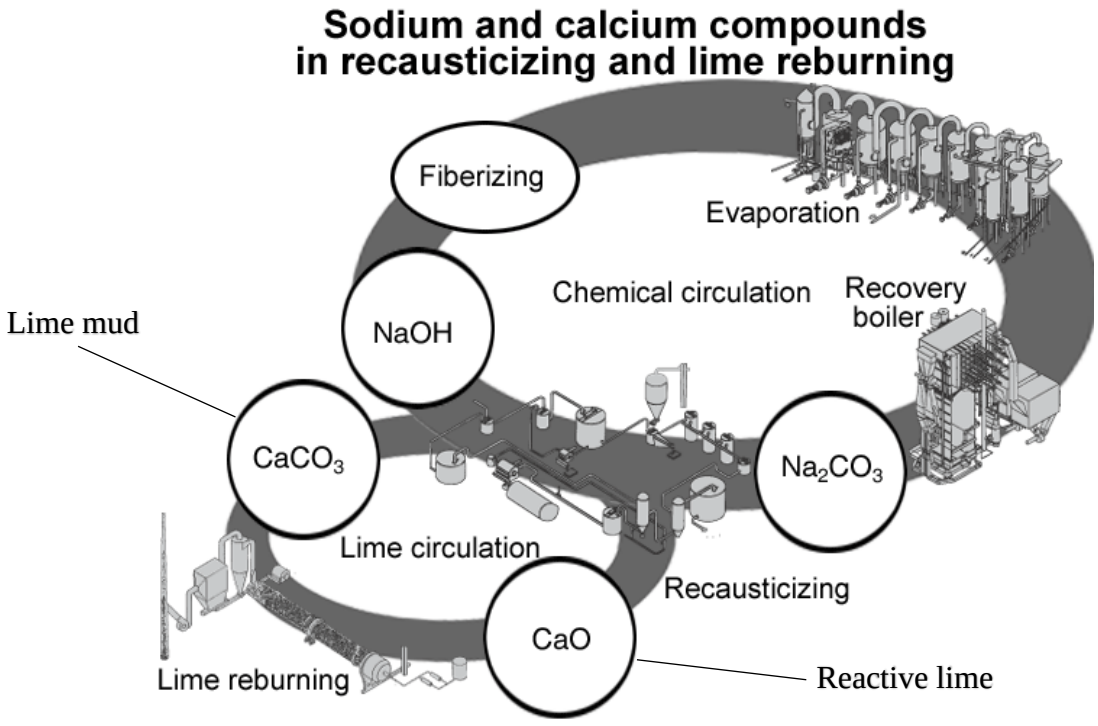

Figure 3. The re-causticizing process; Circulation of sodium and calcium components. (KnowPulp 2016)

The smelt is drained from furnace bottom to a dissolving tank, where weak wash is added to make green liquor. Green liquor containing mainly Na_2CO_3 is filtered and mixed with CaO (calcium oxide or reactive lime) in a slaker to produce NaOH (sodium hydroxide) and $CaCO_3$ (calcium carbonite or lime mud). NaOH is then recycled back to the fiberizing

process for pulping. The lime mud is burned in a kiln, which produces reactive lime. Reactive lime is then directed back to the slaker. (Gullichsen & Fogelholm 1999, pp. 10-11 & 135)

2.1.3 Environmental operation

The recovery boiler has two key challenges from the environmental perspective: Gas emissions and reuse of effluents within the pulp mill. Gas emissions include, in the case of kraft process, particulate emissions, SO_2, total reduced sulphur gases (TRS) HCL, NH_3, CO, methanol and other organic compounds. Modern recovery boiler uses wet scrubbers and precipitators to control these emissions. Non-condensable gases (NCGs) produce TRS emissions in, for example, digesters and kilns. These gases can be collected and directed to the recovery boiler for incineration, which has the capacity to capture the emerging Sulphur oxides. Effluent reuse inside the pulp mill is desired, which essentially means reducing water usage and the need for chemical makeup. (Tran and Vakkilainen n. d., p. 1.1-3)

2.2 Black liquor combustion

Black liquor is the residual component of pulping, and typically contains dissolved wood with some digestive chemicals. To be precise, black liquor composes of organic wood substances, lignin, hemicellulose, cellulose, inorganics, sodium and sulphur compounds and inert material (Gullichsen & Fogelholm 1999, pp. 37-38). The organic material from wood covers approximately 60% of the total black liquor dry-solids. It is usually very hard to determine standard black liquor characteristics, like density, viscosity and heat capacity because of the complex nature of the mixture. (Adams et al. 1997, p. 61) Typically the black liquor supplied to the furnace is mixed with process steam, make-up salt cake (or some other equivalent) and dust from the flue gases, which further increases complexity. (Adams et al. 1997, p. 19) Black liquor elemental composition might resemble something like in table 2.

Table 2. Elemental composition of black liquor presented as percentage values (%). (Adams et al. 1997)

Element		Black liquor	Ash, as chemical	Sulfated ash, as chemical	Sulfated ash, as NaOH
Carbon	C	35.0	3.8	-	-
Hydrogen	H	3.3	-	-	0.9
Oxygen	O	35.7	23.1	28.7	14.4
Sodium	Na	19.7	19.7	19.7	19.7
Potassium	K	1.6	1.6	1.6	1.6
Sulfur	S	4.0	4.0	14.4	-
Chloride	Cl	0.6	0.6	-	-
Inerts	Si, Al, Fe, Ca, etc.	0.1	0.1	0.1	0.1
Total		**100**	**52.9**	**64.5**	**36.7**

On top of controlling a combustion process in the furnace, the chemical cycle has to be maintained while minimizing emissions in the flue gases. The char bed also needs to be maintained at a certain height and shape so that the bed doesn't solidify at the smelt spout entrance, which will cause the spouts to plug. These challenges can be overcome with careful air and black liquor supplying systems and furnace design.

Combustion inside a recovery boiler furnace is most intense where the combustion air is supplied in to the furnace. This naturally affects the heat flux profile to the water circulation. A heat flux distribution obtained by CFD calculation is presented in figure 4 and 5.

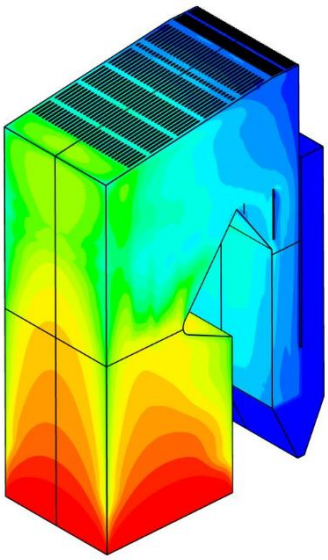

Figure 4. Heat flux distribution on the top part of the boiler. (Sirainen et al. 2017, p. 3)

As the flue gases are cooled by the water circulation system, the less intensive the heat flux gradients are. Figure 5 describes more clearly the asymmetric nature of heat load of the furnace below the bull nose.

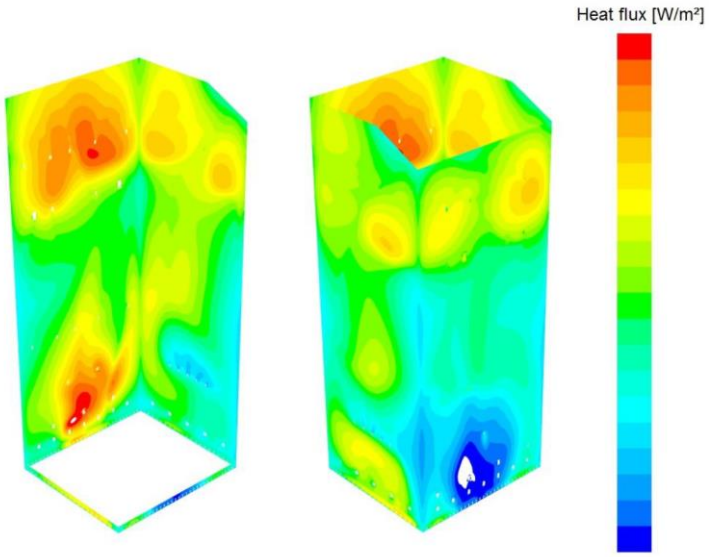

Figure 5. An example of the lower furnace heat flux profile. (Sirainen et al. 2017, p. 5)

The heat flux profile on furnace walls is quite dynamic. However, the corners are usually colder compared to the center wall, because of the distance to the main combustion volume. Heat flux from the bed to the floor isn't shown in the figure.

2.2.1 Black liquor feed

Black liquor is sprayed to the furnace through liquor guns fixed on the furnace walls (see figure 6). The guns are equipped with a nozzle to spread the spray. Most commonly used is the splash plate type. The splash plate is a simple plate, its surface angled towards the flow. The contact angle determines how well the spray mixes into the furnace. (Adams et al. 1997, p. 9)

While there are many types of nozzles which have different mixing effects to the spray, the droplet size of sprayed black liquor remains between 0.5-5mm, which is coarse compared to droplet sizes encountered with fossil fuel combustion. The burning reaction also has a strong effect on the droplet size; black liquor particles ignite, then swell and devolatilize and finally shrink after the volatiles are burned. The relatively large size of the droplets reduce entrainment, enable them to dry and pyrolyze during their fall to the char bed, but limit the

burning so that unburned material will end up on the char bed. Smaller droplets would be carried away with the flue gases which is not preferred. (Gullichsen & Fogelholm 1999, p. 109; Adams et al. 1997, p. 9)

2.2.2 Char bed

The char bed consists of a char layer on the top of a smelt pile. Hot and burning black liquor solids that have totally or partly pyrolyzed reside in the char layer. The smelt on the other hand consists of inorganic chemicals present in black liquor; approximately 66% is Na_2CO_3 (Sodium carbonate) while the rest being Na_2S (Sodium sulfide) (Adams et al. 1997, p. 3). Ideally, the inorganics in black liquor should fall into the bed in a reduced state and separate from the burning organic part. The bed provides an environment for compounds like CO (Carbon monoxide), CO_2 (Carbon dioxide), Na_2CO_3 and Na_2S to form, while minimizing the oxidization of Sulphur to avoid unnecessary emissions in the flue gas and on the other hand to keep Sulphur in the chemical cycle. (Adams et al. 1997, p. 163)

Another way of dividing the char bed into different parts is by activity. The top layer of the bed is called an active layer, because of the chemical and physical (mixing) activity enabled by burning and high temperatures. Underneath the active layer resides the chemically and physically inactive core, below the inorganic melting point. The physical characteristics of the active layer remain same in different boiler types, but the inactive layer characteristics prove to be more complicated. (Adams et al. 1997, p. 164) The thermal properties of black liquor char and smelt are shown in **Table 3**. The bed temperature can vary from 230°C to 1200°C, while the bed density also varies widely across the bed.

Table 3. Thermal properties of black liquor and smelt. (Adams et al. 1997, p. 166)

Property	Active zone	Inactive zone	Molten smelt	Solidified smelt
Density [kg m^{-3}]	290-460	480-1330	1923	2163
Heat capacity [kJ kg^{-1} K^{-1}]	1.25	1.25	1.34	1.42
Thermal conductivity [W m^{-1} K^{-1}]	0.28-0.38	0.078	0.45	0.88

Cooling of the low conducting bed can take a long time. During an emergency shut down of the boiler, it can take up to five days for the total bed of 3m height to solidify. However, the surface temperature of the bed will fall much faster. A large temperature distribution will

develop across the bed because of the insulating behavior of the smelt. (Adams et al. 1997, pp. 177-178)

Smelt spouts are used to transfer the smelt from the active layer to the dissolving tank. Depending on the boiler type the amount of available fluid smelt, size of the active and inactive layers varies. Furthermore, the char bed shape and size vary according to black liquor properties, design of the boiler, air and black liquor feed systems. (Adams et al. 1997, p. 164)

2.2.3 Air feed

There are usually multiple horizontally positioned combustion air ports present in a recovery boiler furnace. This configuration enables good control of the burning phenomena, which brings certain advantages including efficient mixing of gases and black liquor burning while minimizing possible emissions in the flue gases. The air is supplied with fans connected to the ports via wind boxes and ducts.

According to Adams et al. (1997) most of the air is supplied through the primary air level. However, this information seems to be a bit outdated, since a process design manual by Andritz Oy (2018) dictates that primary air should only be 30-20% of the total supplied air. Secondary and tertiary air levels supply almost an equal amount of air according to the design rules, but optimization will have an effect on the ratio. The function of primary air is to keep a desired char bed shape and position, while also burning the char and pyrolysis gases to keep the bed hot and fluid. The secondary air ports are fewer and larger compared to the primary ports. Typically these are also positioned on the front and rear walls while primary ports circulate all walls. The function of secondary air is to control the bed height while also burning pyrolysis gases and CO (carbon monoxide). It is common to use primary and secondary air naming scheme for ports under liquor guns. Above the liquor guns is the tertiary air level, which completes the combustion process. Quaternary air level can be utilized above the tertiary air to minimize possible air emissions. (Adams et al. 1997, p. 9-11) The air port and liquor gun positioning are shown in figure 6.

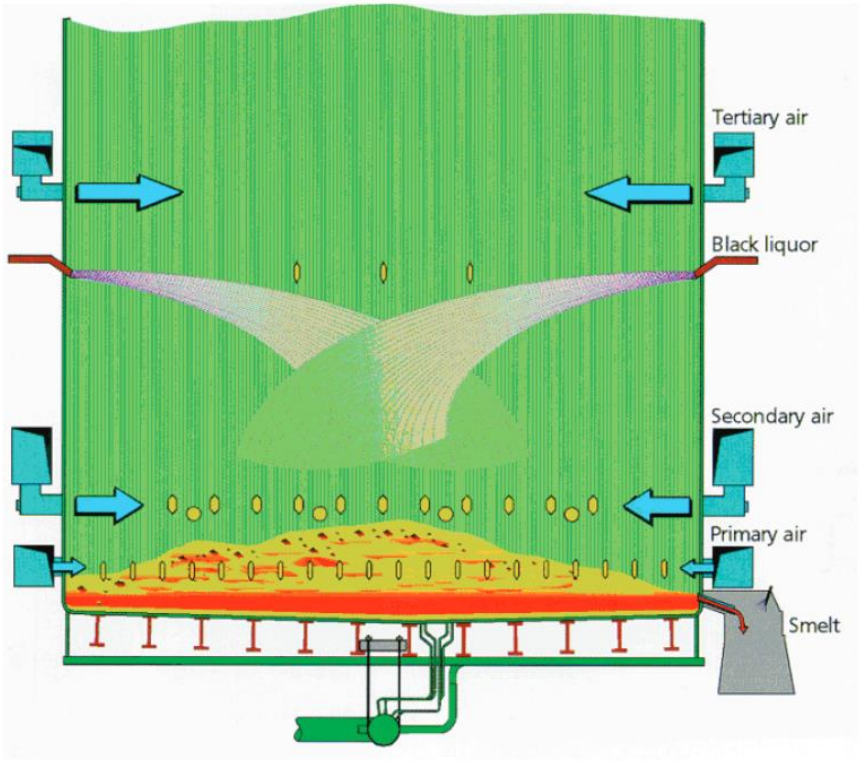

Figure 6. Combustion air supply into the recovery boiler furnace. (Vakkilainen 2005, p. 4-8)

2.2.4 Flue gases

Recovery boiler flue gases include pollutants such as SO_2 (sulphur dioxide), NOx (nitrogen oxides), HCl (hydrochloric acid), volatile organic compounds (VOC), heavy metals and PAH (polycyclic aromatic hydrocarbons). High flue gas temperature in the lower furnace has a positive effect on sodium volatilization, meaning the formation of Na_2SO_4. High flue gas temperature in the upper furnace reduces SO_2 formation, which is directly connected to HCl emissions. (Adams et al. 1997, p. 217, 240-241)

2.3 Water circulation system

A recovery boiler is a water tube boiler that utilizes natural circulation to circulate the water through the boiler. To produce steam, the recovery boiler needs feedwater and a system to transfer the combustion heat of black liquor into the water. This system is referred to as water circulation system and it includes all evaporative surfaces. A modern recovery boiler utilizes a single-drum design, wide spaced superheaters and vertically oriented boiler bank. Single-drum design was adopted to gain improved safety and availability. Wide super heaters

reduce fouling and corrosion while the vertical orientation of the boiler bank make it easier and more efficient to clean. (Vakkilainen 2017, pp. 250-251)

2.3.1 Steam drum

Feedwater is pumped from the feedwater tank, through preheaters such as economizers, to the steam drum. The steam drum aims to separate steam from water coming through the riser channels. The separation is done by gravity, cyclones and de-mister elements (Gullichsen & Fogelholm 1999, p. 122). Cyclones spin the flow and centrifugal forces separate the water to the sides while steam rises from the middle. Steam is dried from droplets in the de-mister which is commonly a grid mesh or a maze of baffle plates (Vakkilainen 2017, p. 102). Cyclones direct water downwards to mix with the drum water, and eventually, to get back to the natural circulation through a downcomer. A steam drum is shown in figure 7

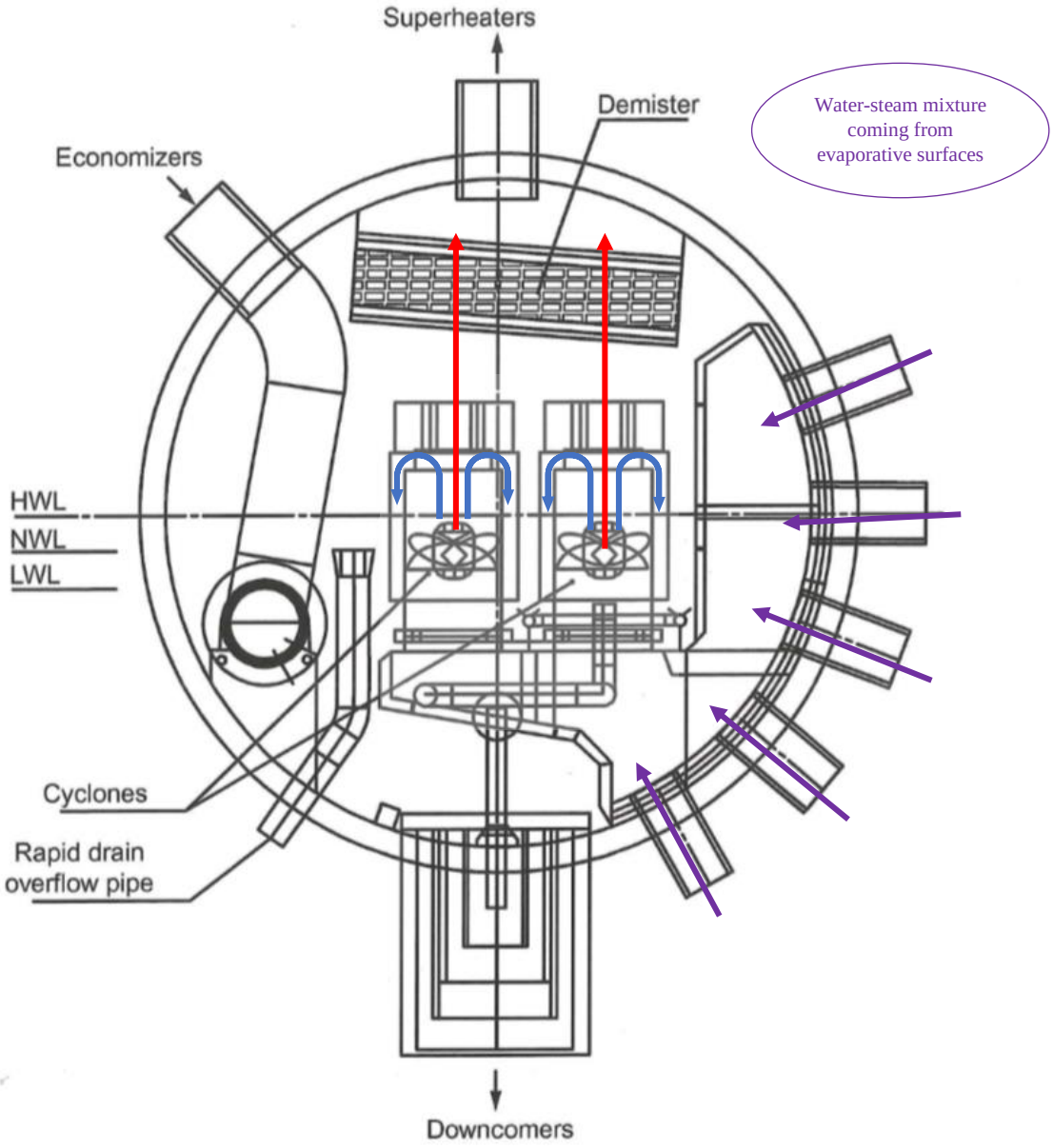

Figure 7. A steam drum. HWL stands for high water level, NWL for normal water level and LWL for low water level. Blue stands for water, red for steam and purple for mixture of both. (Vakkilainen 2017, p. 101)

Steam drum water level should be kept constantly at the NWL, since too high water level can carry over water to the superheaters and too low water level can cause steam to enter the downcomers. Superheater tubes are sensitive to droplets in the steam. Steam in downcomer tubes cause cavitation and decrease circulation due to lower density of the steam.

2.3.2 Evaporative surfaces

Evaporation in the boiler happens in dedicated evaporative components. These components consist of tubes that are fixed to each other with fins. The tubes then form the evaporative

surface, through which the combustion heat is transferred. Figure 8 elaborates the configuration further.

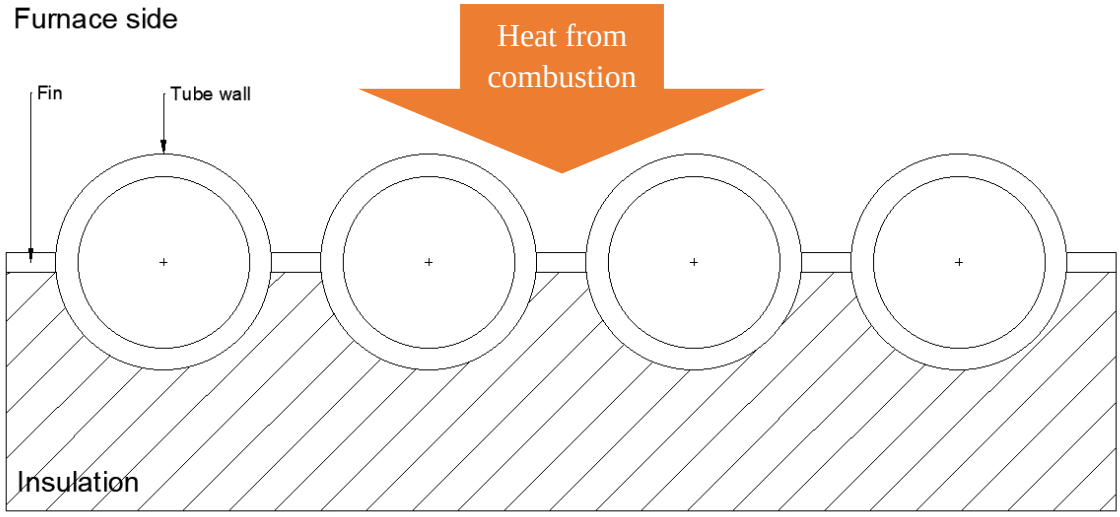

Figure 8. Furnace wall cross-area. The cold side is usually well insulated. For screens and boiler bank platens the construction is similar, but there is no insulation and the heat enters basically through the entire perimeter.

Walls and boiler bank are the most common evaporative components in the water circulation system. Sometimes a rear wall screen, a furnace screen, a pre-boiler bank or a combination of these is utilized. Most of the evaporation occur in the furnace walls, while 10-25% occur in the boiler bank (Gullichsen & Fogelholm 1999, p. 123). Figure 9 presents one possible arrangement of the evaporative components.

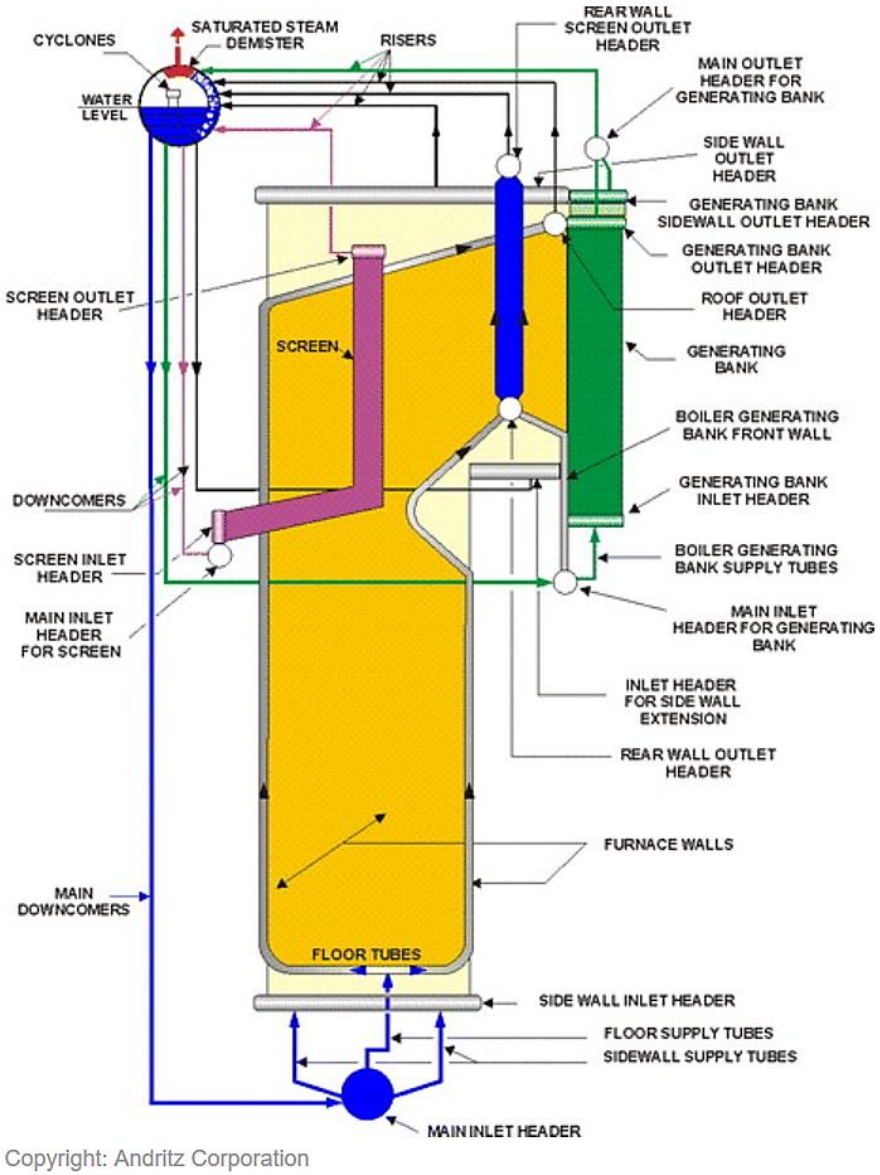

Figure 9. The main parts of a water circulation system. (Andritz Oy 2017)

Evaporative tubing are connected to the steam drum and downcomers via headers. Vakkilainen (2017) describes that connections are done with upper and lower collecting headers, divider tubes and wall headers. It is customary design to have all evaporative tubing to start and end with a header. (Vakkilainen 2017, p. 99) Header utilization, however, is different according to manufacturer.

Downcomers distribute the water to the evaporative tubing. In some cases the furnace screen is directed upwards through the nose and integrated within the boiler bank platen tubes. The boiler bank volume also contains tube walls, which are supplied from the same inlet header as the platens. Sometimes a furnace screen is used in recovery boiler design to reduce the

radiating heat of the furnace to the hottest superheater tubes (Vakkilainen 2017, p. 256). The screen is positioned right below the first superheaters. By reducing radiation heat flux to the superheaters, corrosion is reduced significantly. Nowadays, it's more common to place the screen through the nose, unlike shown in the figure above. The boiler bank construction is shown next in figure 10.

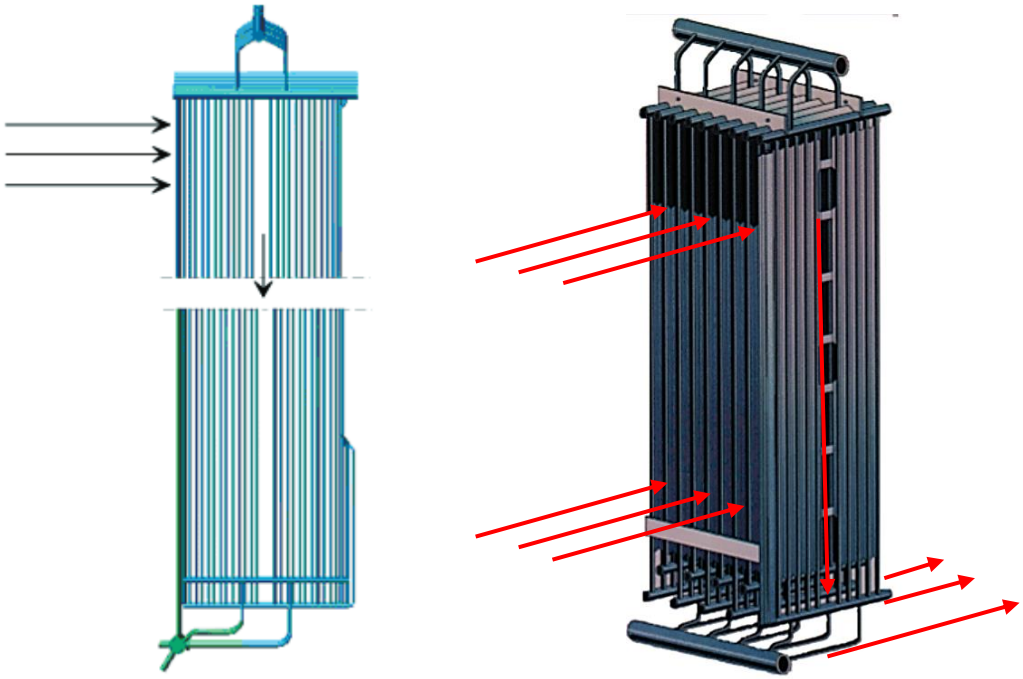

Figure 10. Boiler bank construction on the left, and an economizer on the right. The greatest difference between them lies in the spacing of tubes, which is wider in the economizer. The arrows indicate flow direction of the flue gases. (Vakkilainen 2005, p. 6-15)

Flue gases travel around the flat tube platens of the boiler bank and flow downwards, while the water inside the tubing rises up, forming a counter flow heat exchanger. Fins are positioned between tubes of the same platen. Rear wall of the boiler bank consists of the last platen tubes that are connected together with fins. The economizer is of similar construction, but is used for pre-heating water instead of boiling it.

2.3.3 Tube material characteristics

Typically, tube materials are made of different kinds of steel to suit different requirements. For example, carbon steel (CS) is easily corroded at high temperatures and lacks creep strength, but is economical to use up to operating temperatures of 510°C (Haribhakti et al. 2018, p. 88). The upper furnace usually consists of CS, because it resists most corrosion in

an oxygen-rich environment. Floor tubes can also be built from CS, but the lower furnace is usually too corrosive for CS. Compound steel can be utilized in this case. (Vakkilainen 2017, pp. 253-255) Compound steel consists of two components that are metallurgically combined to form a tube with different inside and outside characteristics. The components share a bonding zone which connects the materials. The outside material is usually some high alloy steel, which provides corrosion resistance, while the inside component is utilized for load bearing. For example, CS can be utilized as the load bearing component. (Forberg 2015, p. 53)

According to Haribhakti et al. (2018) tubing materials must have adequate strength at elevated temperatures to counter creep and rupture. Creep is a transient deformation event for material that is being exposed to a load in elevated temperatures. Long exposure to creep can lead to rupture, which translates to the mechanical failure of the material. Tube materials must also have resistance to withstand cyclic loading. In addition, the materials should have low coefficient of thermal expansion, good thermal conductivity and good resistance against oxidation and corrosion. (Haribhakti et al. 2018, pp. 88, 149) Table 4 presents some common tube materials used in today's boilers.

Table 4. Example of boiler tube materials and limit temperatures. (Vakkilainen 2017, p. 175)

Class	Temperature [°C]	Typical material (common name)	EN number	ASME
Steel	Up to 400-450	P235GH, P265GH	EN1.0425	SA/A-210 Gr A-1
Alloyed	Up to 540-580	16Mo3, 13CrMo4-5, 10CrMo9-10	EN1.5415, EN1.7335, EN1.7380	SA/A-204, SA/A-387 12, SA/A-387 22
Martensite	Up to 550-600	X10CrMoVNb9-1, X20CrMoV11-1	EN1.4903	
Austenistic	Up to 600-720	X10CrNiMo1613, X10CrNiNb1613		

Haribhakti et al. (2018) suggests that the maximum operation temperature for CS is 510°C. Vakkilainen (2017) instead mentions that CS is used up to 400-450°C. (Vakkilainen 2017, p. 174; Haribhakti et al. 2018, p. 101) From table 4 we deduce, that the maximum operating temperatures in the furnace tubing materials range between 400-580°C.

2.4 Evaporative surface fouling

When black liquor is sprayed in the furnace, all of it doesn't burn. Instead, the inorganic part of the fuel and possibly some organic parts are not combusted and end up on evaporative surfaces, superheaters, economizers, ash hopper or in the dust precipitator. This matter is called carryover, fume or dust depending on the way of deposition and particle size. Figure 11 describes where deposits originate from and where the different types are generally found.

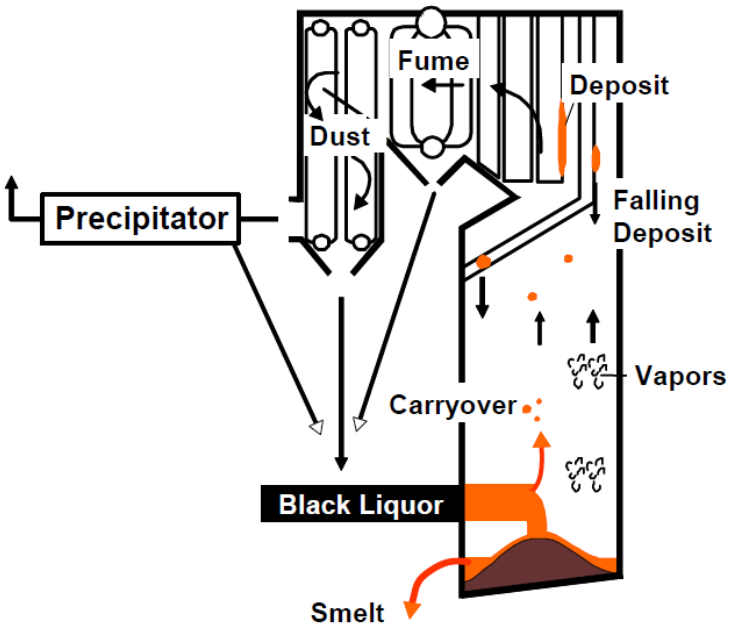

Figure 11. Deposit circulation in the furnace. (Honghi Tran 2015, p. 2)

Figure 12 presents deposition on a probe inserted in the superheater region.

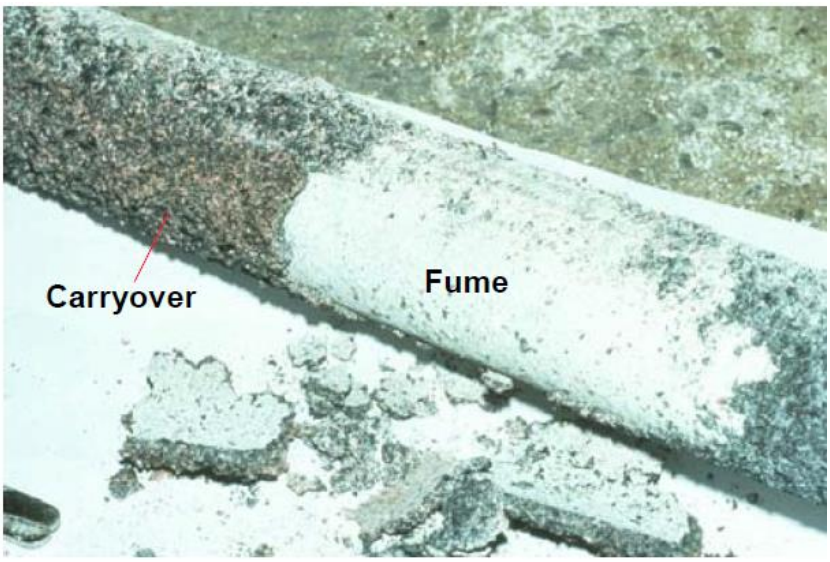

Figure 12. Carryover and fume deposits on a probe from superheater region. (Honghi Tran 2015, p. 1)

Carryover layer is shown on top of a fume layer. In some cases the platens of boiler bank or superheaters can get completely plugged of deposit. Figure 13 presents massive deposit accumulation on boiler bank tubing.

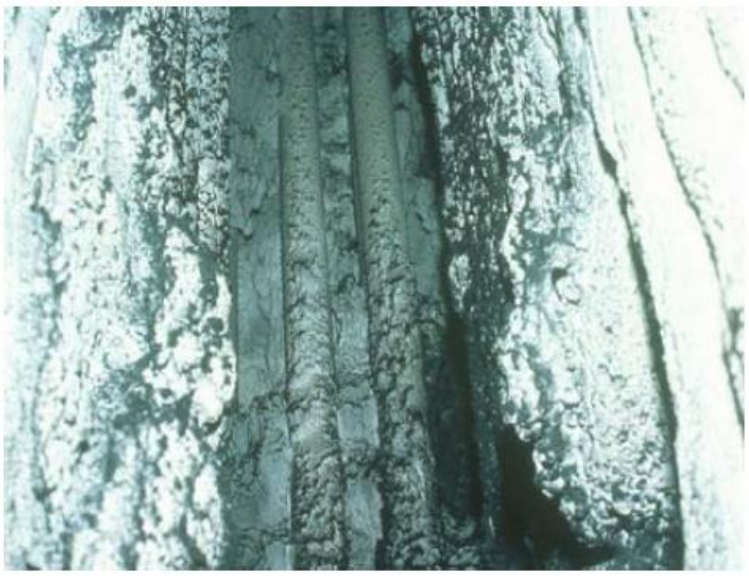

Figure 13. Massive deposit on boiler bank tubing. (Honghi Tran 2015, p. 7)

2.4.1 Carryover

Carryover deposit consists of black liquor particles that are literally carried over by the flue gases from the boiler furnace. The particle size of carryover is around 20µm-100mm, which means the particles deposit by inertial impact. These particles can contain smelt components

as well as unburned organic components. Carryover entrainment behavior is related to its temperature, and can exhibit stickiness as well as hardness. (Adams et al. 1997, p. 249)

2.4.2 Fume

Fume is formed when sodium and potassium compounds condensate in the flue gases and then deposit on a surface (indirectly) or condense directly to a cooler surface. Fume particles are noticeably smaller compared to carryover; the particles are observed in sizes of around 0.1-1µm. Because of the small size of fume, the particles usually deposit by thermophoresis and turbulent diffusion. Fume deposits are described as soft, but in some cases may sinter in high temperatures. (Adams et al. 1997, p. 249)

2.4.3 Dust

When flue gas temperature decreases low enough (around boiler bank), carryover and fume form a stream of dust. Most of the dust is collected from boiler bank, economizers and the ESP (electrostatic precipitator) with ash hoppers underneath each component, while only a small amount passes through the stack with flue gases. Dust can be utilized in the black liquor feed, by mixing the dust in a mix tank to the fuel flow, since it includes expensive cooking chemicals such as Na and S. (Adams et al. 1997, 252-253)

2.4.4 Deposit

Deposit is a mixture of fume, carryover and dust. Its characteristics are different according to location inside the boiler. Roughly estimating, in the lower superheater, carryover is dominant in the deposit. In places where the temperature is lower, like the back side of the boiler bank, fume is dominant. Deposit mixture composition varies accordingly, but mostly composes of Na_2CO_3 (up to m-35%) and Na_2SO_4 (up to m-87%). (Adams et al. 1997, p. 256)

Deposit thickness on the wall is mainly dependent on deposit temperature, Cl-concentration and K-concentration. Concentration of these compounds affect the sticky temperature (T_{15}) and the radical deformation temperature (T_{70}). The subscripts indicate the amount of liquid smelt in mass-percentage. T_{15} is the temperature, when the deposit can literally stick to a furnace wall or tubing. T_{70} is achieved when the accumulated deposit on a wall will not stay in place, and will be pulled down by gravity. Temperatures T_{15} and T_{70} are important

parameters in examination of super heater and boiler bank deposition accumulation; it is expected, that only between these temperatures (in the sticky region) fast and large scale accumulation of deposits can occur. Figure 14. Elaborates the case further. An exception is the sintering of fume to the cooler parts of the boiler. (Adams et al. 1997, p. 258)

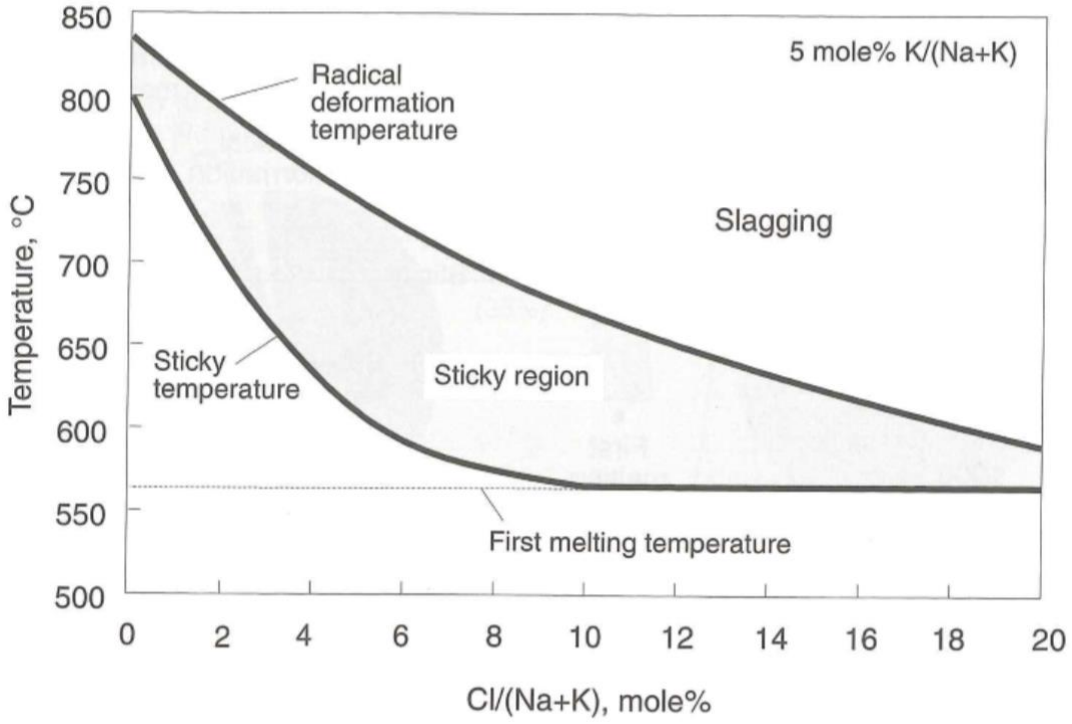

Figure 14. Sticky and radical deformation temperature presented against the Cl-concentration. Sticky temperature is always above the first melting temperature, which determines the first temperature point when the deposit has a liquid phase. The second melting temperature is above the radical deformation temperature and determines, when the deposit is fully liquid. (Adams et al. 1997, p. 258)

Deposit layer size changes according to temperature of the wall surface and the flue gases. The deposit layer will grow, until the layer grows thick enough to insulate the cooling effect of steam/water and the surface achieves the radical reduction temperature, which will deny further accumulation. Figure 15 presents layer thickness growth until a steady-state is reached. (Adams et al. 1997, p. 261)

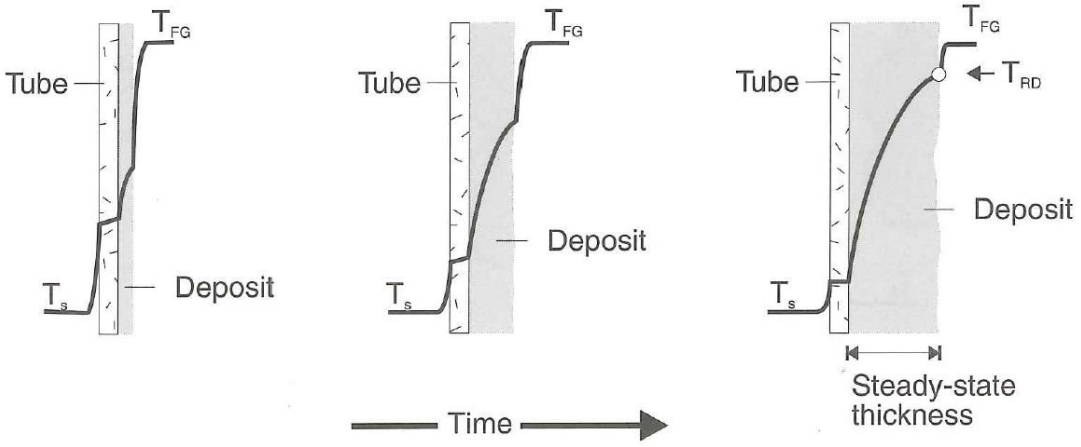

Figure 15. Deposit growth on a vertical surface inside the boiler. (Adams et al. 1997, p. 261)

Since deposit chemical composition, microstructure and porosity are far from constant, it is hard to determine thermal conductivity of the deposit. Porosity can have an order of magnitude difference when comparing chemically similar porous and non-porous compounds. Thermal conductivity has been observed to increase when particle size of the deposit grows. Sintered, non-porous, deposit has thermal conductivity similar to air. (Baxter et al. 2001, p. 135)

Two experiments were conducted by Baxter et al. (2001) to determine thermal conductivity dependency on porosity. The results are shown in figure 16. Comparing the graphs it is shown how solid fraction affects thermal conductivity of deposit.

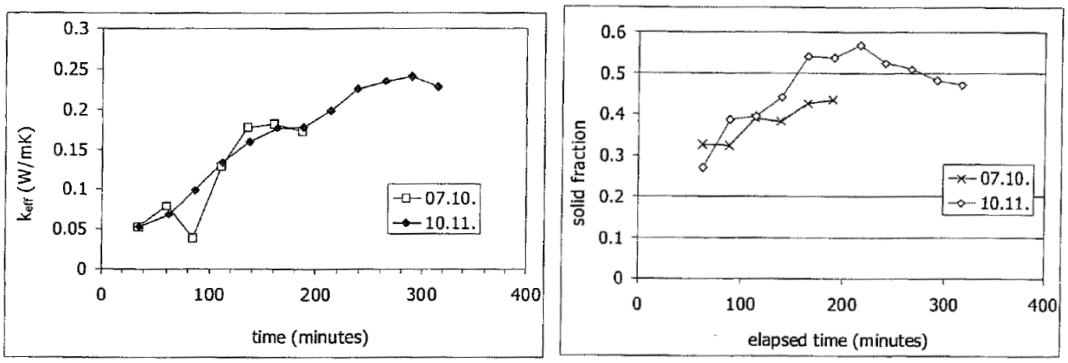

Figure 16. Thermal conductivity and solid fraction change of deposit with increasing time. (Baxter et al. 2001, p. 136)

Li et al. (2012) studied water wall temperatures of recovery boiler furnace with CFD modeling and infra-red cameras. The cameras were used to determine deposit temperature on the wall, while CFD models were used to determine the tube wall temperature. The study

found out that deposit temperatures were higher on the lower furnace on front and rear walls where liquor gun spray was hitting the wall. The deposit build-up on the front and rear walls was also larger compared to the side walls. (Li et al. 2012, p. 46) The measurements are presented in figure 17.

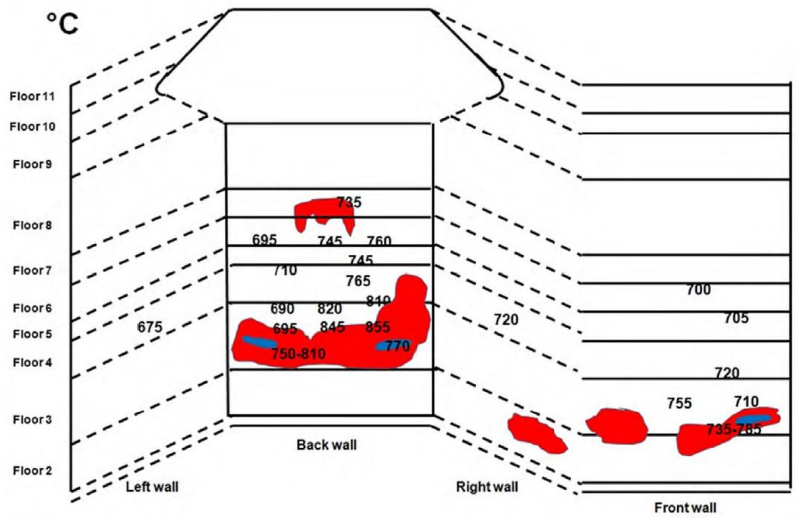

Figure 17. Wall temperature measurements done with infra-red cameras. (Li et al. 2012, p. 45)

Higher temperatures are caused mainly by the continuing combustion of liquor on the furnace wall. Cold blue areas are formed where the accumulation of liquor is most intense. The area is cool, because rapid liquor flow prevents efficient combustion. Red areas represent the hottest areas. (Li et al. 2012, p. 46)

3 NATURAL CIRCULATION IN RECOVERY BOILER

Natural circulation type boilers are commonly used in recovery boiler designs. The advantages of a natural circulation boiler include operation without a pump circulating the water inside the boiler and flexibility towards load shifting. Natural circulation inside the boiler tubing is caused by density difference between saturated and sub-cooled water in the downcomers and steam-water mixture in the evaporative tubing. The natural circulation mechanism makes these boilers more sensitive to flow instabilities than pump driven boilers. While a pump creates a constant pressure which drives the circulating flow, in natural circulation boilers the pressure difference varies by changing the heat load to the circuit.

3.1 Heat transfer from combustion to water circulation

Conduction, convection and radiation are the governing modes of heat transfer in many natural phenomena. Conduction is transfer of heat through a stationary medium and is useful to take into account when determining heat transfer through the isolating deposit layers. Convection on the other hand refers to heat transfer between a solid surface and a moving fluid, and is the main mechanism of heat transfer from the tube wall to the boiler water and steam. Lastly, thermal radiation refers to heat transfer by electromagnetic waves. (Incropera et al. 2003, p. 2-3)

The idealized thermodynamic system consists of a flue gas flow in the furnace, a furnace side deposit on a tube wall, a tube wall and water flow in the boiler tube as is shown in figure 18.

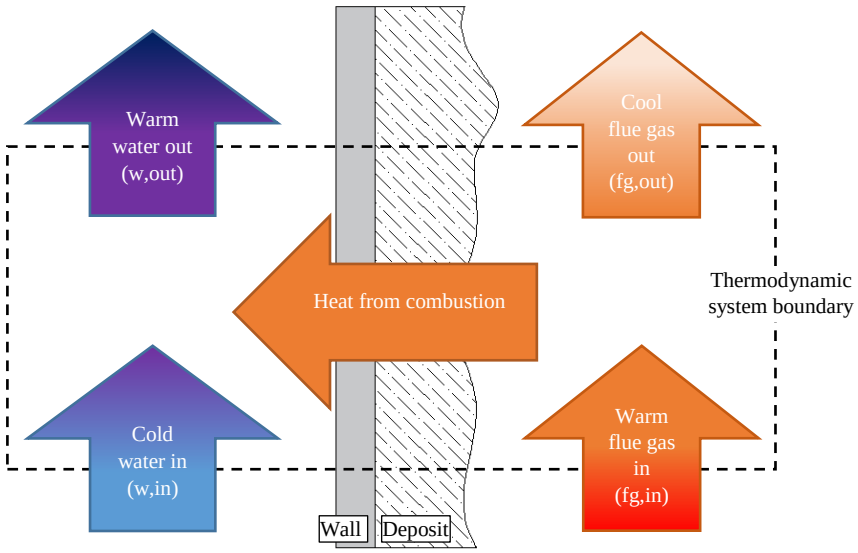

Figure 18. Thermodynamic representation of combustion heat transfer boiler water. Flue gases heat the deposit layer by convection and radiation. Deposit conducts heat further to the cooler tube wall. Tube wall is cooled by the water/steam flow.

Heat from combustion is transferred to the boiler water. For a discrete part of the wall, the conservation of energy requirement states that

$$(\dot{E}_{fg,in} + \dot{E}_{w,in}) + \dot{E}_g - (\dot{E}_{fg,out} + \dot{E}_{w,out}) = \frac{d}{dt} E_{st} \qquad (1)$$

, where $\dot{E}$ refers to flow of energy, which is in this case only heat. $\dot{E}_{fg,in}$ and $\dot{E}_{w,in}$ represent the heat of incoming flue gas and water, while $\dot{E}_{fg,out}$ and $\dot{E}_{w,out}$ represent the heat of outgoing flue gas and water flowing out of the system. The term $\dot{E}_g$ describes a heat sink or a source of heat in the system volume.

3.1.1 Flue gas convection

The deposit receives heat from the flue gas flow. Most of the heat is transferred by convection. The tube wall releases heat again to water by convection. Convection is presented simply as a product of convection coefficient h, heat transfer surface A and temperature difference ΔT between the fluid and the surface

$$q = hA\Delta T \tag{2}$$

(Incropera et al. 2003, p. 383). The convection coefficient is commonly determined with the dimensionless Nusselt number (Nu), which expresses the ratio of convection to pure conduction heat transfer

$$Nu = \frac{hL}{k} \tag{3}$$

, where L is the characteristic length of a surface and k is the conduction coefficient of the fluid. (Incropera et al. 2003, p. 409). Nusselt number can be determined using empirical correlations found in literature, or experimentally by varying the fluid, geometry and flow velocities to obtain new correlation equations.

3.1.2 Steady-state conduction through the deposit and wall

Let us assume that the flue gas and water flow properties of figure 18 stay constant. Then a simpler system can be derived:

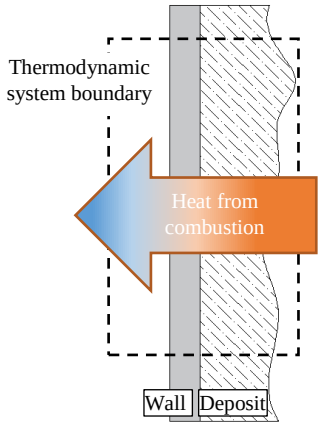

Figure 19. Simplified thermodynamic system of the tube wall.

For which,

$$\dot{E}_{in} - \dot{E}_{out} = \frac{d}{dt} E_{st} \tag{4}$$

, where $\dot{E}_{in}$ representes heat from combustion and $\dot{E}_{out}$ heat to the water circulation. During a steady-state event the heat energy change in the wall materials is zero (Incropera et al. 2003, p. 116).

$$\frac{d}{dt} E_{st} = 0 \tag{5}$$

The discrete wall-deposit system is divided to three interfaces, as is shown in figure 20.

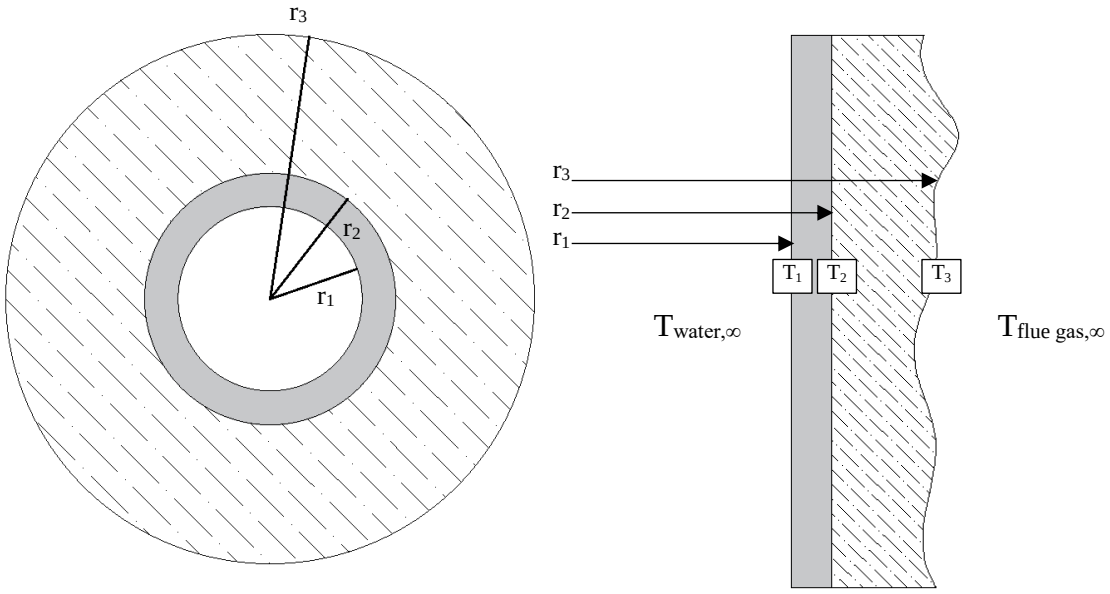

Figure 20. Specific surface temperature can be determined for the system interfaces. 1: Inner wall surface, 2: outer wall surface/inner surface of the deposit layer, 3: Outer surface of the deposit layer.

A radial heat conduction equation, with steady-state operation and no heat generation, is applied:

$$\frac{1}{r}\frac{d}{dr}\left(kr\frac{dT}{dr}\right) = 0 \tag{6}$$

(Incropera et al. 2003, p. 136). Equation (6) is integrated twice to obtain temperature as a function of radial distance:

$$T(r) = C_1\, ln(r) + C_2 \tag{7}$$

, where C refers to an integration coefficient (Incropera et al. 2003, p. 137). Introducing boundary conditions $T(r_2) = T_{s,2}$ and $T(r_3) = T_{s,3}$, to calculate transfer through the deposit layer, the complete equation is obtained

$$T(r) = \frac{T_{s,2} - T_{s,3}}{ln\left(\frac{r_2}{r_3}\right)} ln\left(\frac{r}{r_3}\right) + T_{s,3} \tag{8}$$

(Incropera et al. 2003, p. 137). From equation (8) it is evident that the radial temperature profile is logarithmic. This is shown in figure 21.

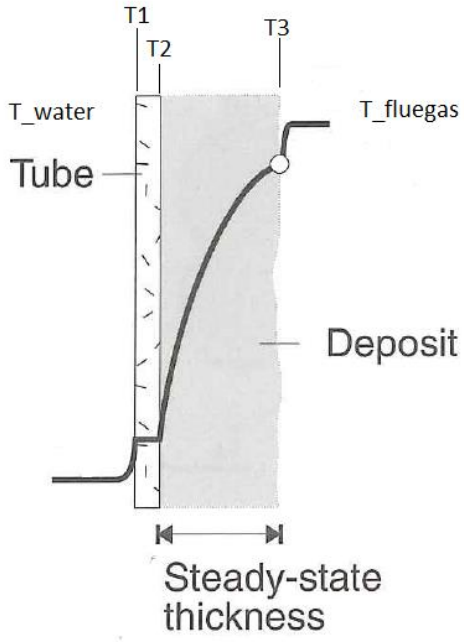

Figure 21. Temperature profile of evaporator tube surface in steady-state.

In figure 21, the temperature distribution is displayed with a thick line. Heat is transferred from flue gas side to the water side, hence the temperature descends from right to left. The largest temperature difference is between T_3 and T_2 where the deposit layer resides. The radial heat transfer rate can be expressed with Fourier's law:

$$q_r = -kA\frac{dT}{dr} = -k(2\pi rL)\frac{dT}{dr} \quad (9)$$

, where k refers to thermal conductivity, A to heat transfer surface, T to temperature L to tube length and r to radial distance (Incropera et al. 2003, p. 136). Now, substituting equation (8) to equation (9) the discrete form for radial heat transfer is obtained

$$q_r = \frac{2\pi Lk(T_{s,2}-T_{s,3})}{ln\left(\frac{r_3}{r_2}\right)} \quad (10)$$

(Incropera et al. 2003, p. 137). The same equations can be utilized for the tube wall as well to determine heat flow between points 1 and 2.

3.1.3 Resistance of the thermodynamic system

Since the term $kr\frac{dT}{dr}$ is independent of r, it follows that the radial heat transfer is constant:

$$q_{(system)} = q_{(water-wall)} = q_{(wall)} = q_{(deposit)} = q_{(deposit-fluegas)} \quad (11)$$

, where q stands for radial heat transfer rate, which is constant for a radial system. This heat flow can be expressed with temperature difference and thermal resistance.

$$\underbrace{\left(\frac{T_{fluegas}-T_{water}}{R_{tot}}\right)}_{system} = \underbrace{\left(\frac{T_1-T_{water}}{R_1}\right)}_{water-wall} = \underbrace{\left(\frac{T_2-T_1}{R_2}\right)}_{wall} = \underbrace{\left(\frac{T_3-T_2}{R_3}\right)}_{deposit} = \underbrace{\left(\frac{T_{fluegas}-T_3}{R_4}\right)}_{deposit-fluegas} \quad (12)$$

, where R stands for thermal resistance (Incropera et al. 2003, pp. 114-115). The total thermal resistance can be determined as the sum of thermal resistances between the flue gas and water flows. These resistances can be expressed with material thickness and heat transfer coefficient

$$R_1 = \frac{1}{2\pi r_1 Lh_{water}},\ R_2 = \frac{ln\left(\frac{r_2}{r_1}\right)}{2\pi k_{steel}L},\ R_3 = \frac{ln\left(\frac{r_3}{r_2}\right)}{2\pi k_{deposit}L},\ R_4 = \frac{1}{2\pi r_3 Lh_{fluegas}} \quad (13)$$

, where h refers to convective heat transfer coefficient (Incropera et al. 2003, pp. 114-115). The total resistance is therefore

$$R_{tot} = R_1 + R_2 + R_3 + R_4 \tag{14}$$

$$R_{tot} = \frac{1}{2\pi r_1 L h_{water}} + \frac{ln\left(\frac{r_2}{r_1}\right)}{2\pi k_{steel} L} + \frac{ln\left(\frac{r_3}{r_2}\right)}{2\pi k_{deposit} L} + \frac{1}{2\pi r_3 L h_{fluegas}} \tag{15}$$

Total thermal resistance describes the ability of the system to resist heat transfer. R_3 is usually the largest term in the system, since the deposit has low thermal conductivity and commonly higher thickness compared to the tube wall. Relatively, R_3 is at least 1000 times larger than other resistances. Large resistance creates a large heat gradient, as is shown in figure 21, where the temperature between T_3 and T_2 is larger compared to differences between other interfaces.

3.1.4 Transient conduction

In reality, the deposit layer responds slowly to the surrounding thermodynamic changes, which shows in the heat distribution inside the wall and deposit materials. The general heat diffusion equation

$$\frac{\partial}{\partial x}\left(k\frac{\partial T}{\partial x}\right) + \frac{\partial}{\partial y}\left(k\frac{\partial T}{\partial y}\right) + \frac{\partial}{\partial z}\left(k\frac{\partial T}{\partial z}\right) + \dot{q} = \rho c_p \frac{\partial T}{\partial t} \tag{16}$$

can be reduced by assuming constant thermal conductivity, constant density, constant specific heat capacity, no heat generation and 1- dimensional radial conduction to

$$k\frac{\partial^2 T}{\partial r^2} = \rho c_p \frac{\partial T}{\partial t} \tag{17}$$

, where α refers to thermal diffusivity. Heat diffusion inside the wall materials is dependent on heat capacity (c_p), density (ρ) and thermal conductivity (k) of the wall and deposit materials. These properties together are commonly referred to as thermal diffusivity

$$\alpha = \frac{\rho c_p}{k} \tag{18}$$

Which reduces equation (17) to

$$\frac{\partial^2 T}{\partial r^2} = \frac{1}{\alpha}\frac{\partial T}{\partial t} \leftrightarrow \frac{\partial T}{\partial t} = \alpha\frac{\partial^2 T}{\partial r^2} \tag{19}$$

The time derivative of temperature change is directly proportional to thermal diffusivity. In essence, larger thermal diffusivity means that heat is transferred faster in relation to the ability of the substance to store heat.

3.2 The principle of natural circulation

Natural circulation is a phenomenon that recovery boiler water-steam circulation relies on. Driving force of the circulation is the difference in bulk fluid density between evaporative tubing and downcomers. A density difference, in essence temperature and void differences, is created when a heat flux is established to the evaporative tubing. In case of a single channel, the difference in density creates a pressure gradient along the channel. Equation (20) elaborates the pressure difference mathematically.

$$\Delta P = \left(\rho_{down} - \rho_{up}\right) g H \tag{20}$$

, where ΔP is the pressure difference between riser and downcomer tubes, ρ_{down} is average downcomer fluid density, ρ_{up} is average riser fluid density, g is gravitational acceleration and H is height of the circulation. (Vakkilainen 2017, p. 99) To be precise, the effective circulation height is determined between steam drum water level and the start of nucleate boiling in the evaporator tubes.

In a recovery boiler, the density differences between water and steam drive the flow. Water isn't a very compressible, but steam on the other hand compresses much more easily. Indicative densities of downcomer water and a water-steam mixture generated in the evaporating components are shown in table 5.

Table 5. Densities of downcomer water and average water-steam mixture in an evaporative component. Thermodynamic properties are cited from NIST chemistry WebBook (Lemmon et al. 2018).

Parameters	**Downcomer water (275°C, 80bar)**	**Saturated water (80bar)**	**Saturated steam (80bar)**	**Water-steam mix (x=0.5, 295°C, 80bar)**
Density [kg m^{-3}]	760	722	42,5	382

3.3 Fluid flow inside vertical and horizontal tubes

Single and two-phase flow are both present in the boiler water circulation system. The system flow directions also vary from horizontal to vertical in divider tubes, screens and the bull nose, while most of the flow will be traveling vertically or horizontally. Flow is restricted by change in the shape of tubing, such as outlets and inlets of channels, bends and friction of the tube wall. The extensive properties such as velocity and temperature have an effect on the turbulence of water and steam inside the tubing. Known flow patterns help to understand the dynamic water-steam phenomena inside an operating recovery boiler.

3.3.1 Single-phase flow

Single-phase flow will occur with gases and liquids alike. Flow of the fluid can be turbulent or laminar. Turbulence emerges from fluid flow contact with a surface. Flow near the surface will be slower than the bulk flow and theoretically it will be zero on the surface. This slower flow area is called the boundary layer. Eventually in the right conditions, the boundary layer will grow and develop a turbulent region that covers the whole flow area. This transition is described in figure 22.

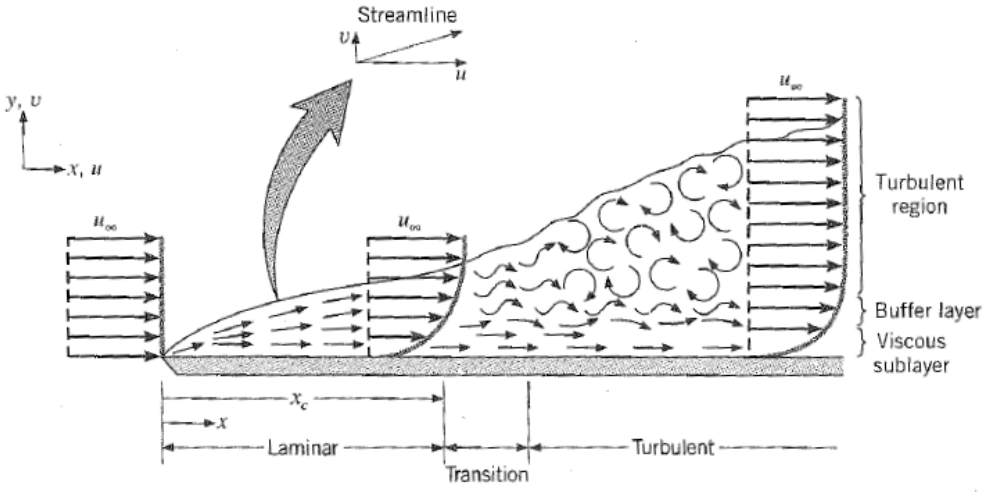

Figure 22. Change from laminar to turbulent boundary layer on a flat plate. (Incropera et al. 2003, p. 389)

Development of a laminar boundary layer in a circular tube is shown in figure 23.

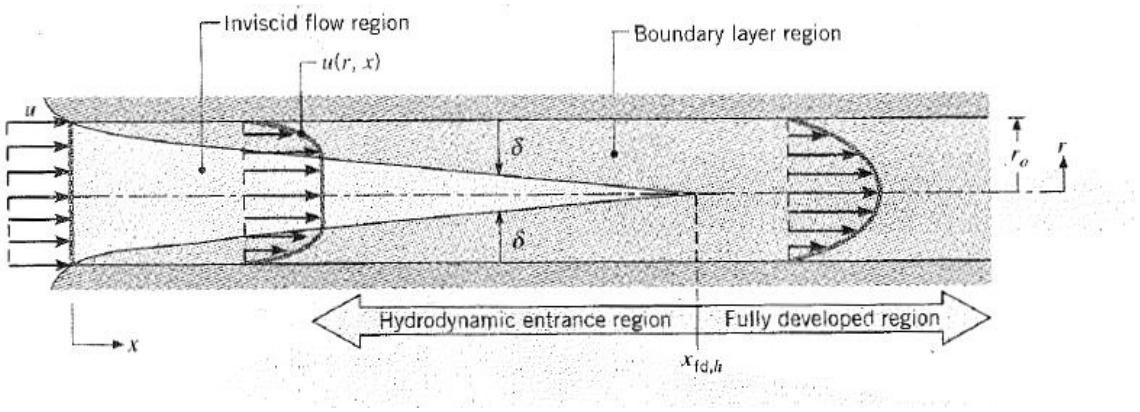

Figure 23. Laminar boundary layer development in a circular tube (Incropera et al. 2003, p. 518). For a turbulent tube flow the profile would be more flat in the developed region.

A dimensionless parameter Reynolds number can be utilized to determine turbulence of the flow. A high Reynolds number means the flow is turbulent, while a lower number indicates laminate flow.

$$Re_D = \frac{\rho u_m D}{\mu} \tag{21}$$

, where Re_D is Reynolds number, ρ is fluid density, u_m is mean velocity, D is the hydraulic diameter and μ is dynamic viscosity of the fluid. Laminar flow is considered dominant for Reynold's number under 2300. (Incropera et al. 2003, p. 519)

3.3.2 Two-phase flow

In essence, two-phase flow is a bulk fluid motion of a liquid and gaseous mixture. Inside a vertical tube a radial symmetry in the flow of water and steam mixture can usually be approximated. When the flow is horizontal, the density difference between water and steam makes the flow not so symmetric in the radial direction. With small inertial forces of the fluid, the difference between vertical and horizontal flow patterns is noticeable. (Baehr & Stephan 2006, p. 474) figure 24 and figure 25 present different types of two-phase flows.

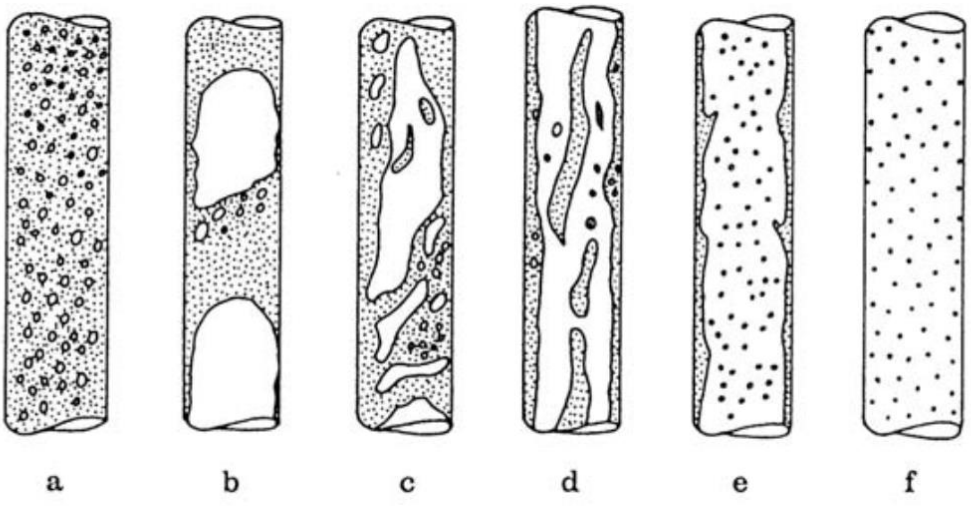

Figure 24. Two-phase flow inside an unheated vertical tube. Flow patterns are defined as bubble flow (a), plug flow (b), churn flow (c), wispy-annular flow (d), annular flow (e) and spray or drop flow (d). (Baehr & Stephan 2006, p. 473)

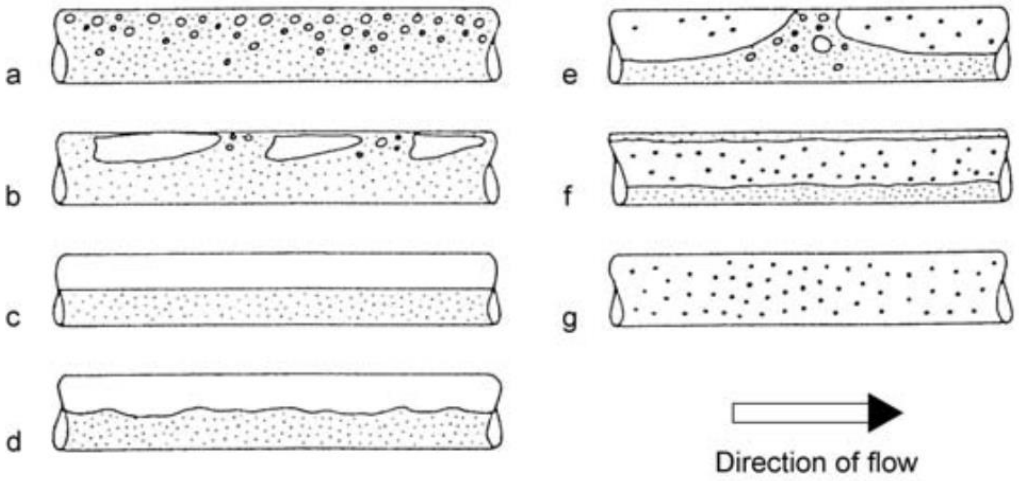

Figure 25. Two-phase flow inside an unheated horizontal tube. Flow patterns are defined as bubble flow (a), plug flow (b), stratified flow (c), wavy flow (d), slug flow (e), annular flow (f) and spray or drop flow (g). (Baehr & Stephan 2006, p. 474)

Because of the complex nature of a non-adiabatic vapor-liquid flow, caused by irregular heat fluxes to the flow, forming and collapsing of drops and other deviation of hydrodynamic and thermodynamic equilibrium, the flow patterns do not occur sequentially. The patterns might be mixed and some might not occur at all. (Baehr & Stephan 2006, p. 473-474)

3.3.3 Pressure loss inside a tube

The total pressure loss of a single-phase flow consists of losses from fittings, flow entering a tube, flow exiting a tube and friction losses. There can be as many fitting losses as there are fittings. Pressure losses inside tubing are presented in equation 22.

$$\Delta p_t = \Delta p_l + \Delta p_i + \Delta p_o + \Delta p_f \tag{22}$$

, where Δp_t is total pressure loss, Δp_l are fitting losses, Δp_i are inlet pressure losses, Δp_o are outlet pressure losses and Δp_f are friction losses (Vakkilainen 2017, p. 104) All of these losses are dependent on the dynamic pressure p_d:

$$\Delta p_t = p_d(\Sigma\zeta_b + \zeta_i + \zeta_o + \epsilon\frac{L}{d_i}) \tag{23}$$

, where ζ refers to a pressure loss coefficient, ϵ to friction loss coefficient, L to tube length and d_i to inside diameter. Dynamic pressure is dependent of fluid density and velocity:

$$p_d = \frac{\rho\omega^2}{2} \tag{24}$$

, where ω is the velocity of the fluid. Pressure and friction loss coefficients are usually determined experimentally.

Total pressure loss for a two-phase flow is determined with local wall friction loss (Δp_f), acceleration loss (Δp_a), hydraulic loss (Δp_g) and fitting loss (Δp_l)

$$\Delta p_t = \Delta p_f + \Delta p_a + \Delta p_g + \Delta p_l. \tag{25}$$

The acceleration loss addresses losses originating from growing volume of the fluid due to evaporation. These parameters are determined with the homogeneous or the separated model. Homogeneous model assumes that the flow can be modelled after single-phase behavior. This model is used, when the fluid has high or low steam quality, high flow rate or is at higher pressures. The separated model treats steam and water as separate streams, and is used when the homogeneous model fails. The separated model is more difficult to

utilize, because it requires use of correlations, which often are not public information. (Kitto & Stultz 2005, p. 5-9, 5-10, 5-11)

3.3.4 Boiling

The change from single-phase to two-phase flow is subtle; when a heat flux is directed to the flow, bubbles start to form on the heated surface while the bulk liquid is still subcooled. For a heated tube, the flow experiences multiple two-phase flow patterns in the flow direction, which are presented in figure 26.

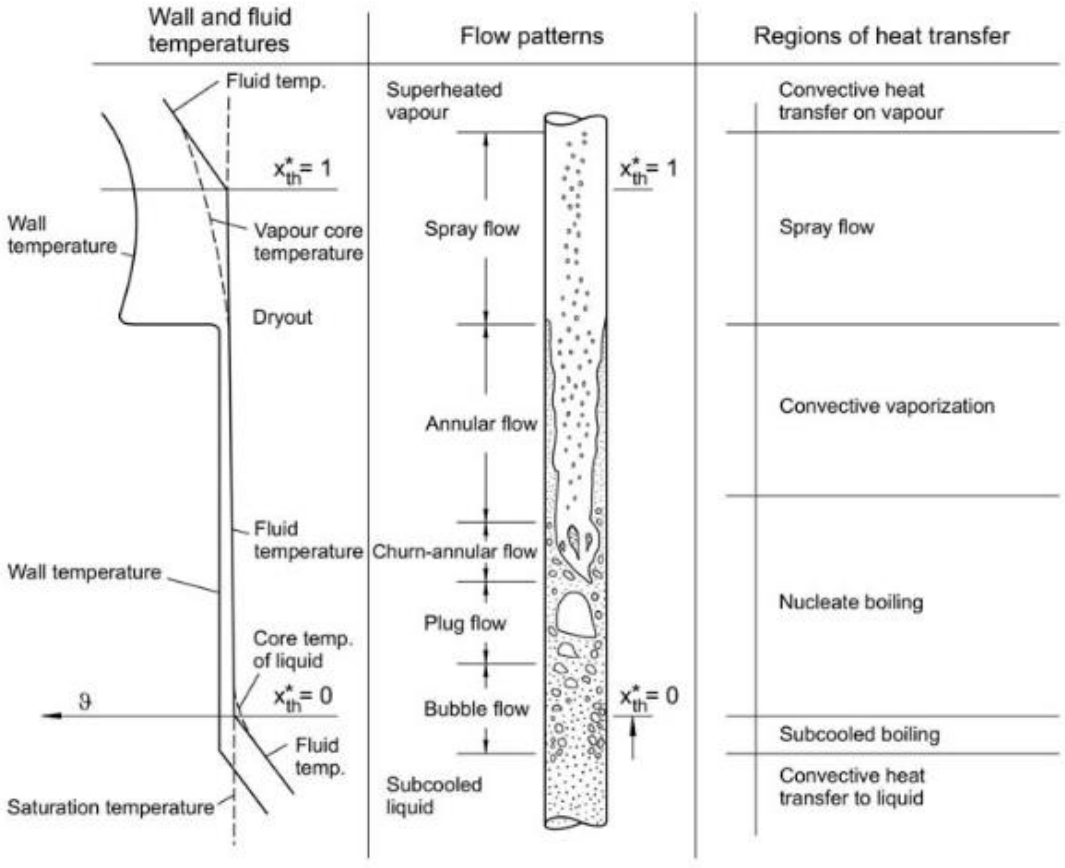

Figure 26. Forced convection boiling inside a vertical tube. Flow patterns are explained with wall and fluid temperatures and with regions of heat transfer. (Baehr & Stephan 2006, p. 488)

Bubbles start to form as soon as the wall temperature reaches the boiling temperature of water. Incropera et al. (2003) suggests that in the saturated flow boiling region (nucleate boiling and convective vaporization in figure 26) the overall heat transfer coefficient for the

fluid is higher, than in the other regions. At dryout point a steam film develops on the surface of the tube, which acts as an insulator immediately rising the wall temperature. (Incropera et al. 2003, p. 671) For relatively low flow velocities, forced convection boiling in a horizontal tube looks something like presented in figure 27.

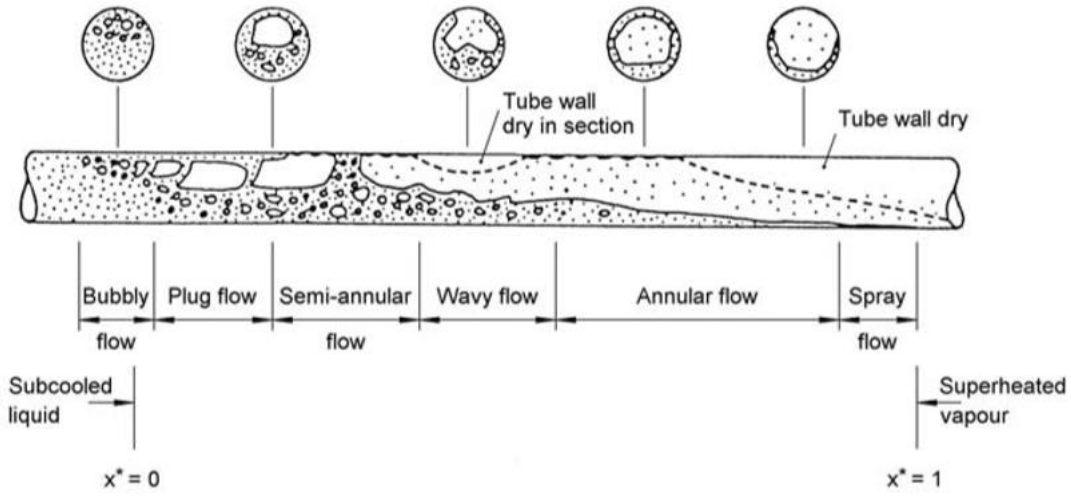

Figure 27. Horizontal forced convection boiling inside a tube according to Collier (1972) (cited in Baehr & Stephan 2006, p. 475)

3.3.5 Critical heat flux

Boiling crisis, or dryout, is a state that represents a reduced heat transfer coefficient of the fluid and, in essence, reduced heat flux to the cooling fluid. Boiling crisis is achieved with a CHF (critical heat flux) value. With a large enough heat flux, the fluid can exhibit film boiling on the surface of the tube, even when the majority of the fluid is still water. On the other hand, when quality of the flow is high enough, and the last water film on the surface has been dissipated, the flow reaches CHF and enters a dryout zone. Figure 28 elaborates the two cases further.

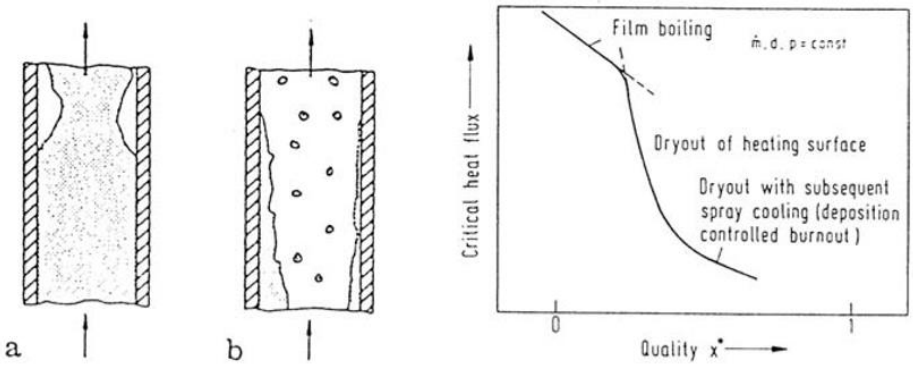

Figure 28. Critical heat flux occurrence in film boiling (a) and dryout (b). (Baehr & Stephan 2006, p. 493)

A plotted boiling curve is shown in figure 29. A dynamic instability is observed in the boiling curve when the CHF is passed, causing a massive temperature rise immediately.

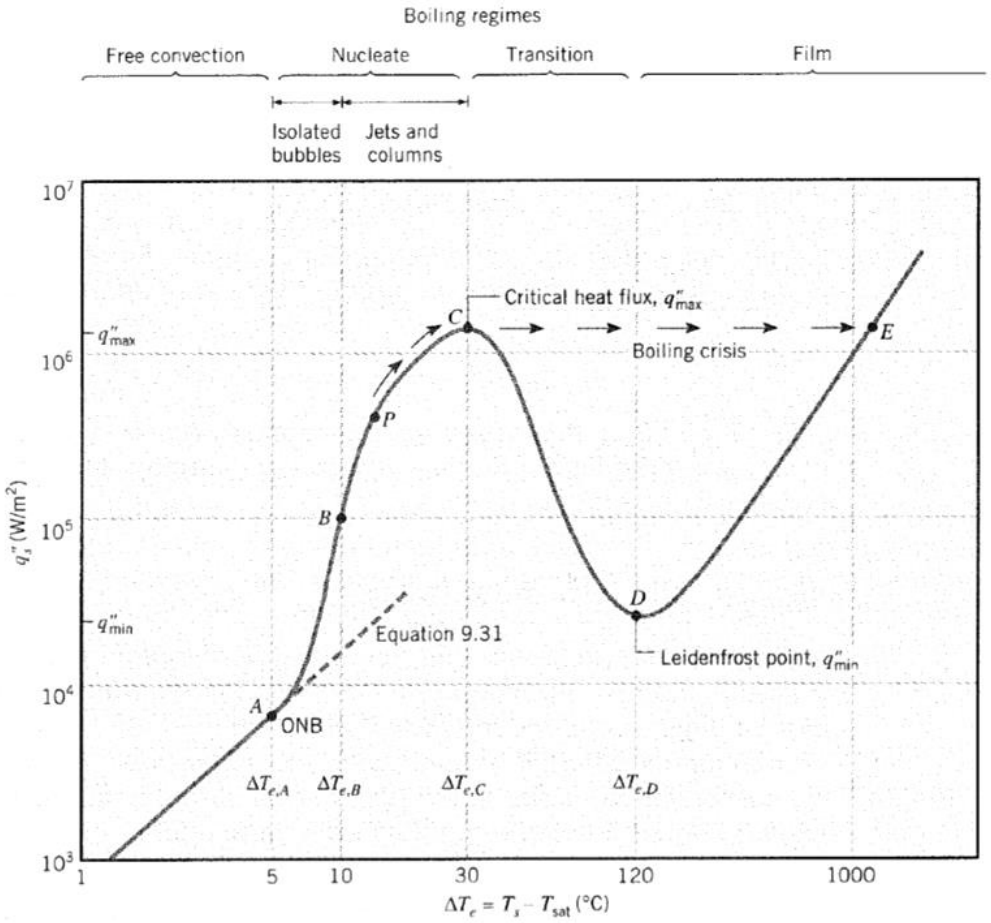

Figure 29. Pool boiling curve in 1atm pressure. Surface heat flux is presented as a function of excess temperature. (Incropera et al. 2003, p. 658)

3.4 Flow instability phenomena

Flow instability problems, eventually resulting to failure, can be found after startup of new boiler design configurations. Permanent changes in the flow direction of individual tubes, and stagnation of fluid have led to severe tube failures. (Linzer & Walter 2003, pp. 2363, 2370) Unstable flow might damage piping by allowing periodic or constant exceeding of CHF inducing unnecessary thermal stresses to tube structure.

3.4.1 Pressure density oscillation

Flow excursion combined with a compressible volume (located upstream from heated channel) enables pressure drop oscillation (PDO). An example system is shown in figure 30, while the oscillation phenomena is presented in figure 31.

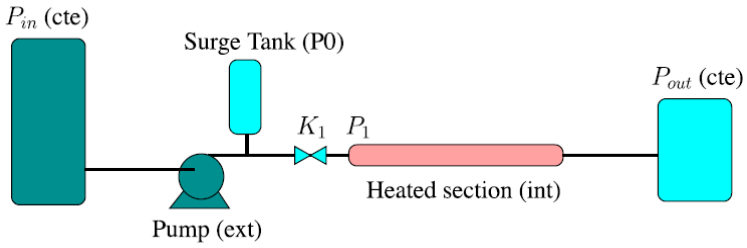

Figure 30. An example of a system, where PDO is possible. (Ruspini et al. 2014, p. 255)

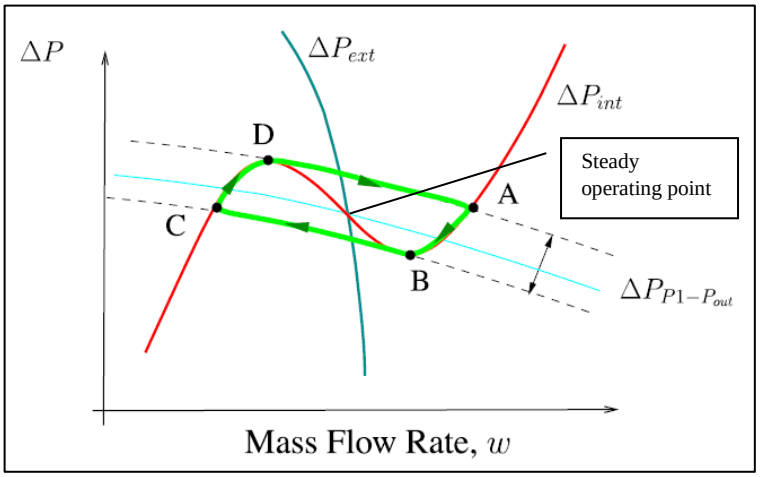

Figure 31. Flow excursion induced PDO. (Ruspini et al. 2014, p. 525) The colors correspond to figure 30 components. Surge tank compressibility enables shifting of the surge tank characteristic curve (cyan line). CD - Compressible volume compresses, which triggers a flow excursion. DA - much of the fluid evaporates. AB - Mass flow is now much higher, so the surge tank volume releases pressure. BC - Flow excursion happens and much of the fluid condense back to liquid.

Operating point nucleates around the intersection point of the internal and external characteristic curves, enabled by the surge tank volume and expressed with the characteristic curve of the surge tank. This behavior is driven by flow excursions which deny the system to reach the steady operating point.

3.4.2 Density wave oscillation

Ozawa et al. (2001) suggests that density wave oscillations (DWO) are the most common two-phase flow instability encountered in parallel-channel boiling systems, systems with upstream compressibility and natural circulation systems. DWO emerges from the time-delay of void wave propagation and the feedback effect between flow rate and pressure drop. (Ozawa et al. 2001, p. 391) Ruspini et al. (2014) establishes that the main mechanisms of DWO are the delay in propagation of disturbances and the feedback processes that condition the inlet parameters (Ruspini et al. 2014, p. 526). In comparison to PDOs the DWO frequency is much smaller, as is shown in figure 32.

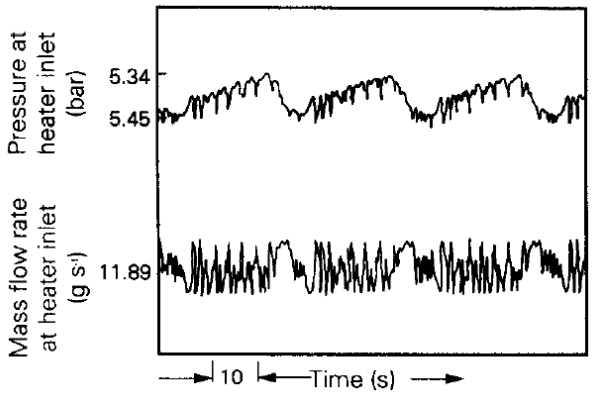

Figure 32. PDO and DWO phenomena captured in experiment results. (Padki et al. 1992, p. 527) The high frequency oscillation is DWO while PDO phenomena cycle time is about 25 seconds.

3.4.3 Thermal oscillation

Thermal oscillation (ThO) is observed in a heated tube wall. The phenomena is usually triggered by other thermo-hydraulic instabilities such as PDO and DWO. When ThO is low frequency and high amplitude oscillation, it is likely triggered by PDO. Then the temperature shifting is caused by the vertically shifting dryout point. (Ruspini et al. 2014, p. 527)

4 BLACKOUT DEFINITION

A power blackout happens when external supply of electricity (by the electric grid) to the recovery boiler is lost. Diesel-generators will usually provide enough electricity for IC-systems (information and control). The backup feedwater pump might be steam driven. Nominal steam drum pressure should be maintained as long as possible to avoid losing water reservoir, in case of backup pump failure and long blackout duration.

4.1 Boiler shut down

In the worst case, emergency power generation fails and no electricity is provided through the normal electrical network nor through the backup network. Normal operation of the boiler stops; air supply, black liquor guns and feedwater pumps stop operating (Finnish recovery boiler committee 2013, p. 4). The state of the boiler can be quite unique, since no shut down protocols can be adequately executed without power. An example of this was a case where during blackout, the sootblowers were left inside the boiler with the steam temperature adjustment valves open, which meant that there was a possibility of feedwater finding a way through the sootblowers to the smelt. (Finnish recovery boiler committee 2013, p. 15). Manual operation of valves is difficult, because the IC-system can't provide the operators any information (Finnish recovery boiler committee 2013, p. 4).

The feedwater pump runs on external electricity as well, and will stop at the start of blackout. A backup pump is then needed to be activated. The backup pump is driven either with live steam from the boiler or electricity. It is not unusual, however, for the backup pump to fail to operate. When the backup pump fails, flow of cooling water to the boiler stops and the furnace char bed needs to be cooled with the remaining water inside the boiler. A method used to cool down the boiler is to keep the boiler pressure constant, while reducing the mass flow of steam out of the boiler. Boiler pressure must be kept, in case the backup pump doesn't start operating and the blackout lasts a long time. Possible feedwater flow is controlled with the start valve, while the steam flow out is controlled with the main steam valve.

4.2 Impacts

The most severe impact is a steam explosion, which emerges from water-bed interaction while the bed is still hot (Finnish recovery boiler committee, 2009, p. 11). Water or steam can flow in to the furnace from cracked wall tubes caused by unusual operation of the boiler. If water is found inside the furnace, it will be pooling somewhere on the bed (bed surface will be solidified at this point). The explosion is activated by a falling deposit or some other phenomena that lets the water interact with the inner hot bed, creating large amounts of steam in an instant.

5 BLACKOUT STUDY

A blackout study is conducted to discover if problems in material temperatures emerge. The study utilizes an Apros model of the boiler water circulation. A worst case scenario approach is chosen as the method to determine necessary assumptions and boundary conditions. Sensitivity analysis is conducted for the furnace side deposit thickness using the blackout study as a base case.

5.1 Model

Apros Combustion was chosen as the dynamic modelling software for this work. The choice was easy, since there were similar simulations already done in Andritz with the software. Apros is also a widely used software that uses model libraries, which have been validated against real plant data as well as test facility experiments.

The dynamic model steady-state is determined with combustion heat data, deposit thickness, the thermodynamic state of feed water, blow out water and produced steam amount. Heat from combustion is determined with an iterative process described in chapter 5.1.3. During blackout, all heat in the deposits is assumed to transfer to the water circulation. The thermodynamic states are provided with the boiler calculation tool of Andritz. Deposit size is defined according to previous measurements. Assumptions are made and boundary conditions chosen according to worst case scenario approach.

5.1.1 Apros

Apros Combustion version 6.07.05.06 is used to model the water circulation inside a recovery boiler. Apros is a dynamic, 1-dimensional, simulation program which enables the user to build a model with diagrams and process components (see figure 33). Creation of models is backed up with model libraries. In this thesis, a six-equation model with separated fluid phases is utilized to model the two phase water-steam flow. The model is based on the conservation equations of mass, momentum and energy for both phases. The water-steam (WS) fluid is used to model the water circulation flow phenomena.

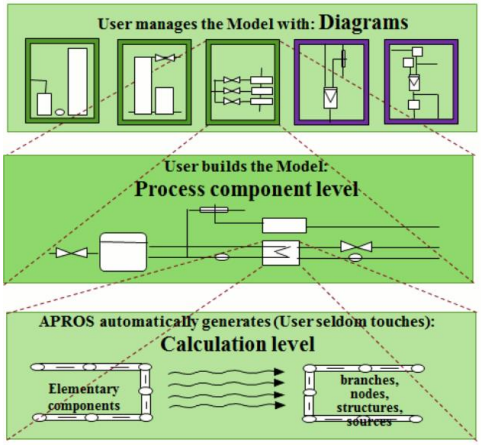

Figure 33. Apros model structure. (VTT 2017)

The model consists mainly of heat tube and point modules. Points are used to determine points in the model space, for example elevation. Heat tubes are connected to these points to model the flow inside the tubes. A heat tube module can be set to contain multiple similar tubes to reduce model iteration time. Tubes with different bend angles and lengths can also be bundled into one module. Average values of pressure loss coefficients and lengths need to be used for modules containing tubes with different geometry.

The calculation inside the heat tube modules is done by a network of calculation nodes. Creating a module such as a heat pipe generates smaller components, which in essence form the heat pipe module itself. An Apros model is comprised of a composition and a thermal hydraulic network. Both of these networks contain nodes and branches. Together they form a dual network structure, which handles the fluid modeling. A heat pipe module and two heat point modules are presented in figure 34.

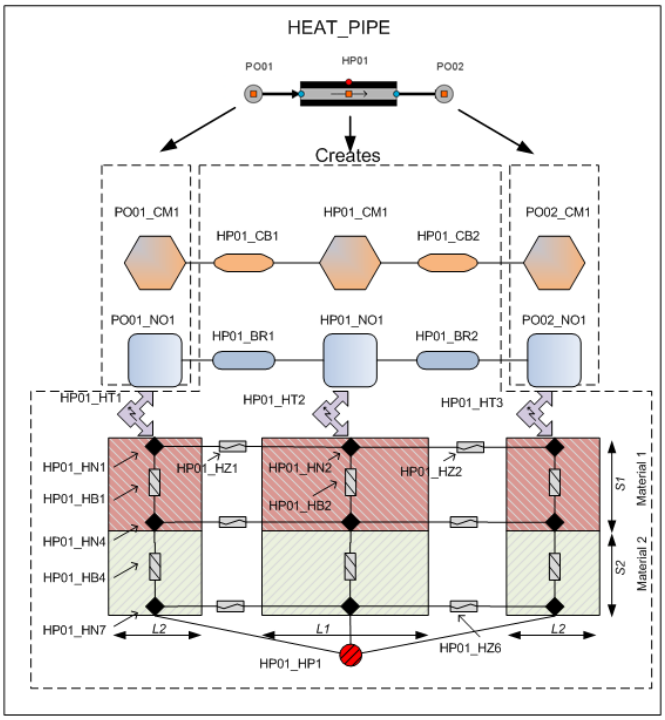

Figure 34. Heat tube module with two material layers. 3 heat nodes (black diamonds) are created in the radial direction. Blue components represent the hydraulic network while the orange components represent the composition network. Nodes inside the red and green material handle the thermodynamic behavior of the tube wall and deposit. (VTT 2017)

Between material 1 and the hydraulic network are heat transfer nodes which communicate the heat transfer between nodes. In radial direction, a calculation node is provided for both inner and outer surfaces of the steel material. Third node in radial direction is positioned at the outer layer of the deposit material. The incoming heat flux to heat tube modules will be set to these outer nodes.

5.1.2 Model structure

The boiler is discretized to following components:

1. Front wall
2. Rear wall
3. Left side wall
4. Right side wall
5. Horizontal screen
6. Vertical screen
7. Boiler bank
8. Rear wall screen
9. Ash hopper

These components are constructed in Apros with heat tube and point modules. Figure 35 presents discretization of the boiler front wall. Modules assigned to model evaporative surfaces are discretized roughly a calculation node per meter of tubes in the module.

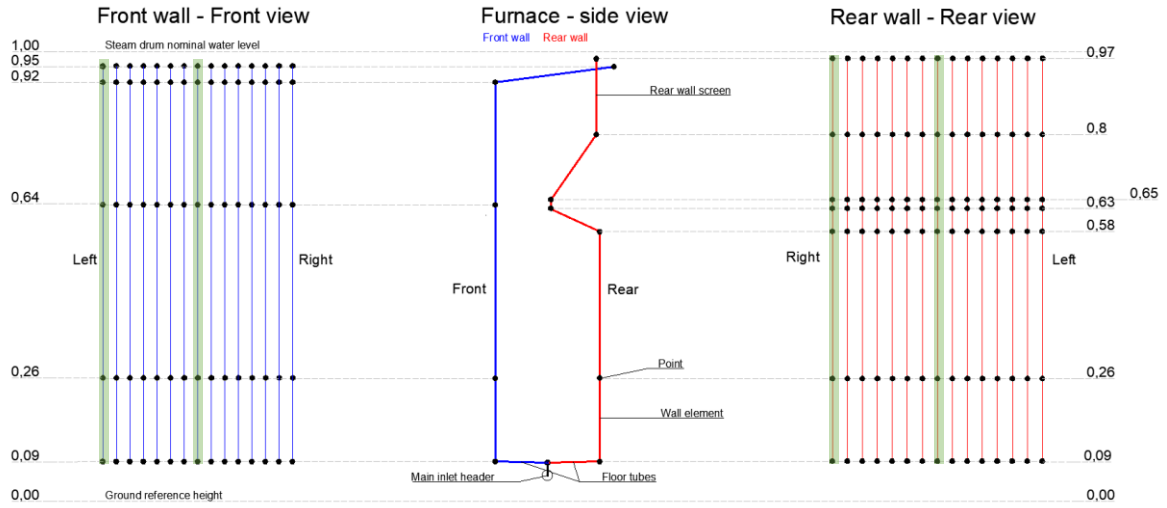

Figure 35. Discreet model of furnace front wall, rear wall and screen. Blue represents the front wall and red the rear wall. The elevation of heat points are presented as a scaled value between 0 and 1, 1 being steam drum nominal water level and 0 being the ground level. Green area emphasizes the modules from which the temperature data is acquired.

Front view presents the horizontal discretization of the front wall into 15 parts. Each wall utilizes the following distribution of tubes into modules:

Table 6. Wall discretization into modules on the furnace walls

Module #	1	2	3	4	5	6	7	8	9	10	11	12	13	14	15
Percentage of wall tubes [%]	2,5	3,0	4,5	6,0	6,0	8,0	12,0	16,0	12,0	8,0	6,0	6,0	4,5	3,0	2,5

Rear wall screen is positioned between 0,8 - 0,97 on the rear wall. The side view presents vertical discretization and elevation differences between points. Side walls are discretized in a similar fashion shown in figure 36.

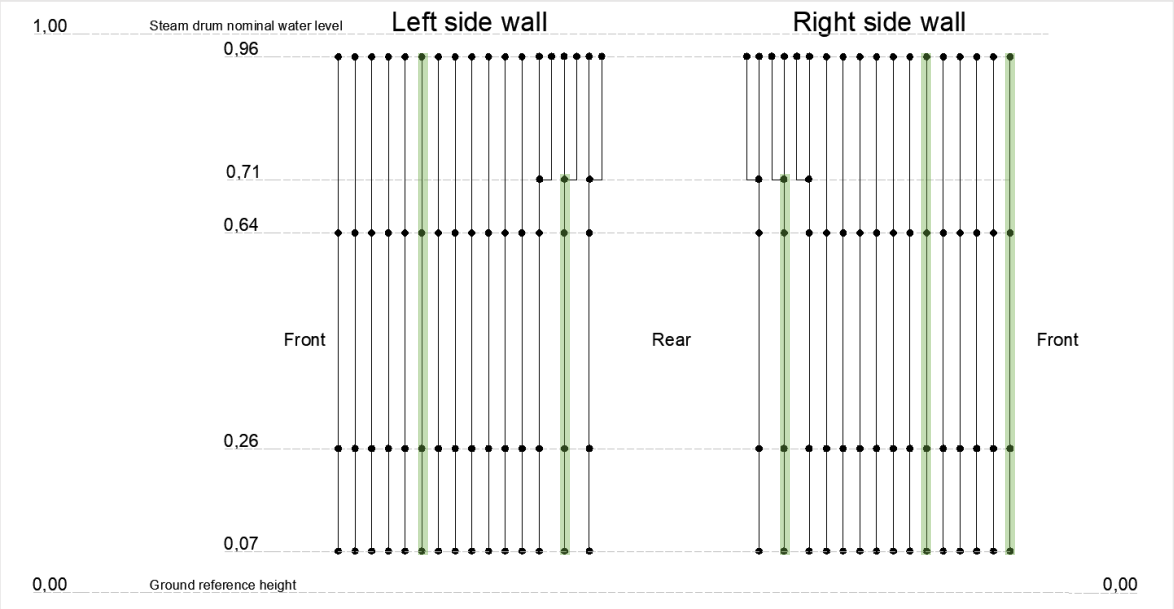

Figure 36. Left and right side wall discretization. Green area emphasizes the modules from which the temperature data is acquired.

The side walls are mirror images of each other. Both walls have a horizontal extension at the upper furnace, which is modelled by dividing single modules into two via a point module.

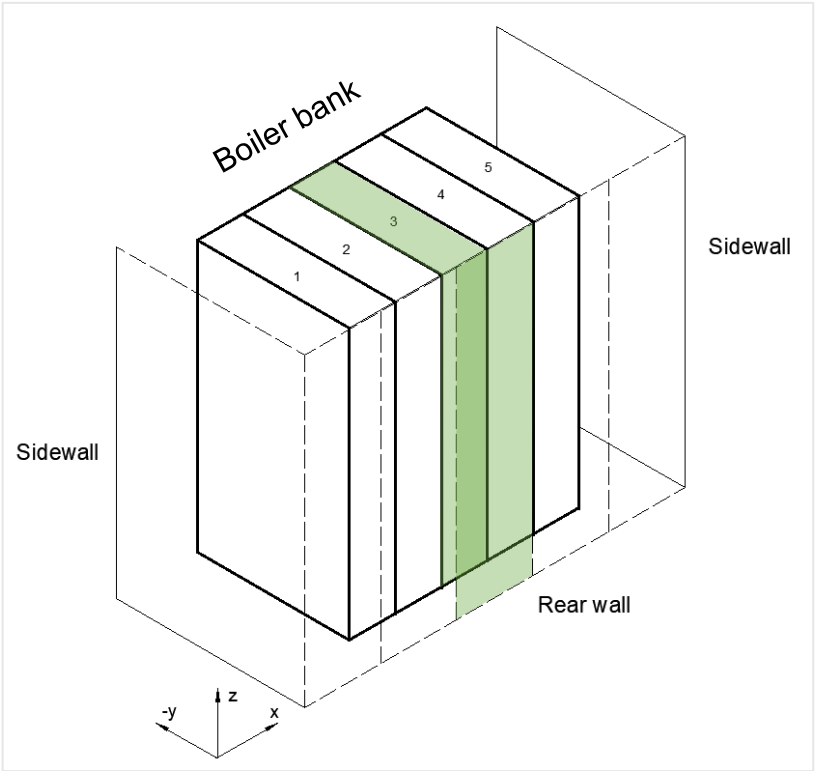

Figure 37. Boiler bank volume discretization. Each numbered volume describes a heat pipe module, which contains multiple tubes. Green area emphasizes the modules from which the temperature data is acquired.

Both sidewalls in the boiler bank are modeled as single heat tube modules. The boiler bank platens and rear wall are each divided into 5 heat tube modules. A part of screen is shown in figure 38.

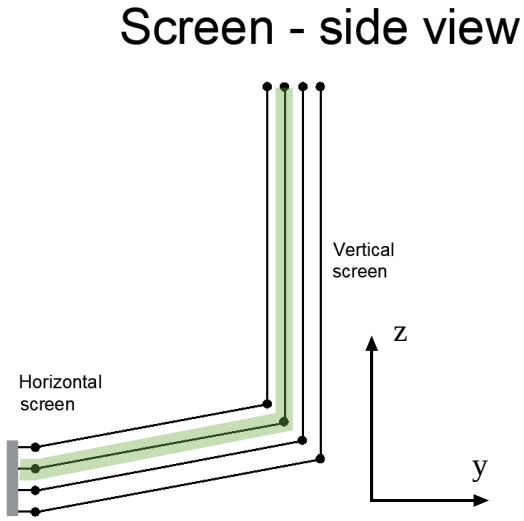

Figure 38. The screen is discretized in 5 of these assemblies along the x-axis adjacent to each other. Green area emphasizes the modules from which the temperature data is acquired. In this case data is acquired from the 3rd assembly (middle), counting from the bottom.

The screen is composed of 5 identical assemblies shown in figure 38.

5.1.3 Combustion model

Heat from combustion must be determined to solve the steady-state of the natural circulation inside the boiler tubing. This would be achieved most accurately with CFD modeling. CFD requires a lot of computation and more accurate determination of boundary conditions, which is why in this case an iterative solving process is utilized to determine the profile. The procedure utilizes a program called ANITA, which calculates the heat balance for certain volumes inside the furnace. The data from ANITA is used as a reference, to which the results from the Apros simulation are expected to match.

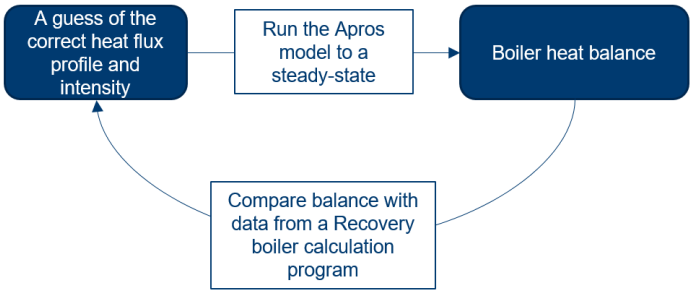

Figure 39. General idea of the combustion heat iteration process.

A sample of generic heat flux data is utilized as a good initial guess for heat flux distribution on the water circulation. CFD-data is provided in the form dedicated by a mesh. Every node in the mesh grid contains a heat flux value. An example is provided in figure 40.

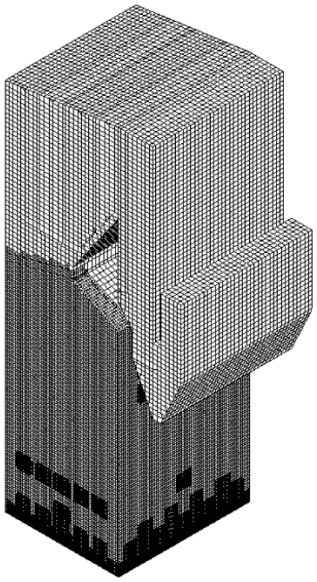

Figure 40. Recovery boiler CFD mesh. (Maakala 2013)

Usually the sample has to be processed before it can be used, since the accuracy of the CFD data is unnecessary high for the Apros model. The sample needs to be scaled to smaller node size and the geometry scaled to current dimensions. Afterwards the processed heat flux sample data is compared with processed data from ANITA. Coefficients are calculated for each evaporative surface. An initial guess for these coefficients must be made. After the initial guess the coefficients are changed via an iterative process according to equation (26)

$$C_{i+1} = C_i \cdot \frac{Q_{Apros}}{Q_{ANITA}} \quad (26)$$

, where C is the thermal coefficient and Q the heat flux. Heat flow values from ANITA are reference values and therefore constant through the process. The heat flow values from Apros are acquired after running the model to a steady state (utilizing the newest thermal coefficients). The iteration process is complete when the new coefficients are approximately 1.

5.1.4 Wall deposits

Wall deposit size is dependent of T_{70} temperature of the deposit and the local heat transfer from combustion. The thickest deposits can be found on the coldest parts of the furnace for example, in the corners, while the hottest wall area is usually on the front wall. A simple geometry is chosen to model the deposit layer on the wall and is shown in figure 41.

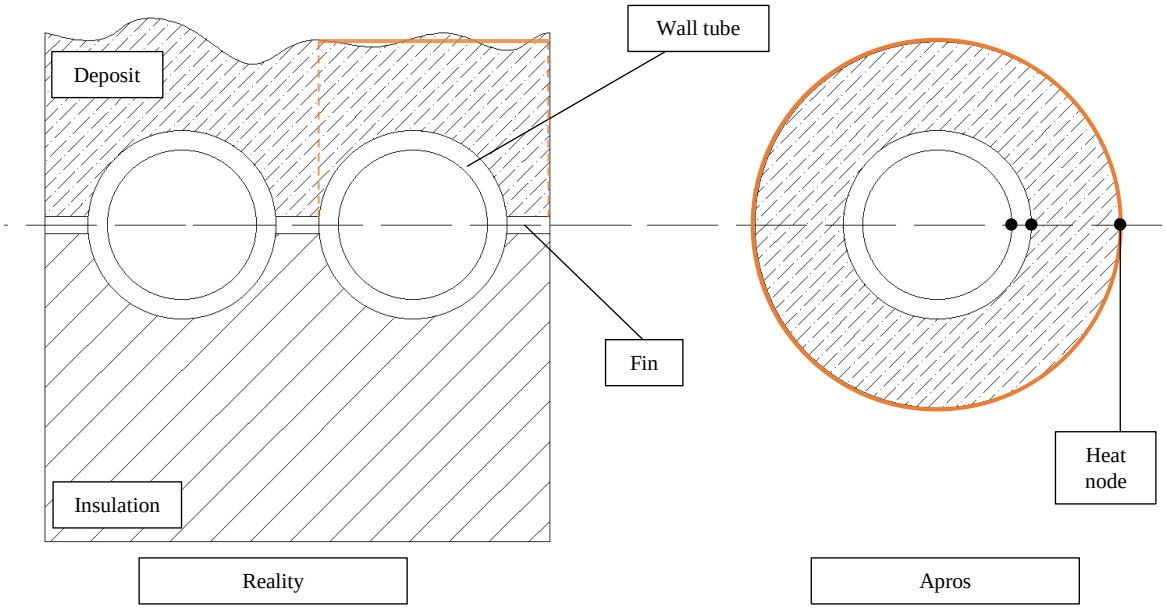

Figure 41. Deposit layer comparison of furnace wall tubing (left) and how it is modelled in Apros (right). The orange solid lines represent the heat transfer area of each case for one tube. Three heat nodes are assigned radially in every heat pipe module to model radial heat transfer.

The heat receiving area of a furnace wall tube is different in the deposit model compared to reality. In Apros the heat is transferred through the whole perimeter of the deposit, while in reality the wall will receive the heat only on the other half the tube and on the fin. To take

into account the difference in geometry, the heat flux data that is set as a boundary condition can be scaled with the relation of the receiving areas:

$$C = \frac{D_{tube}+l_{fin}}{\pi D_{deposit}} \tag{27}$$

, where C is the coefficient used to scale heat flux data, D_{tube} outer diameter of the furnace wall tube, l_{fin} length of a fin and $D_{deposit}$ the diameter drawn from the outer surface of the deposit.

As described earlier in chapter 2.4.3, there are many parameters that determine deposit layer thickness. In this case, it is sufficient to approximate the deposit thickness according to worst case scenario approach. The thicknesses are determined by using the same values as in previous simulation cases done by Andritz, and are presented in table 7. The chosen values have been obtained previously by camera observation inside the furnace.

Table 7. Deposit layer thickness according to location. Thickness values are chosen similarly compared to previous blackout reports. BC1 refers to the base case 1 while BC2 to base case 2.

Location	Deposit thickness [mm]	
	BC1	BC2
Front and rear walls below liquor gun level	60	30
Front and rear walls above liquor gun level	10	10
Side walls below liquor gun level	20	30
Side walls above liquor gun level	10	10
Extended side walls	10	10
Ash hopper wall	10	10
Boiler bank	20	20
Rear wall screen	10	10
Vertical screen	20	20
Horizontal screen	1	1

The thermodynamic properties are set constant and are presented in table 8.

Table 8. Thermal properties of deposit.

Property	Value
Specific heat capacity [kJ kg^{-1} K^{-1}]	1,4
Thermal conductivity [W K^{-1}]	0,8
Density [kg m^{-3}]	2000

As a boundary condition, the deposit temperature is limited to its radical deformation temperature of 850°C. Since the modelled cross-section area of the wall deposit is noticeably

larger than in reality, the steady-state temperature of modelled deposits rise much higher than 850°C. This problem is solved by reducing the deposit thickness of each module so that 850°C is not exceeded. After the combustion has ended, the deposit thickness is returned to previously determined values as shown in table 7.

5.1.5 Blackout simulation

During blackout the boiler stops operating and the combustion process stops. It is approximated, that by keeping the operating-steady state conditions for two minutes before removing combustion heat will suffice to simulate the residual furnace combustion. After this, water circulation is only receiving heat from the deposits. The temperature profiles for the deposits are shown in figures 43 and 44. The profiles are identical for both base cases.

The char bed cools slowly and releases heat directly to the floor tubing of the boiler. Heat flux from the char bed to these tubes is kept at the steady-state value during the blackout simulation. A conservative heat flux value is chosen to represent heat transfer through the floor tubes. A guess has to be made, since the CFD data doesn't provide us with a value. Using conservative value of 900 Wm^{-2} for the heat flux in the Apros model and 9h of simulation time the total heat through the floor tubes can be calculated. When compared to the total energy of furnace wall deposits in BC2, the energy trough the floor tubes is only 3,5% of the total energy stored in the furnace walls. Therefore, there is a marginal error of guessing the floor tube heat flux.

The simulation is divided into three parts. The first two minutes of the simulation the boiler is operating at the design point in steady-state (first part). Second part starts with the blow out and feed water valves closed. The valve is automated with a PID-controller to keep pressure in the steam drum at the nominal value. After two minutes the second part is done. For the third part the total heat flux to the boiler is reduced to only floor tubes. The third part is run for nine hours of simulation time.

5.2 Sensitivity study

Sensitivity analysis is a common tool used to see how a chosen parameter affects the end result of a test. Furnace wall deposits are varied evenly to see how the change of the deposit

mass on the furnace walls affects the water level and tube temperatures during the test. Steam drum pressure variation is also studied with similar intentions.

5.2.1 Deposit thickness

A sensitivity analysis is conducted to study how the deposit thickness and the horizontal distribution of deposit on furnace walls affect the water circulation system. BC2 is used as reference for the analysis. Table 9 presents deposit thickness variation used in the analysis.

Table 9. Cases A-D are analyzed for the sensitivity analysis. Only furnace wall component deposits were varied.

Location	**Deposit thickness [mm]**				
	Reference	**A (+20%)**	**B (+40%)**	**C (-20%)**	**D (-40%)**
Front and rear walls below liquor gun level	30	36	42	24	18
Front and rear walls above liquor gun level	10	12	14	8	6
Side walls below liquor gun level	30	36	42	24	18
Side walls above liquor gun level	10	12	14	8	6
Extended side walls	10	12	14	8	6
Ash hopper wall	10	10	10	10	10
Boiler bank	20	20	20	20	20
Rear wall screen	10	10	10	10	10
Vertical screen	20	20	20	20	20
Horizontal screen	1	1	1	1	1

An arbitrary value of 20% was chosen as a step value to modify the furnace wall deposit thickness. Lastly, a comparison of total deposit mass in the boiler is shown in figure 42.

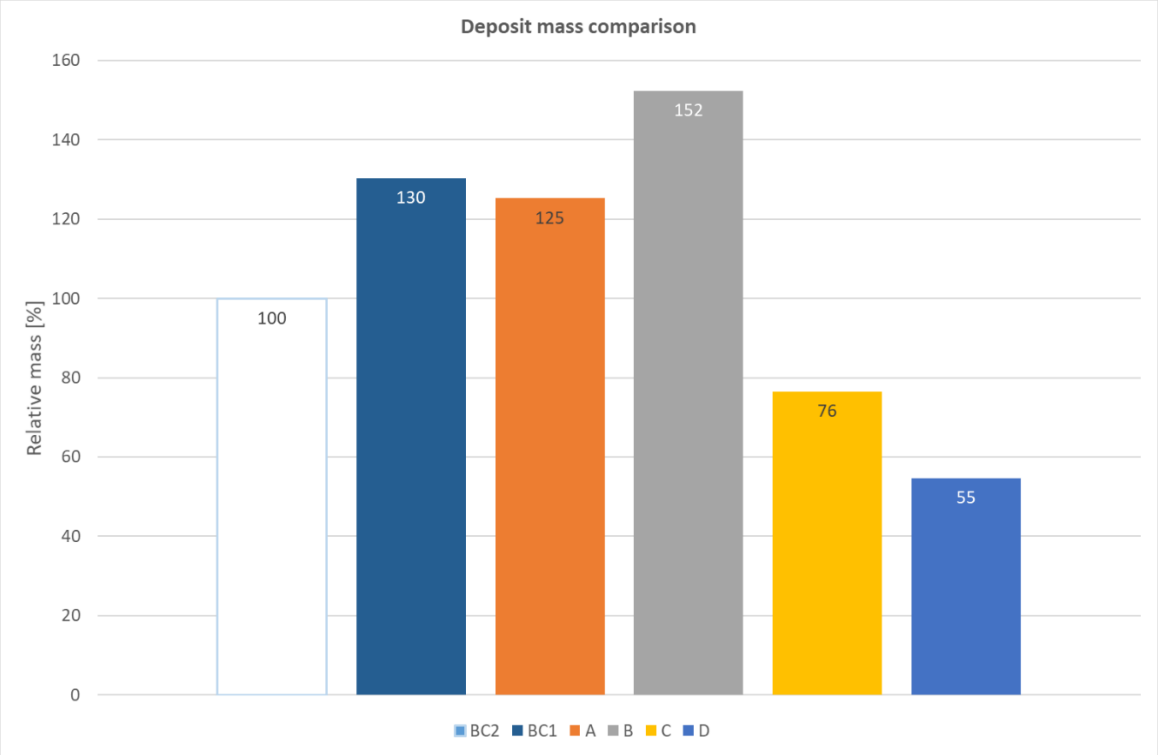

Figure 42. Deposit mass comparison between base cases and cases A-D. BC2 is set as the reference.

5.2.2 Steam drum pressure

Two cases are simulated and compared to the reference case BC2. Both cases have lower boiler pressure than the nominal in BC2.

Table 10. Sensitivity study parameters

Parameter	Reference [%]	SD1 [%]	SD2 [%]
Steam drum pressure	100	91	79

6 RESULTS

The amount of data collected from the simulations is approximately 8 million data points per simulation. The simulation time-step used was 5 seconds to allow reasonable size data files as well as enough resolution for accurate analysis of the results. The observation points were also limited to reduce the data file size. The chosen observation locations and the amount of points for temperature are shown in table 11.

Table 11. Observation point count and location during simulations. Location describes horizontal positioning of the observation points. The observation points are divided equally in the vertical direction in each module.

Component name	**Location**	**# of observation points for temperature [pcs]**	**# of observation points for water level [pcs]**
Downcomers	Center	-	42
Front wall	Center	40	111
	Left corner	40	111
Rear wall	Center	6	-
	Right corner	6	-
Left side wall	Center	34	81
	Extended side wall center	26	-
Right side wall	Center	7	-
	Front-right corner	7	-
	Extended side wall center	7	-
Horizontal screen	Center platen	5	13
Vertical screen	Center platen	10	25
Boiling bank platens	Center platen	14	32
Boiling bank rear wall	Center	14	-
Rear wall screen	Center modules (3pcs)	3	-
Ash hopper	Center	12	22

Water level in evaporative components is plotted for both base cases to elaborate the evaporation rate of water in the boiler. These plots are also informal when examining dryout in tube temperature graphs further on. Deposit temperature on different elevations as a function of time is also presented to describe how heat is dissipated to the water circulation and vertically to adjacent deposits. The initial temperature profiles on the evaporative components are presented in figures 43 and 44.

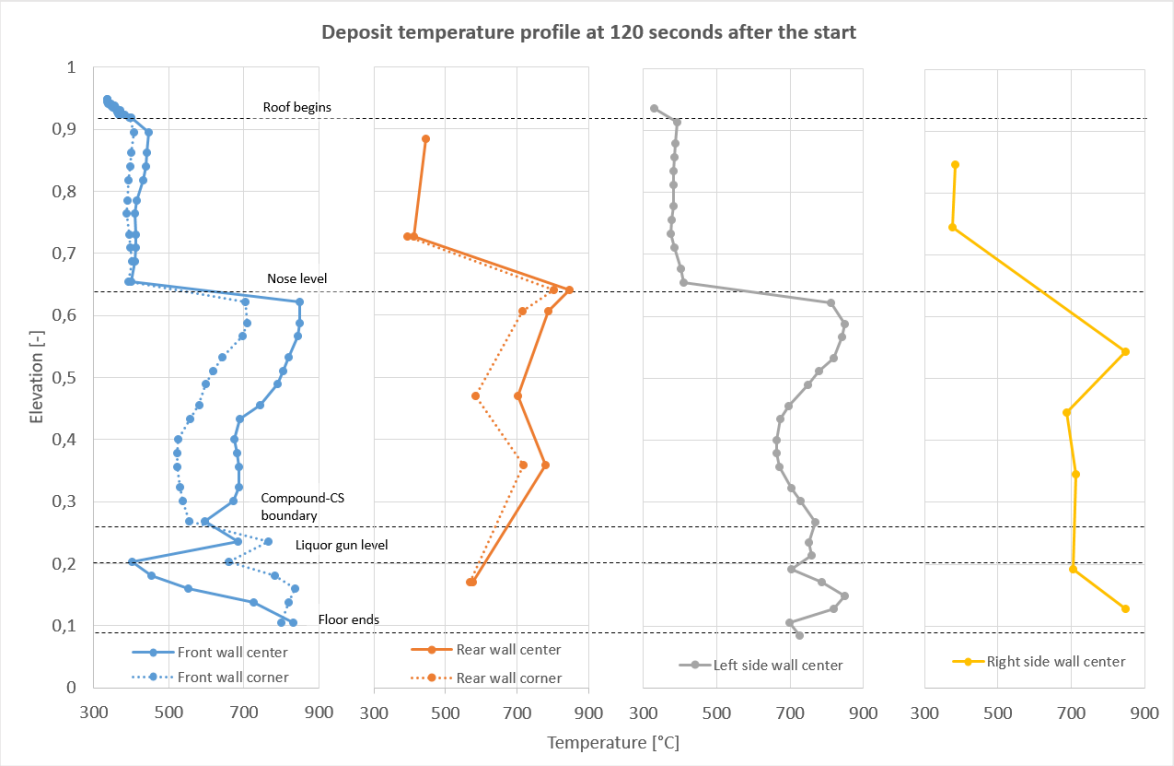

Figure 43. The steady-state temperature profile of furnace side deposits.

We observe the highest temperatures between the compound-carbon steel interface and the nose level. After the nose, the temperature drops because the furnace screen absorbs a lot of heat coming from the lower furnace. The CFD data used contains an area of low heat intensity on the lower front wall, which causes lower temperatures compared to the corner. Generally, corner areas receive lower heat flux, which leads to lower initial temperature of the deposit.

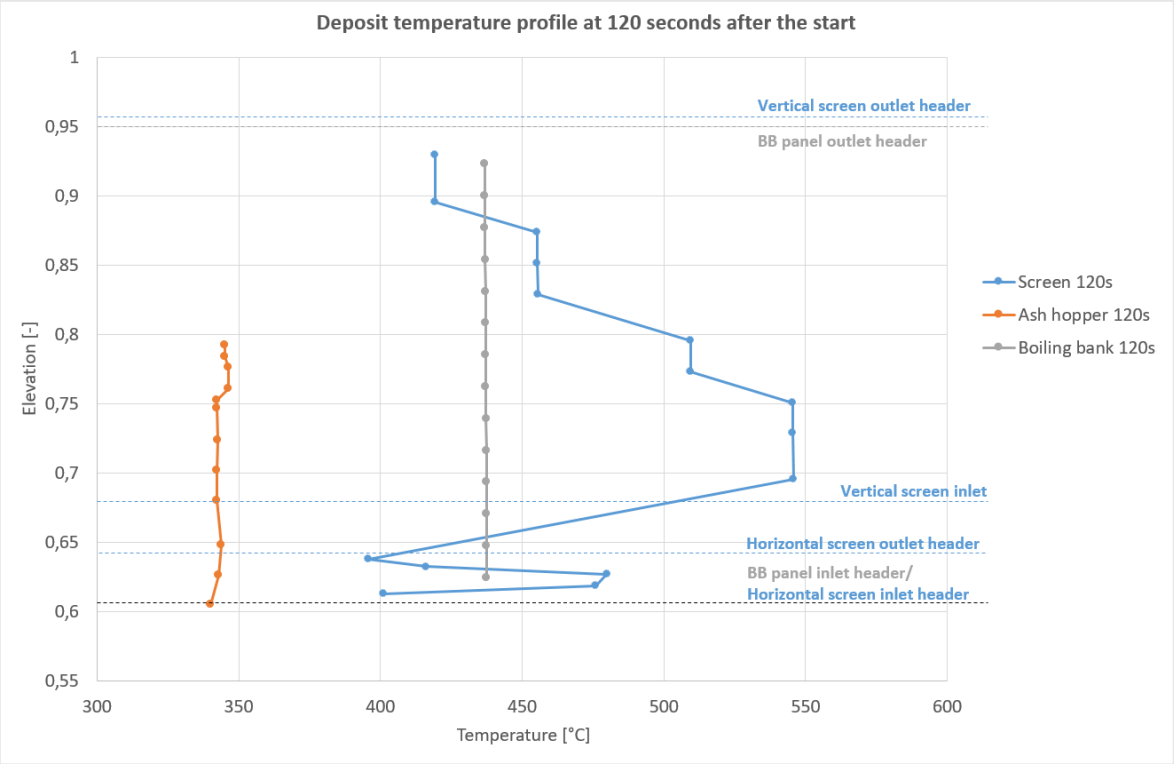

Figure 44. The steady-state temperature profile of deposits in the boiler bank volume and on the horizontal screen.

The initial temperature profiles are identical for both base cases. Different profiles should exist where the deposit thickness is different between cases. The profiles are unique because of the boundary condition of T_{70}. The boundary condition forces us to reduce the module temperatures under 850°C. When this processing is done for both cases, the temperature profiles depend on the CFD sample data, which is same for both cases. All profiles remain unchanged after the feed water valve is closed and the 2 minutes of combustion heat is applied.

6.1 BC1

The simulation starts with two minutes of steady-state operation. At 0:02 the feed water and blowout valves are closed, and the steam valve is operated to keep the nominal steam drum pressure, as is shown in figure 45.

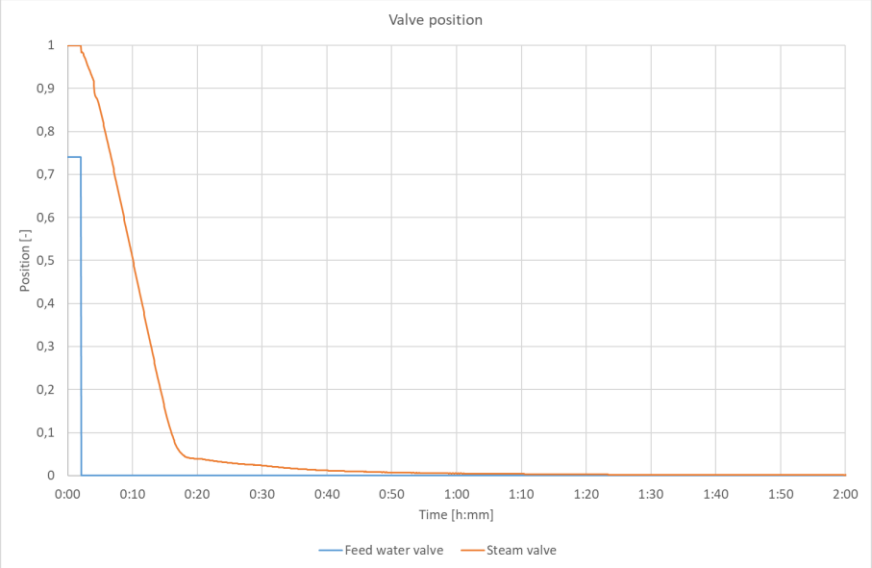

Figure 45. Position of the feed water and steam valve as a function of time. 0 equals to a fully closed valve, while 1 equals to a fully open valve.

The effect of the valve operations is shown in figure 46.

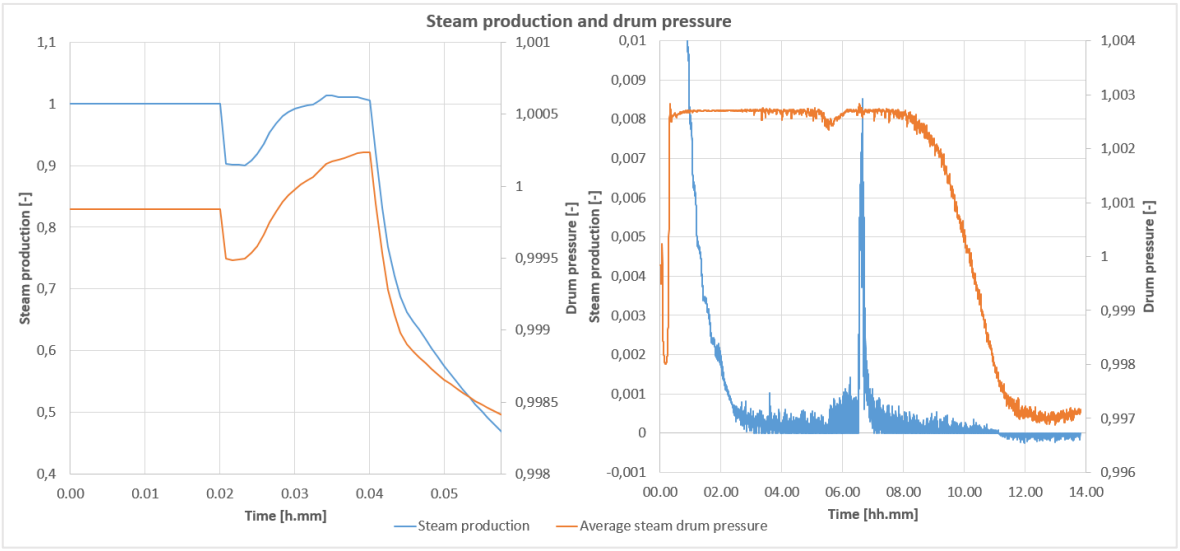

Figure 46. Steam production and drum pressure presented as a function of time. The left figure presents the first five minutes of the simulation, while the right figure includes the rest. Both series have been scaled between 0 and 1, 1 being the nominal steady-state value. Notice that both figures have a secondary axis for the drum pressure.

Steam production reduces right after the feed water valve is closed. Drum pressure and steam production start to decrease as soon as the constant heat flux from combustion is set to 0 at 00:04. Steam production decreases for three hours until 03:00. A peak of almost 1% of nominal steam production is observed at around 06:30. This is caused by the steam valve

controller reacting to a slight pressure rise in the boiler. Water is evaporated at an increasing rate for a short time right after 06:30, which is shown in figure 47.

6.1.1 Water level

Water level in the boiler starts to decrease as soon as the feed water valve is closed. This is observed in each evaporative component. Figure 47 shows the development in the furnace tubing.

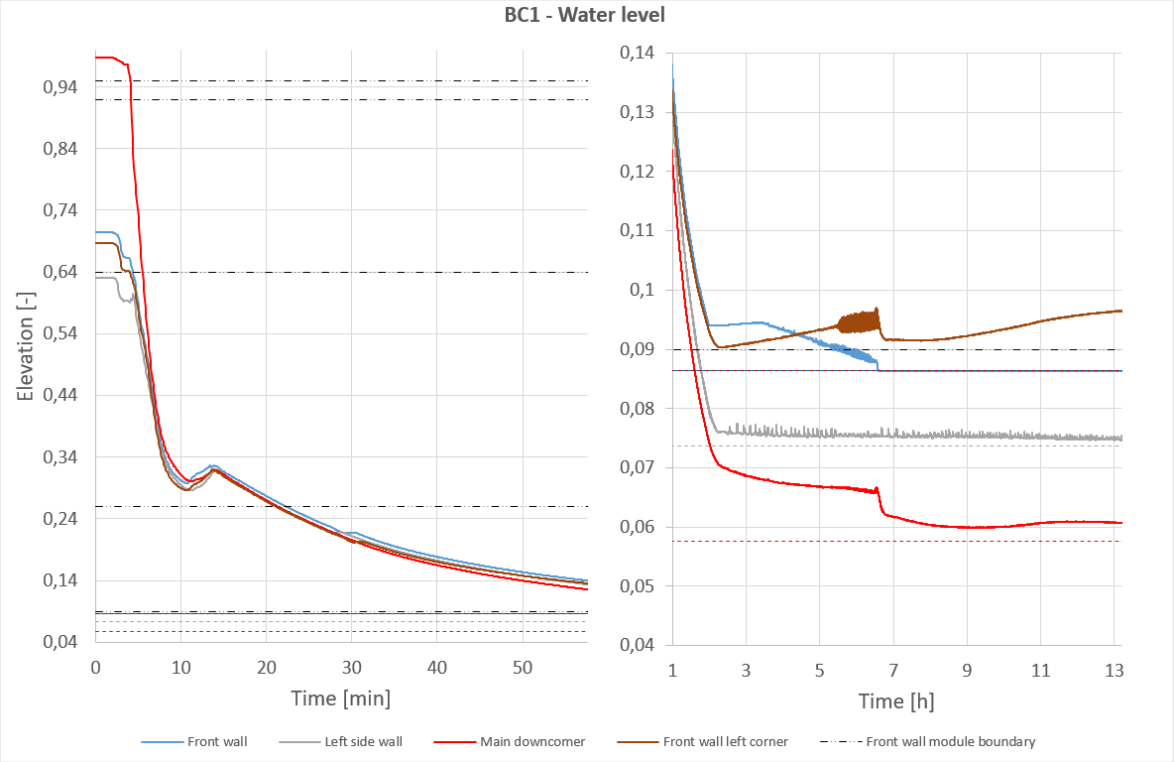

Figure 47. Water level change in the furnace tubes during the simulation. The dashed lines represent local lowest points for each component. Front wall module boundaries are marked with black dot-dot-dash-line. Front wall and front wall left corner share the same lowest point.

The water level in the boiler stays relatively stable during the first 2-4 minutes of the simulation. Between 00:10 and 00:14 water flows from the ash hopper, through the rear wall to fill the furnace walls. Boiler bank and ash hopper are connected by the main inlet of the boiler bank, which means that boiler bank also contributes to the flow. The flow ends at approximately 00:14 when the water level drops below the highest point in the ash hopper (0,8). After two hours from the start, descent of the water level slows down noticeably. Consequently, the evaporation rate slows down. This is caused by the reducing interface area of water and hot tube surfaces. Instead of evaporating water, the deposits heat up steam. The

center module on the front wall dries completely at 06:38, and stays dry for the rest of the simulation. After that, the main downcomer and corner water levels also drop simultaneously.

Towards the end of the simulation, the water level keeps rising in the main downcomer and in the front wall corner. The lowest nodes in the corner are close to saturation temperature and start to cool down after 06:38, which means that steam is starting to condensate, which explains the water level rise. Oscillation of the water level is observed in the front wall corner, center and main downcomer water levels before the peak. In the corner, the oscillation frequency is under 5 seconds while on the front wall the oscillation frequency is approximately 50 seconds. In the center of the left side wall oscillation is observed also after the peak. The water levels in boiler bank, ash hopper and screen stabilize after 1 hour of simulation. The data is presented in figure 48.

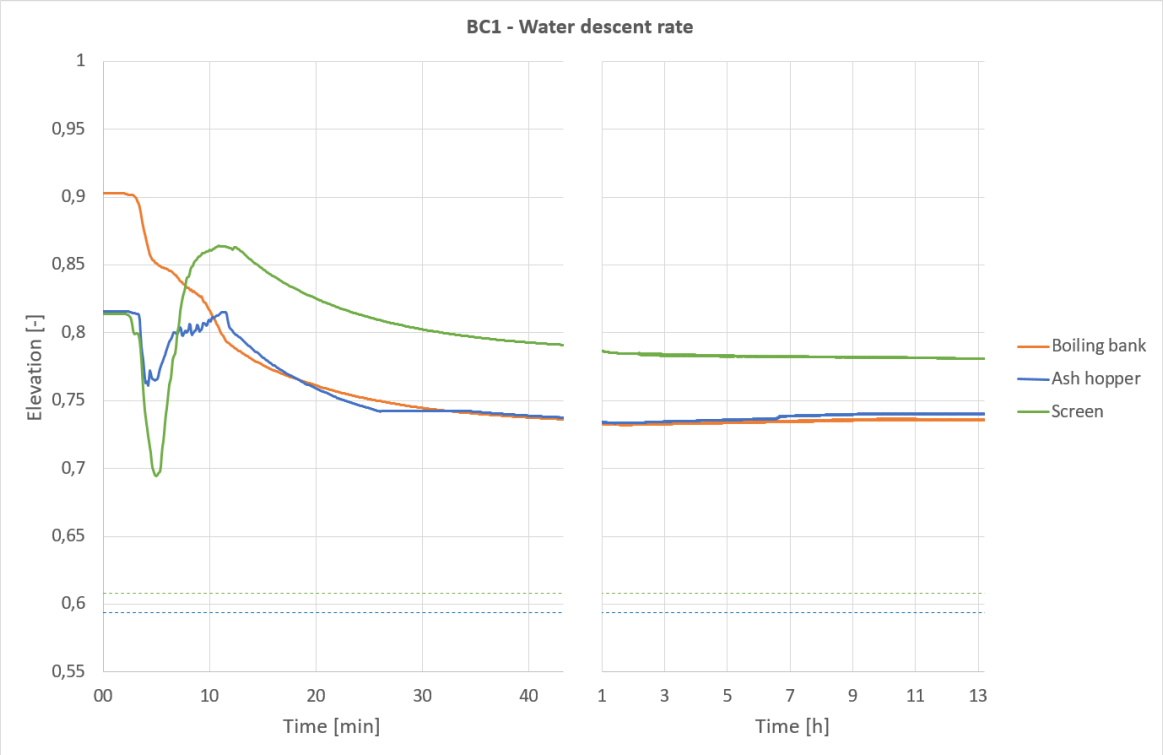

Figure 48. Boiler bank area and screen water levels of the first hour of simulation. The dashed lines represent local lowest points. Boiler bank and ash hopper share the same lowest point. Notice that the time scale is different between the two graphs.

Water level rises slightly in ash hopper and screen components at the start. At 15 minute mark, the levels start to decrease consistently, until at around 1 hour mark the descent ceases.

6.1.2 Tube temperature

High temperatures of over 400°C were found only on the rear and front walls. The findings are presented in figures 49 and 50, where yellow, orange and red represent values above 400°C.

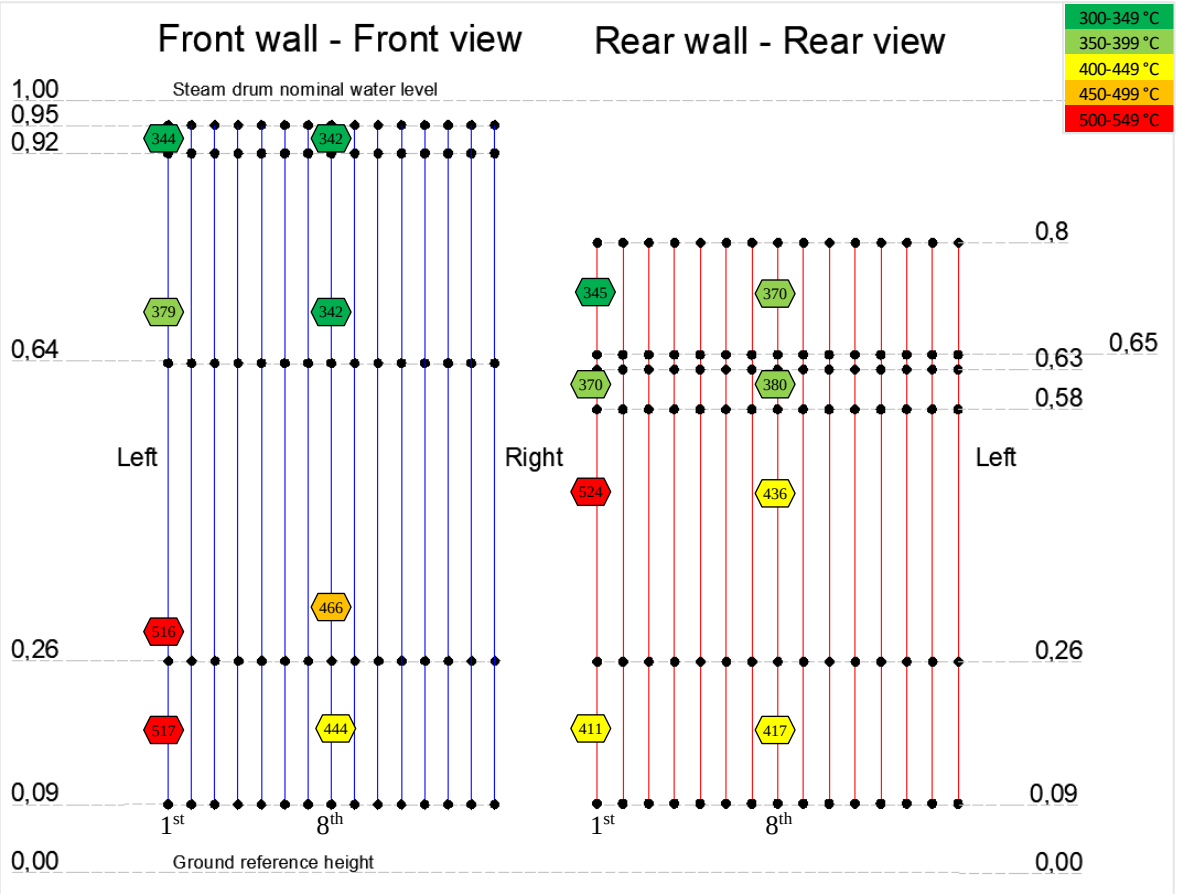

Figure 49. Highest node temperatures of each measured module on the front and rear walls.

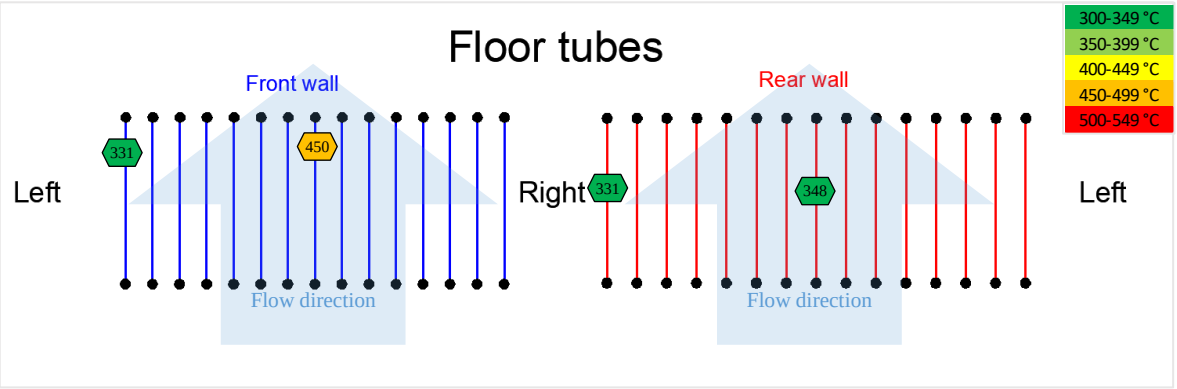

Figure 50. Highest node temperatures of each measured module on the floor tubing.

We see that the most critical temperatures appear between elevations 0,09 – 0,64. Also the temperature of the floor tube module on the front wall center rises quite high. Based on this analysis the critical locations are examined further. Highest values measured from other components are presented in table 12.

Table 12. Highest temperatures below 400°C. The horizontal positioning of the observation point is noted with the component name.

Location	Maximum temperature [°C]
Boiler bank platen, center	361
Boiler bank rear wall, center	343
Vertical screen, center	346
Horizontal screen, center	332
Ash hopper, center	338
Left side wall, center	349
Left side wall, below extended sidewall	374
Right side wall, center	344
Right side wall, below extended sidewall	348

To further explain the high temperatures on the front and rear walls, the node temperatures are presented as a function of time in figures 51 and 52.

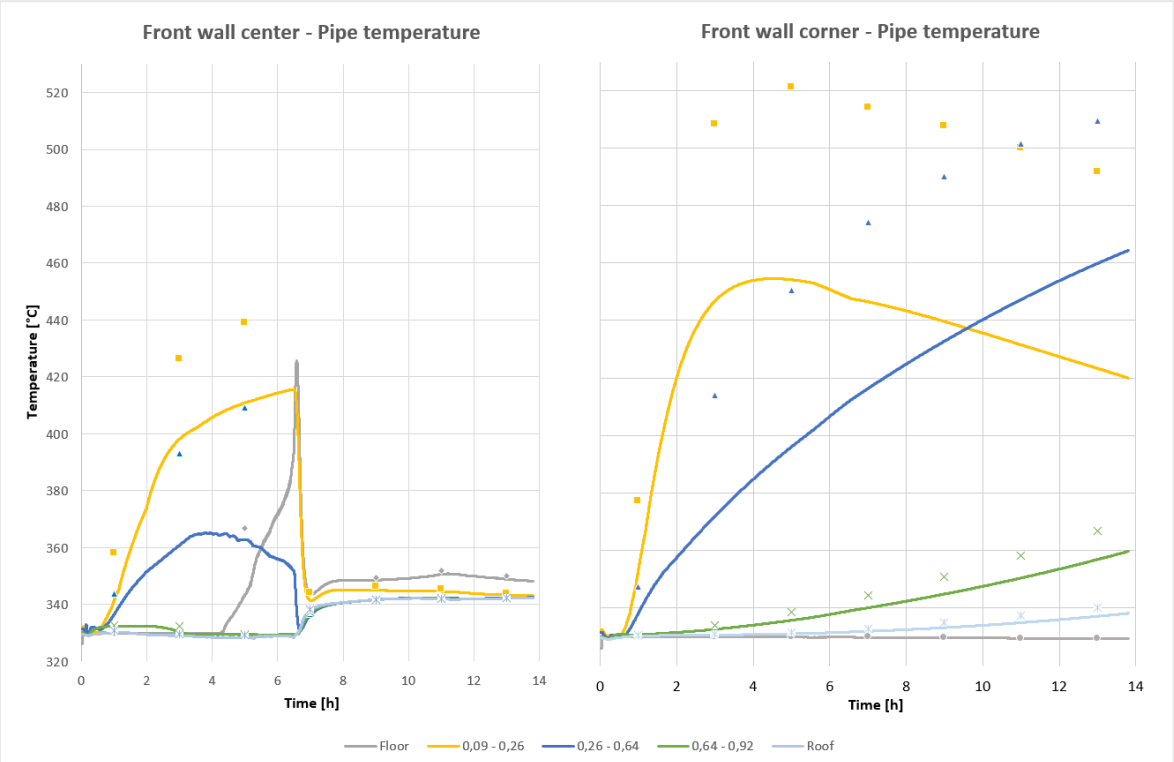

Figure 51. The figure presents average temperatures of modules as a function of time. Temperatures are measured from inner tube walls at the center and at the corner of the front wall. The dots mark standard deviation in the positive direction from the average value to emphasize variance of the sample.

Highest temperatures are observed at the center at around 06:30 hour mark, just before the drop in temperatures. This kind of drop is caused by a steam flow through the front and rear walls, which is initiated when the floor modules of front and rear wall dry completely. The steam flow re–distributes heat around the boiler, essentially cooling the hottest parts. The temperature drop is not observed in the corner, since the floor module contains water and doesn't dry all the way at any point, preventing steam circulation. The highest tube temperature in the corner is located at the lower furnace (0,09 – 0,26) around 04:00–05:00 hour mark reaching the temperature of the deposit. Since the lower module (0,09 – 0,26) contains thick deposits, it eventually conducts heat vertically to the module above (0,26 – 64), while cooling from the lowest point. The module above (0,26 – 0,64) seems to not have achieved its peak during the simulation. Temperatures of the rear wall are shown in figure 52.

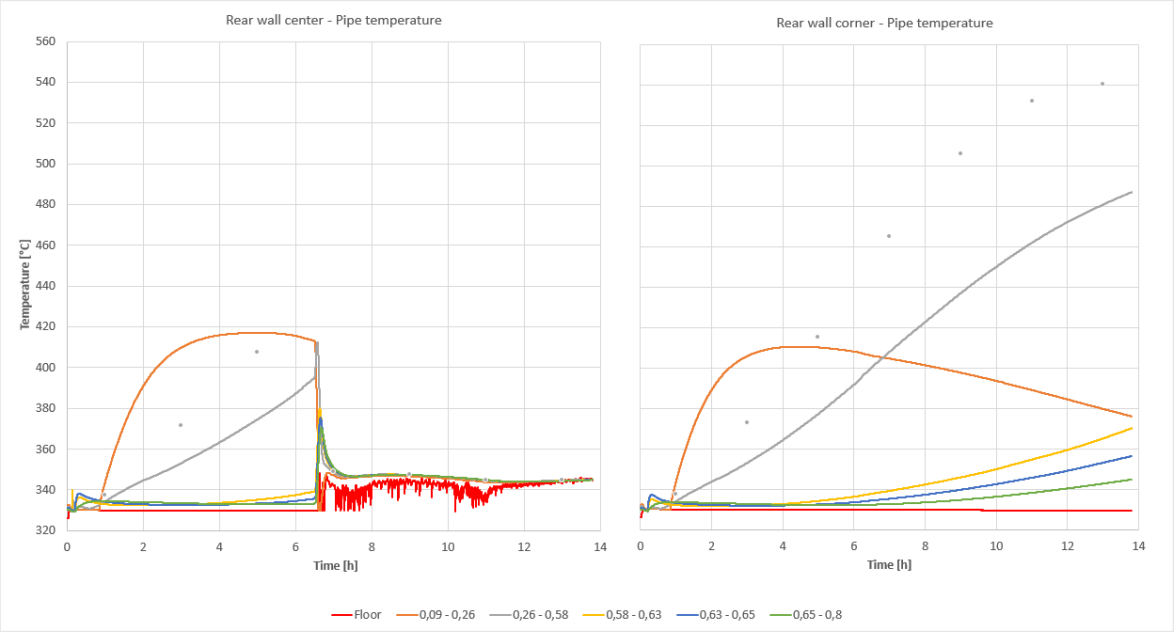

Figure 52. Temperature of modules as a function of time. Temperatures are measured from inner tube walls at the center and at the corner of the front wall. Only one series is calculated from multiple nodes, which is why it has standard deviation in the positive direction plotted in the graph.

The rear wall center and corner exhibit similar behavior compared to front wall center and corner. Some thermal oscillation is observed at the rear wall floor tubing. Third module counting from the bottom (0,26 – 0,58) seems to not have achieved its peak during the

simulation. Temperature changes are examined also on the node level to see the effect of dryout. Lower part of the furnace front wall (0,09 – 0,64) is discretized vertically into 20 calculation nodes. The temperature graphs of the lower front wall center are presented in figure 53.

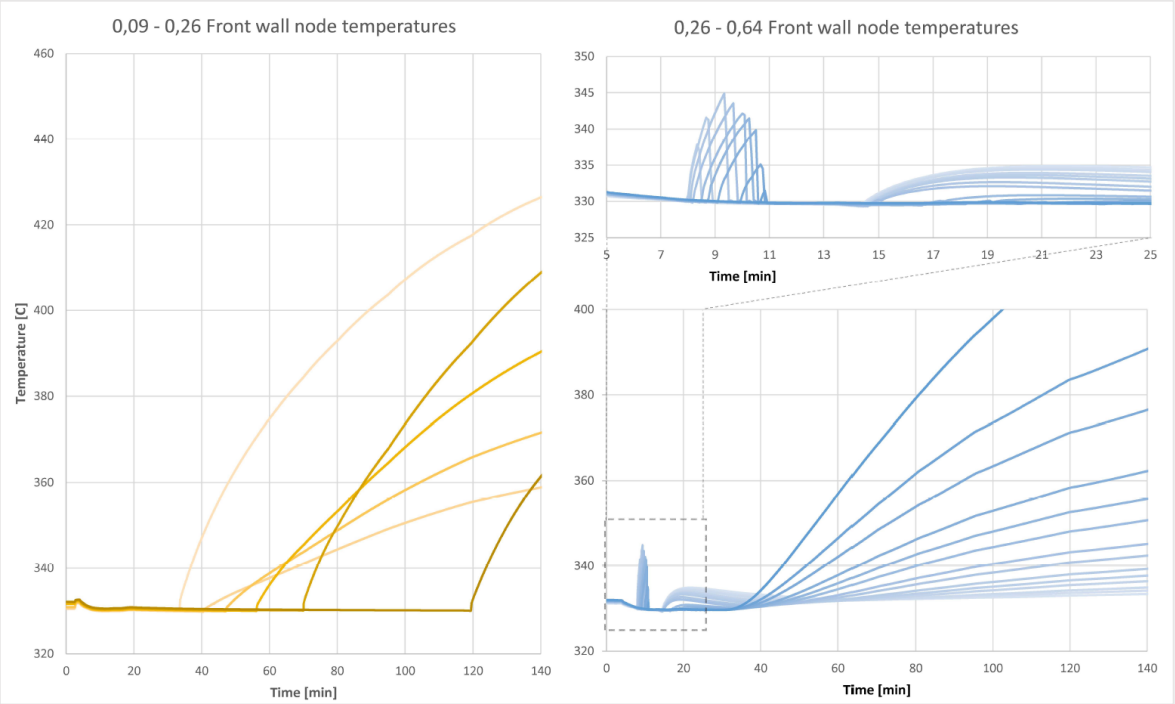

Figure 53. Tube temperatures along two vertically adjacent heat tube modules on the front wall center line. Yellow lines represent temperatures of the lower module (0,09 – 0,26) while blue lines represent temperatures of the higher module (0,26 – 0,64). Lighter colors represent higher elevation of calculation node. The nodes are located evenly in the vertical direction.

Dryout appears in the correct order in both location; starting from the highest node, which is exposed to the dryout first. Node temperatures rise at different rates on the lower module (0,09 – 0,26), because of large initial temperature differences in the nodes (see figure 43). On the higher module (0,26 – 0,64) after dryout the lowest modules start to heat up quickly. This happens because of heat conduction from the lower module. Dryout behavior can be observed on the boiling bank platens as well as on the screen. Node temperatures in the boiler bank platen tubes are shown in figure 54.

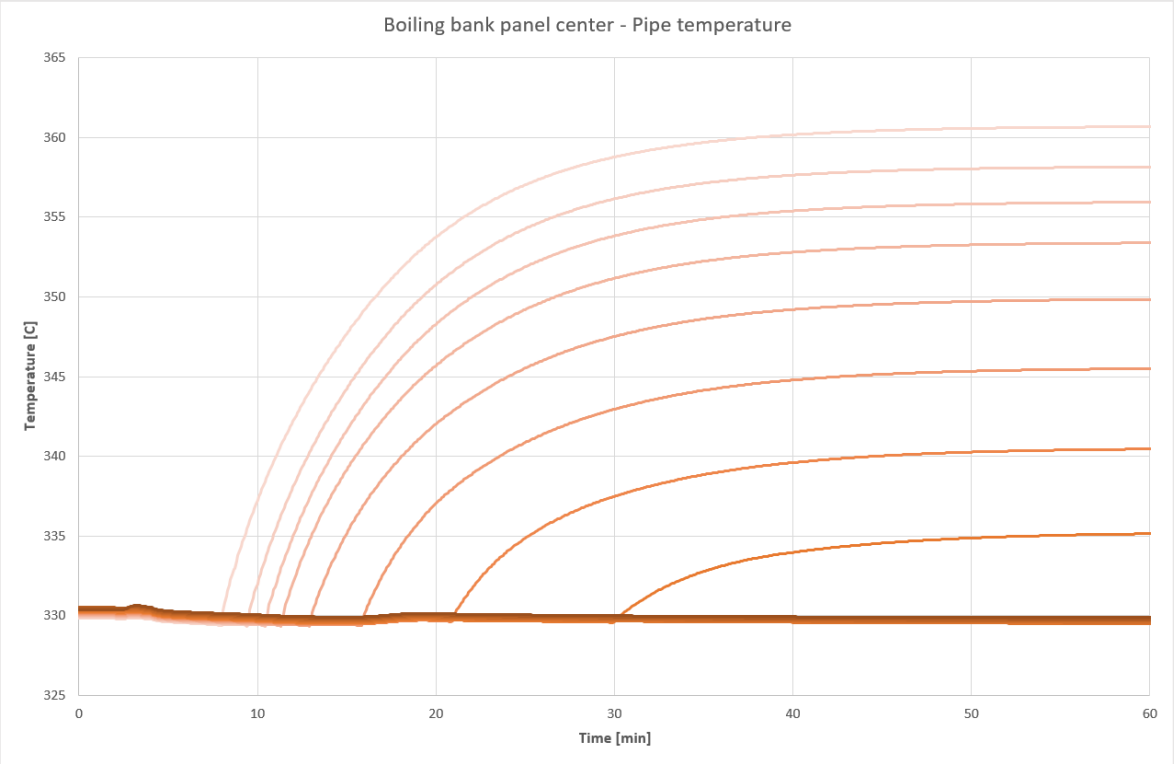

Figure 54. Boiler bank tube temperatures measured from the center platen. Lighter lines represent higher elevation of the calculation node. The nodes are located evenly in the vertical direction.

6.1.3 Deposit temperature

The change in the temperature of deposits indicates from where the heat is diffused to the water circulation system. Front wall deposit temperature as a function of time is shown in figure 55 while the same figures for rear wall deposits is shown in figure 56.

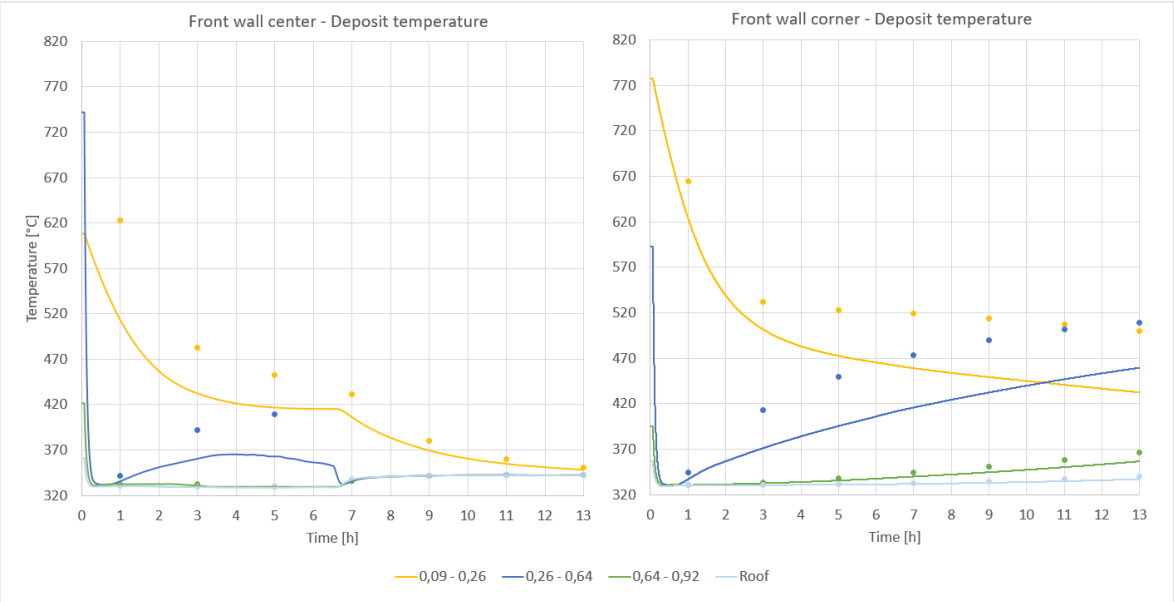

Figure 55. Average temperatures from outer deposit surface in the middle and at the corner of the front wall. The dots represent standard deviation in the positive direction .

On the front wall center the heat of the deposits seems to have dissipated when 13 hours of simulation is reached. The lowest module (0,09 – 0,26) has the thickest deposits, and therefore dissipates heat the slowest. In the corner on the other hand, deposit temperatures remain high between (0,09 – 0,64). Corner deposit temperatures reflect the results of tube temperature observations. Heat is being conducted from the lower module (0,09 – 0,26) to the higher module (0,26 – 0,64).

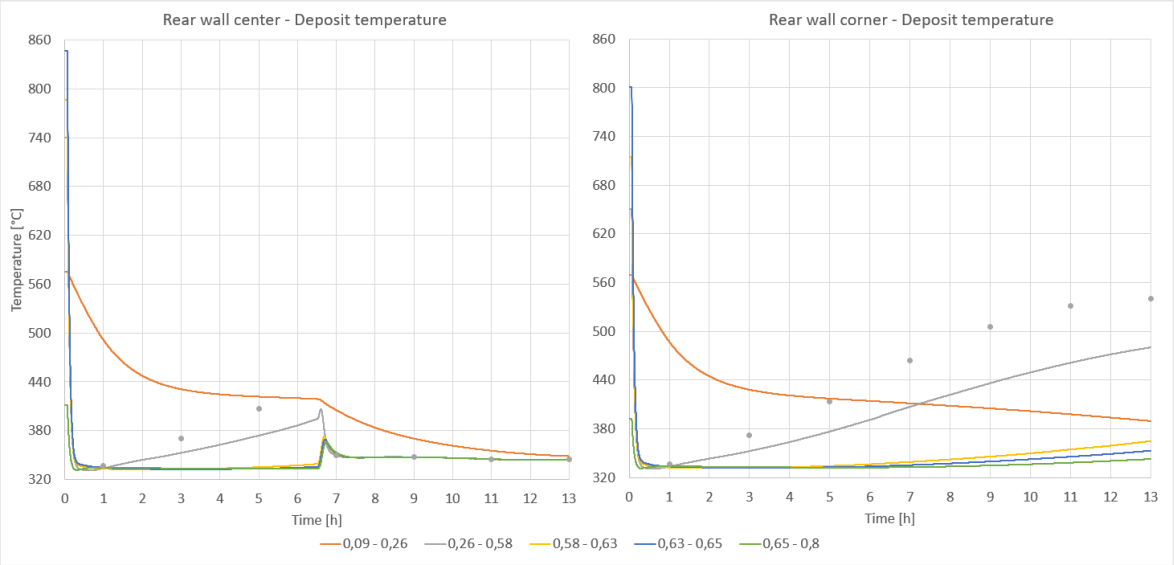

Figure 56. Average temperatures from outer deposit surface in the middle and at the corner of the rear wall. The dots represent standard deviation in the positive direction .

Similar behavior is seen on the rear wall, compared to front wall deposits.

6.1.4 Oscillation

The thermal oscillation observed in the rear wall floor is not apparent in the front wall floor as is shown in figure 57.

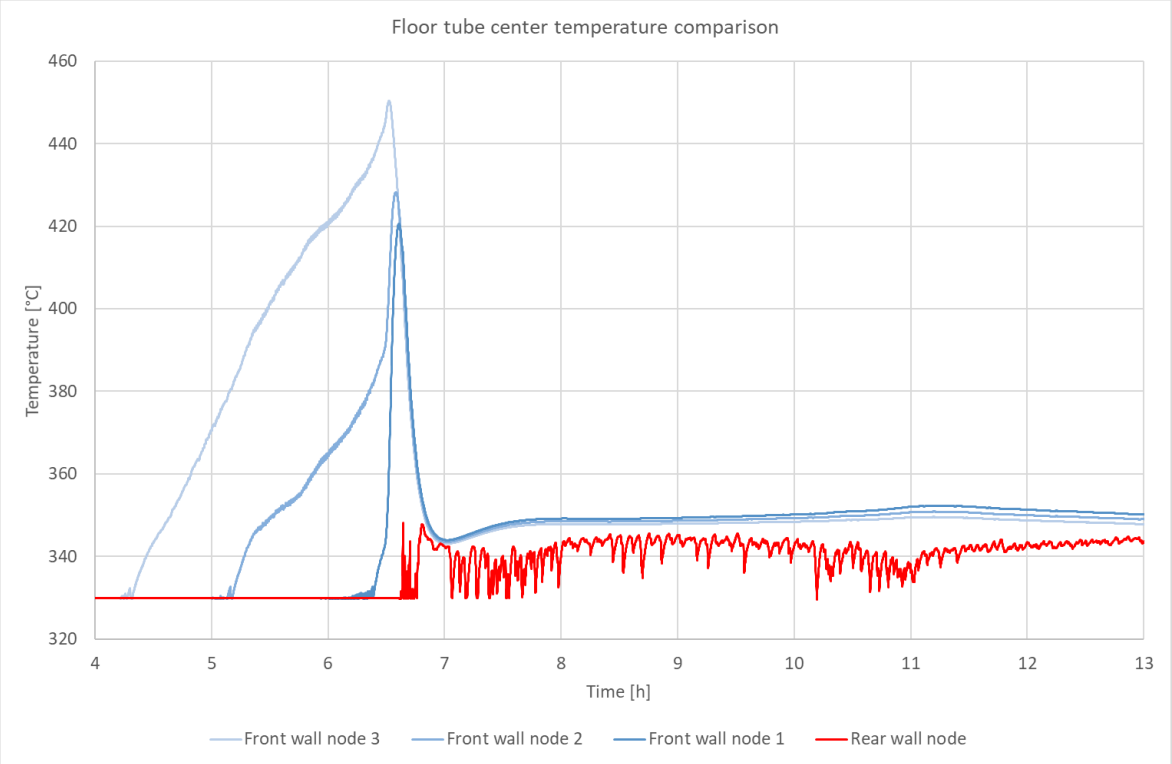

Figure 57. Node temperatures of the floor tubing in the front and rear wall center as a function of time. Lighter color represents location further in the flow direction.

ThO is observed on the center of the rear wall floor. The oscillation begins as soon as the steam circulation has begun through the front wall. Evaporating boiler water explains the temperature oscillation, since the lowest point is in level with the saturation temperature. Boiler water is therefore escaping to the module from adjacent modules. Towards the end of the simulation the oscillation settles. The average amplitude is approximately between 5-10°C.

6.2 BC2

BC2 is run with similar valve operation to BC1. Figure 58 presents the effect of the valve operations.

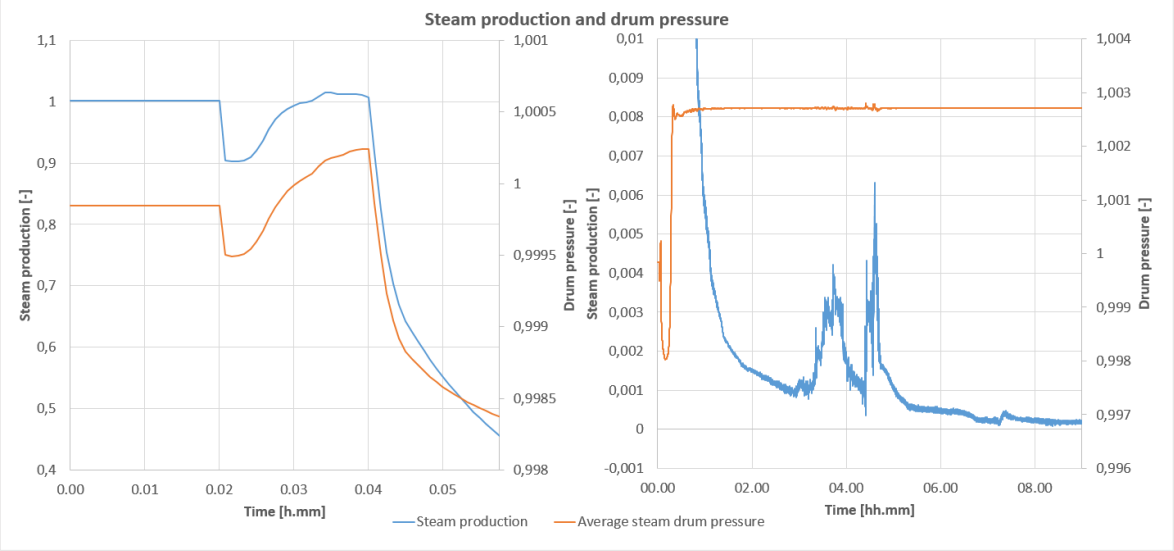

Figure 58. Steam production and drum pressure presented as a function of time. The left figure presents the first five minutes of the simulation, while the right figure includes the rest. Both series have been scaled between 0 and 1, 1 being the nominal steady-state value. Notice that both figures have a secondary axis for the drum pressure.

BC2 has larger steam production during the simulation compared to BC1. Boiler pressure stays also near the nominal value for eight hours in the simulation. Again, the controller of the steam valve reacts to pressure growth in the boiler, releasing steam a few times at approximately 03:30 and 04:30. This sudden growth in boiler pressure is linked to floor module drying.

6.2.1 Water level

Water level in the boiler starts to decrease as soon as the feed water valve is closed. This is observed in each evaporative component. Figure 59 shows the development in the furnace tubing.

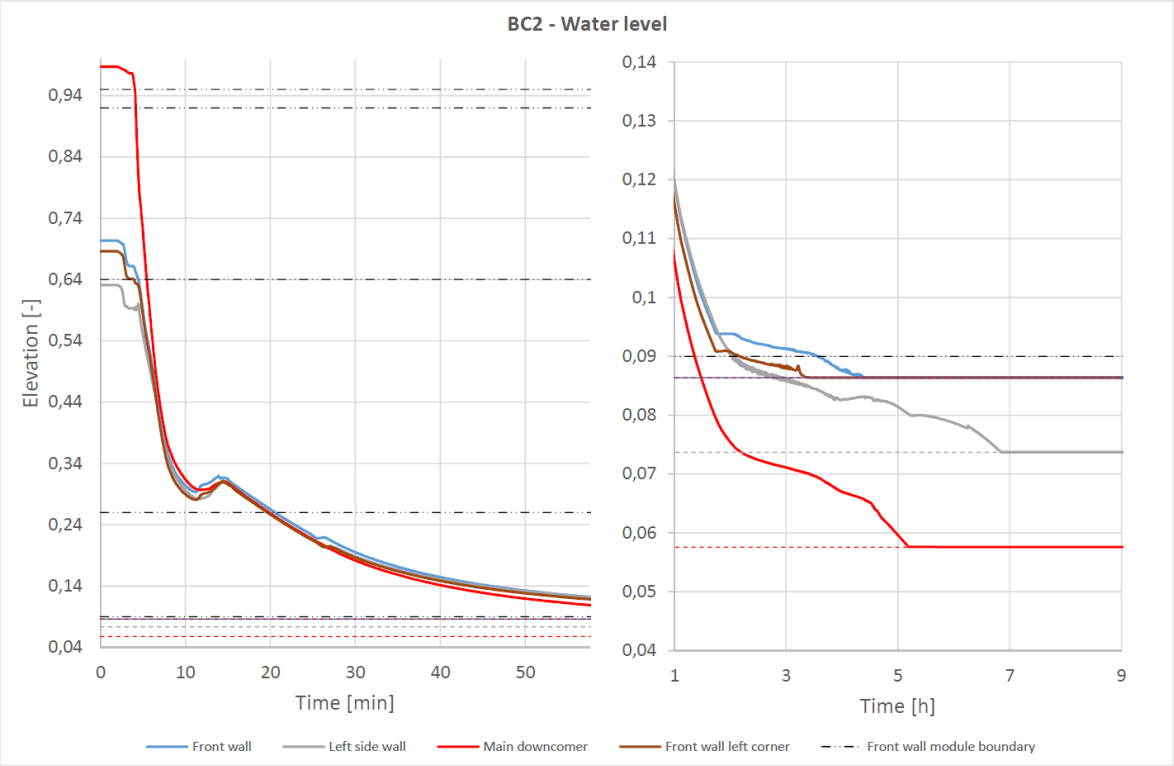

Figure 59. Water level change in the furnace tubes during the simulation. The dashed lines represent local lowest points for each component. Front wall module boundaries are marked with black dot-dot-dash-line. Front wall and front wall left corner share the same lowest point.

The first hour of the simulation is very similar to BC1. After that, the evaporative components dry swiftly one after another. Every observed component is dry just before 07:00. Figure 60 presenting boiling bank, ash hopper and screen water levels is almost identical to BC1.

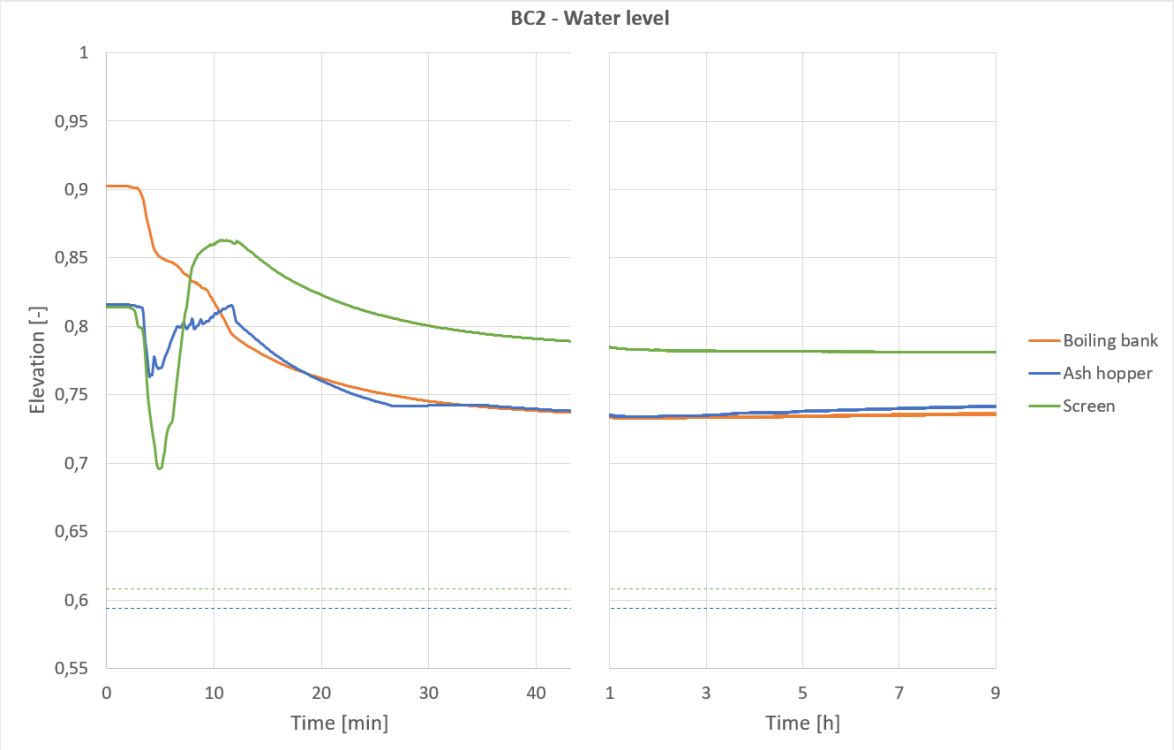

Figure 60. Boiler bank area and screen water levels of the first hour of simulation. The dashed lines represent local lowest points. Boiler bank and ash hopper share the same lowest point. Notice that the time scale is different between the two graphs.

6.2.2 Tube temperature

Highest temperatures were observed on the front and left side walls. Highest node temperatures on front and rear wall are presented in figures 61 and 62.

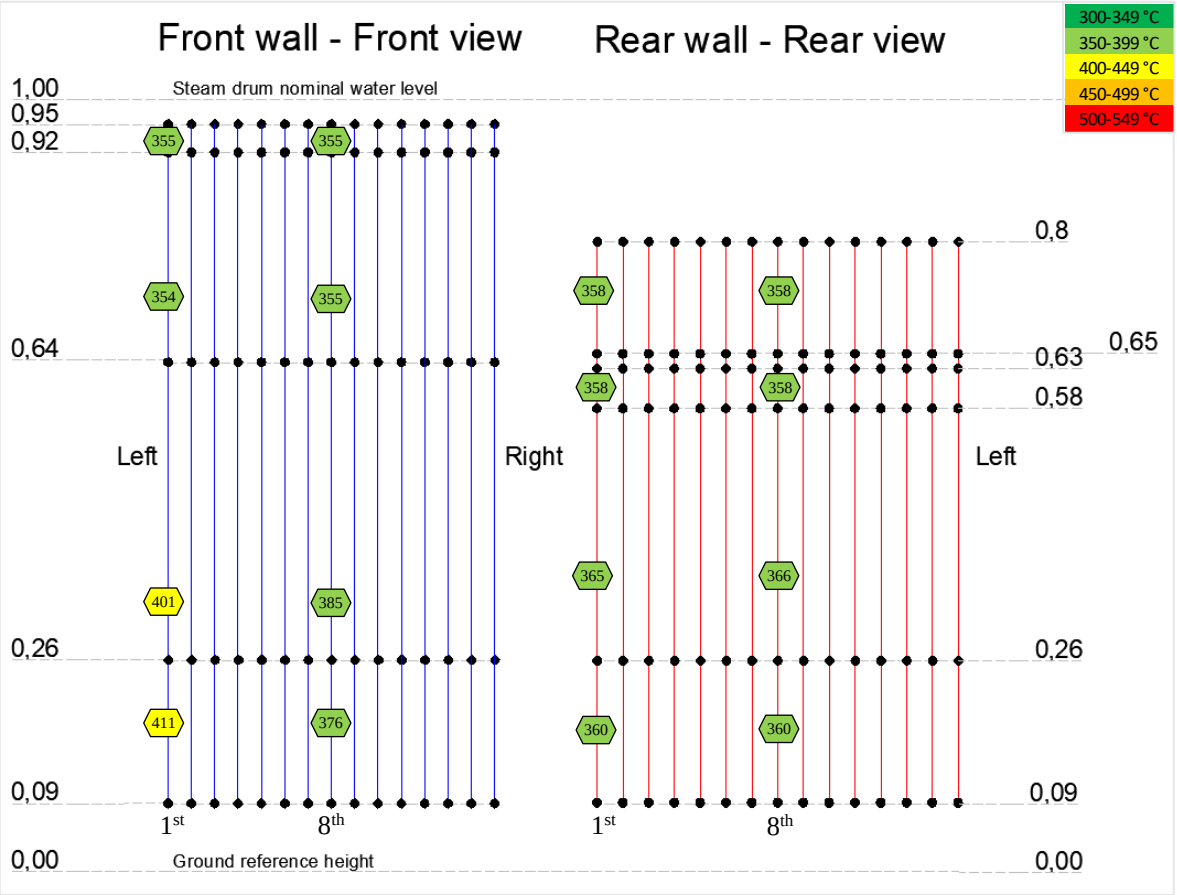

Figure 61. Highest node temperatures of each measured module on the front and rear walls.

On the front and rear wall the observed highest temperatures are much lower than in BC1. The only modules where temperatures rise above 400°C are the lowest corner tube modules.

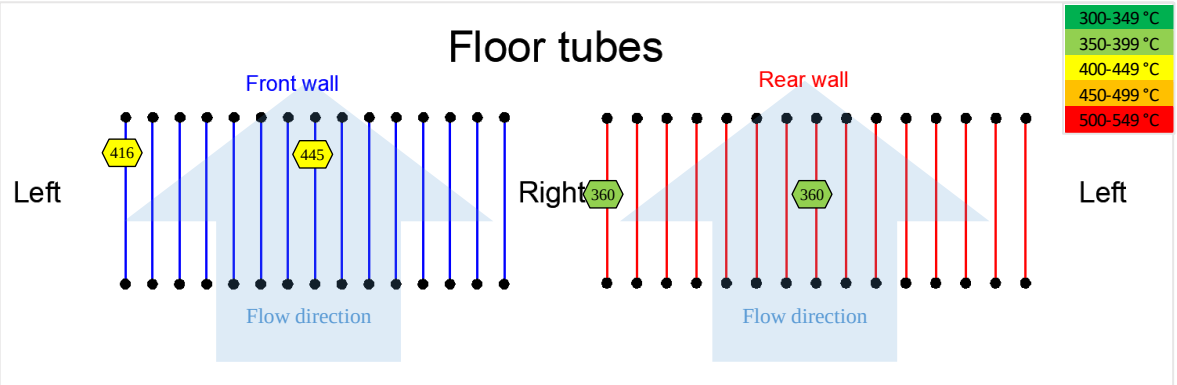

Figure 62. Highest node temperatures of each measured module on the floor tubing.

Temperatures on the front wall floor also rise above 400°C. Instead on the rear wall floor, the temperatures stay relatively low. A few of the lowest module nodes experience over 400°C temperatures as is presented in table 13.

Table 13. Highest observed temperatures in other components. The horizontal positioning of the observation point is noted with the component name.

Location	Highest observed temperature [°C]
Boiler bank platen, center	361
Boiler bank rear wall, center	342
Vertical screen, center	346
Horizontal screen, center	332
Ash hopper, center	341
Left side wall, center	408
Left side wall, below extended sidewall	422
Right side wall, center	390
Right side wall, below extended sidewall	365

Figure 63 presents temperature changes on the front wall.

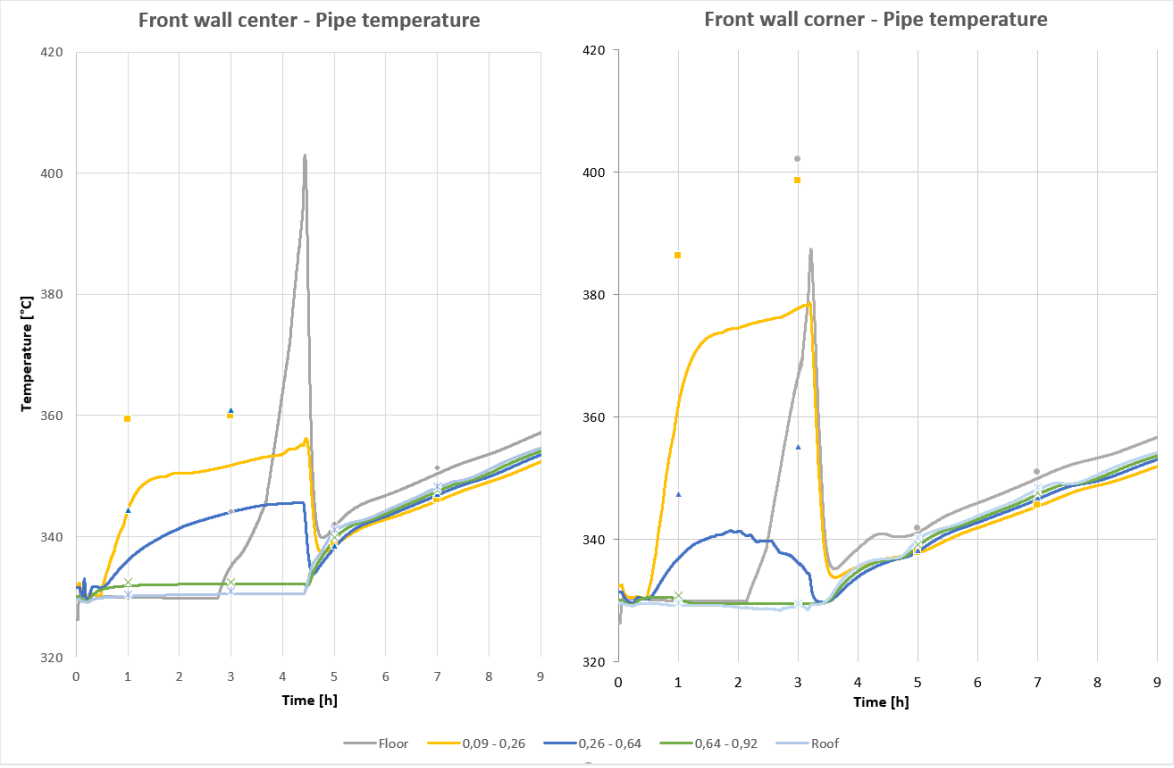

Figure 63. The figure presents average temperatures of modules as a function of time. Temperatures are measured from inner tube walls at the center and at the corner of the front wall. The dots mark standard deviation in the positive direction from the average value to emphasize variance of the sample.

The lowest modules above the floor receive again the highest temperatures. In BC2 the corner tube temperatures don't rise as high as in BC1. A constant rise in the tubes is observed after the steam circulation begins in each module. Figure 64 presents tube temperatures on the rear wall.

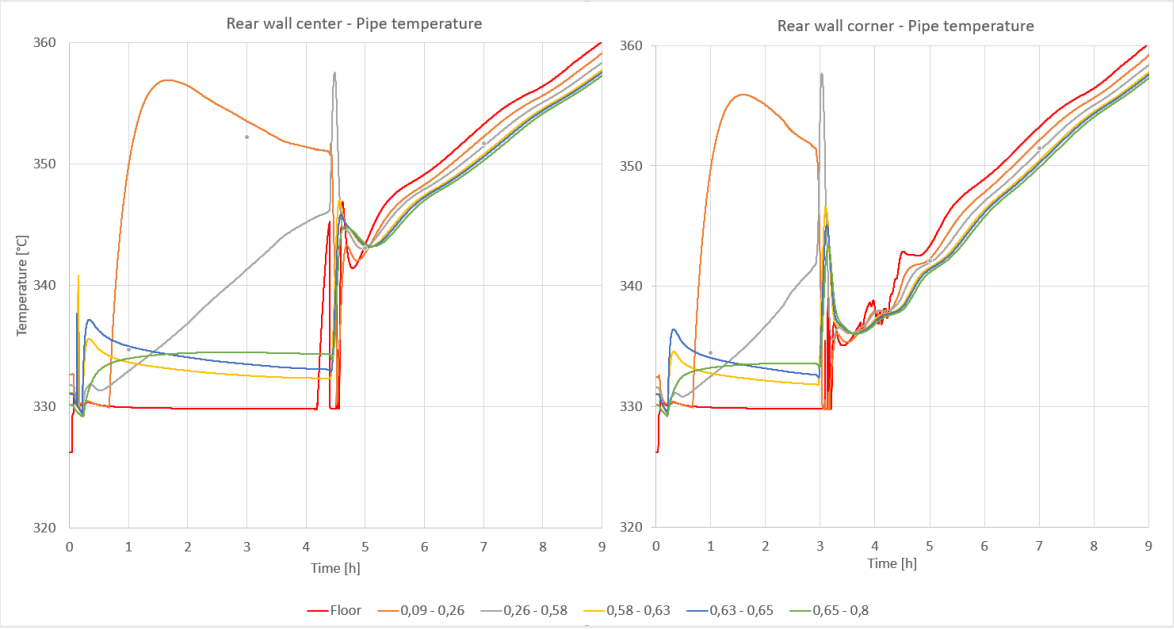

Figure 64. Temperature of modules as a function of time. Temperatures are measured from inner tube walls at the center and at the corner of the front wall. Only one series is calculated from multiple nodes, which is why it has standard deviation in the positive direction plotted in the graph.

The rear wall temperatures stay much lower compared to BC1 rear wall. Similar rise in temperatures is present compared to the front wall. The constant rise in tube temperatures, as well as in deposit temperatures, is caused by the constant heat flux through the floor. The rise in temperature is observed also in the deposit temperature.

6.2.3 Deposit temperature

Deposit temperatures on the front and rear wall are presented in figures 65 and 66.

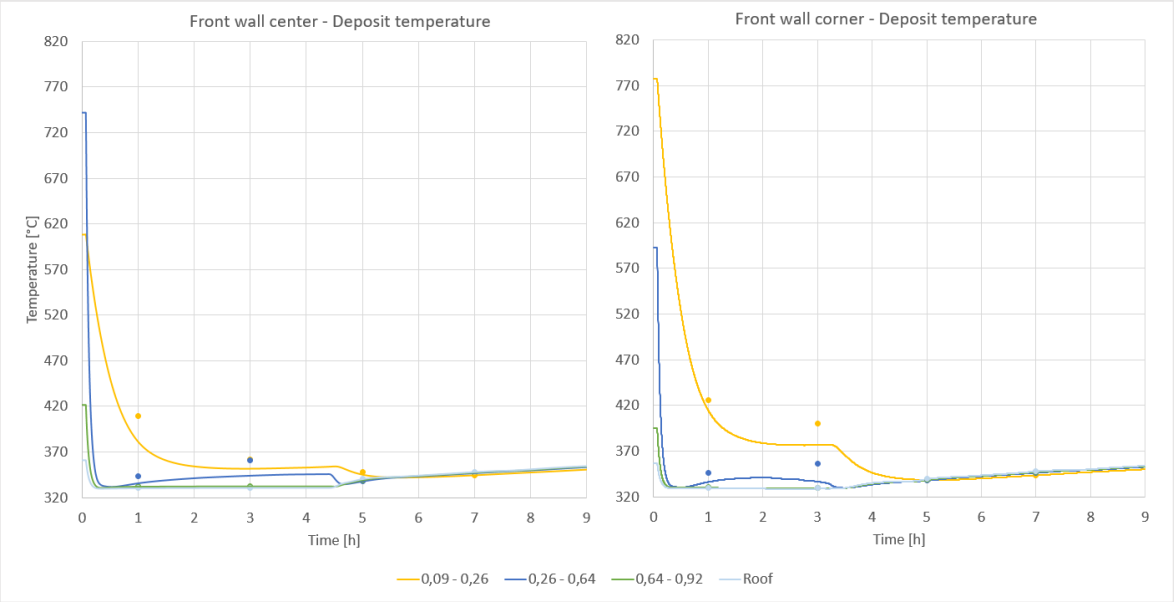

Figure 65. Average temperatures from outer deposit surface in the middle and at the corner of the front wall. The dots represent standard deviation in the positive direction .

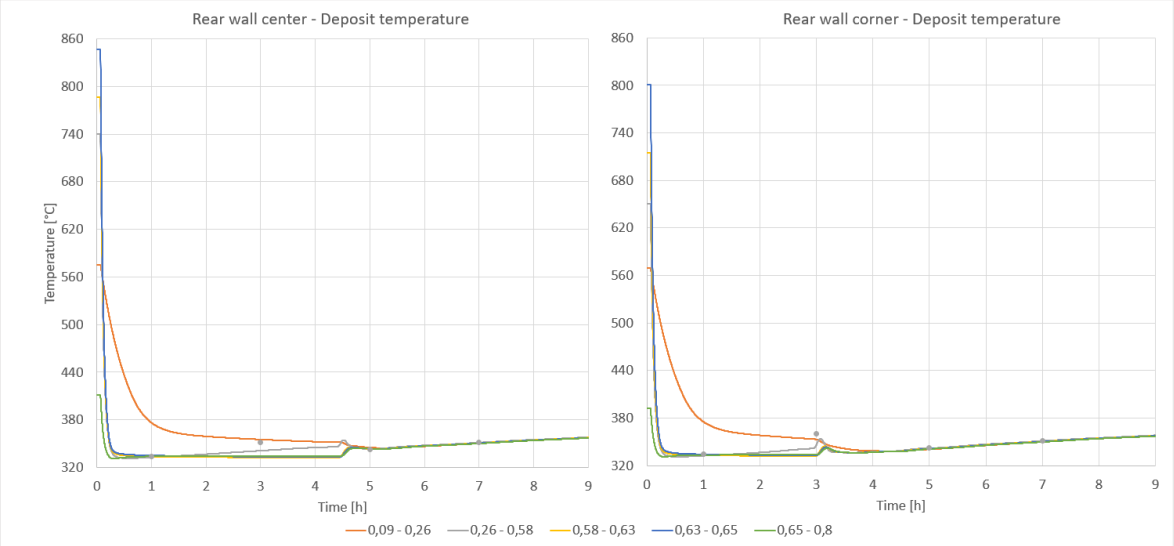

Figure 66. Average temperatures from outer deposit surface in the middle and at the corner of the front wall. The dots represent standard deviation in the positive direction.

The deposits obtain a uniform temperature profile in the center after 05:00 and in the corner after 04:30. The constant rise in tube temperatures, as well as in deposit temperatures, is caused by the constant heat flux through the floor.

6.3 Deposit thickness variation

The water level is displayed for each case in the downcomers and in the front wall center in figure 67.

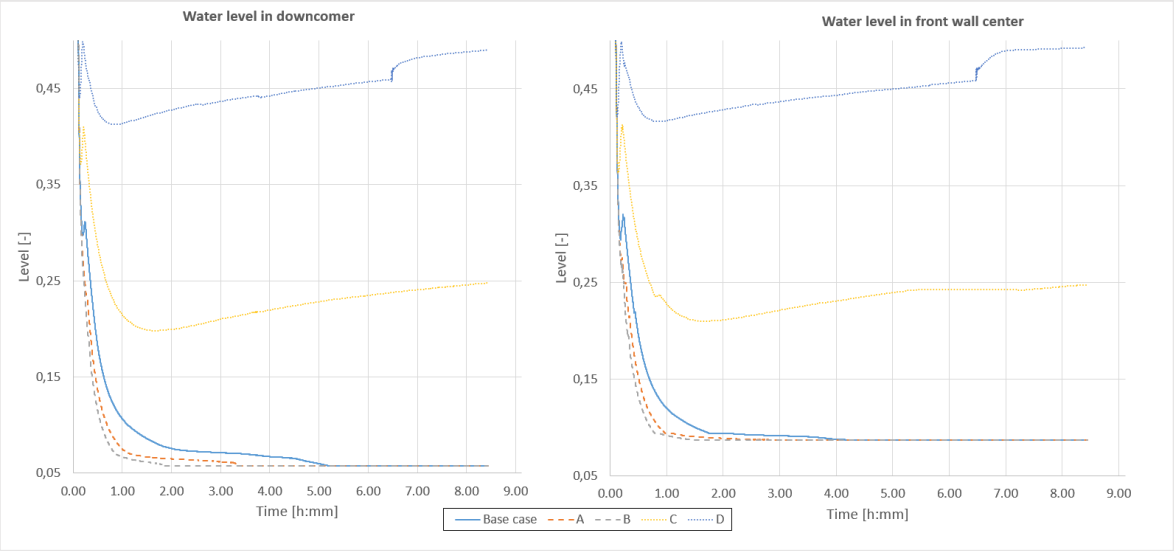

Figure 67. Water level in downcomer tubes and front wall center as a function of time.

In cases C and D the water level is not descending below the lowest points. Cases with lowest deposit accumulation are left with most water in the boiler, because of less heat available for water evaporation. Towards the end, the water level in the furnace walls is rising. Examining the screen water level in figure 68, we see that water is evaporating from the screen and condensing in the walls in cases C and D.

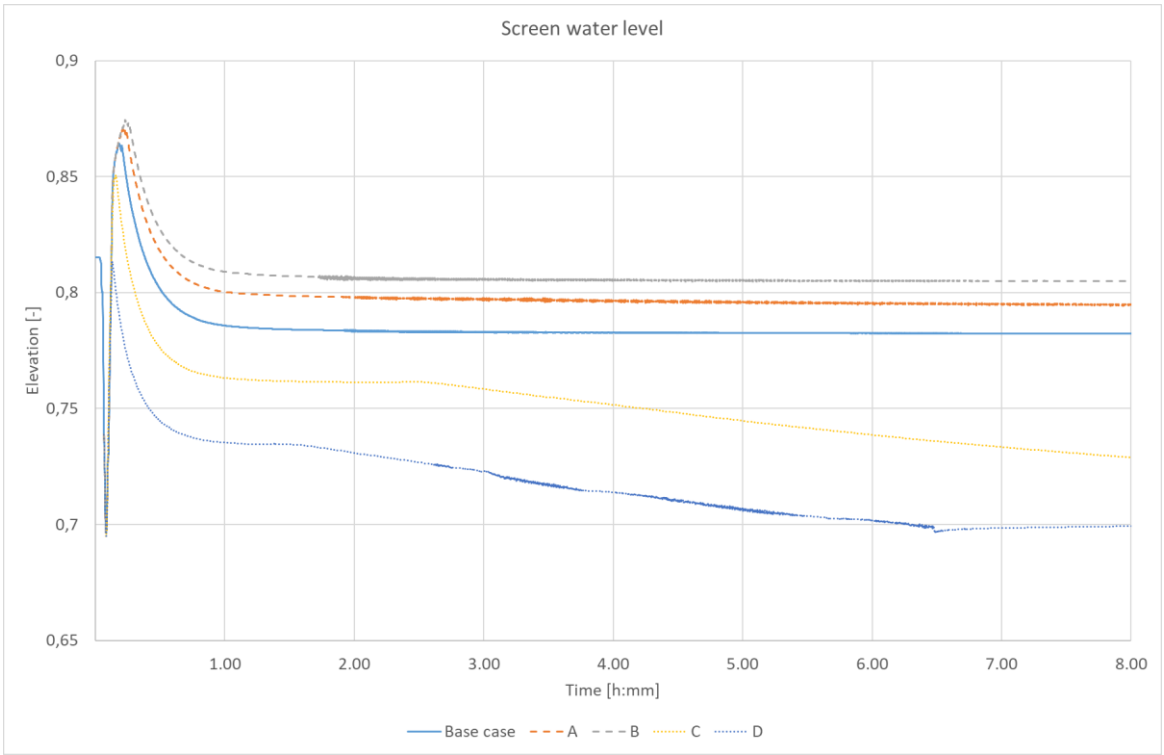

Figure 68. Water level in the screen in each case.

Highest temperatures observed during the simulation are presented in table 14.

Table 14. Highest temperatures and amount of nodes that exceeded 400°C during simulation from the total of 239 nodes.

Case	Highest observed temperature [°C]	Temperature over 400°C in # of nodes [-]
Base case	445	8
A	486	52
B	515	64
C	361	0
D	364	0

In cases C and D the temperature stayed within acceptable levels, while in cases A and B a lot of nodes were observed to go above 400°C. To elaborate the findings further, the highest temperatures of the front wall nodes are presented in figure 69.

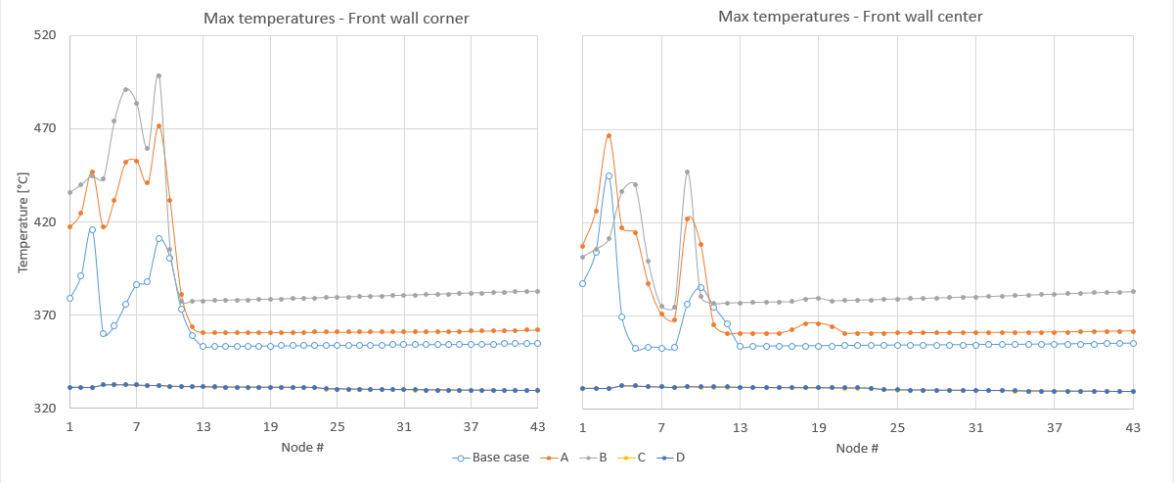

Figure 69. Highest temperatures on front wall nodes. The points display highest observed temperatures in the nodes. Higher node number represents higher elevation.

Cases A and B receive the highest temperatures, while cases C and D receive the lowest. The lowest nodes heat up the most because of thicker lower furnace deposits compared to the higher nodes. We observe inconsistent profiles especially on the lower furnace. On the front wall center cases BC2, A and B have a camelback shape. The drop formed between nodes 7 and 8 is caused by low initial deposit temperature (see figure 43) compared to the adjacent nodes.

Highest temperatures are observer on the front wall corner in cases A and B. Steam circulation begins sooner in the center compared to other modules, which limits temperature

rise in the center. The deposit thickness alone does not determine the highest temperatures. Floor nodes (nodes 1-3) on the front wall center receive higher temperatures in case A compared to case B. Steam circulation starts sooner in case B, which limits the overheating of floor tubes.

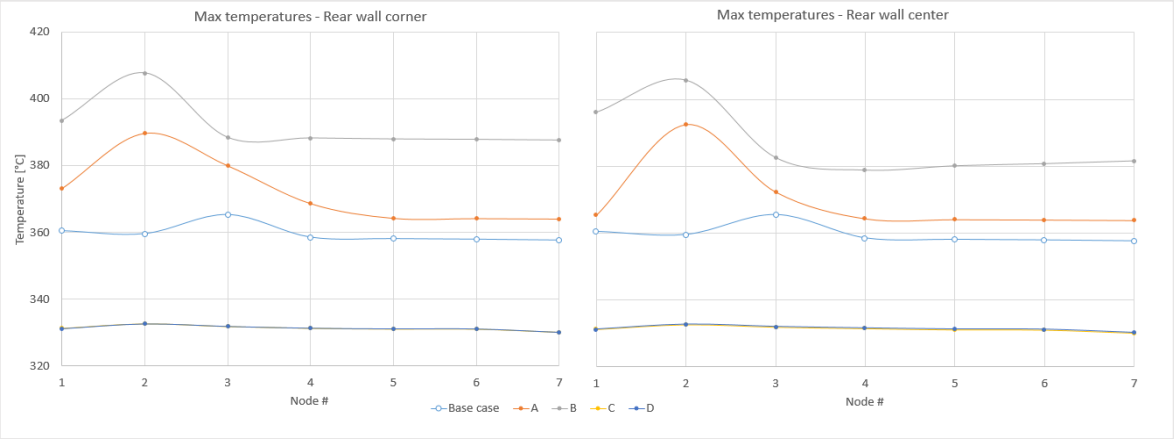

Figure 70. Highest temperatures on rear wall nodes. The points display highest observed temperatures in the nodes. Higher node number represents higher elevation.

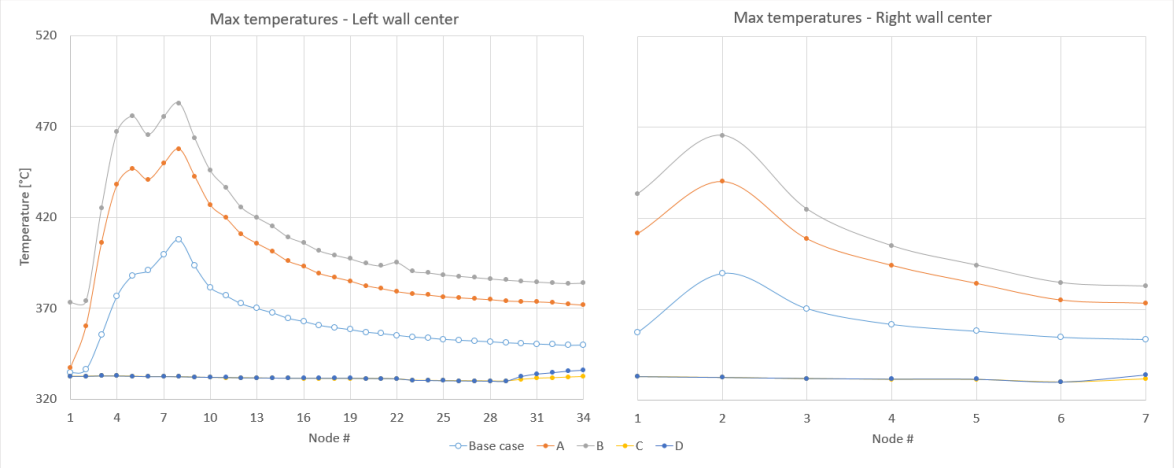

Figure 71. Highest temperatures on rear wall nodes. The points display highest observed temperatures in the nodes. Higher node number represents higher elevation.

For rear and side walls the base case and cases C and D share the same profile shape again, and lower nodes achieve higher temperatures.

6.4 Steam drum pressure variation

Having lower pressure in the steam drum decreases the boiling point of water. Consequently, the water level decreases slower in cases SD1 and SD2 compared to BC2 which is shown in figure 72.

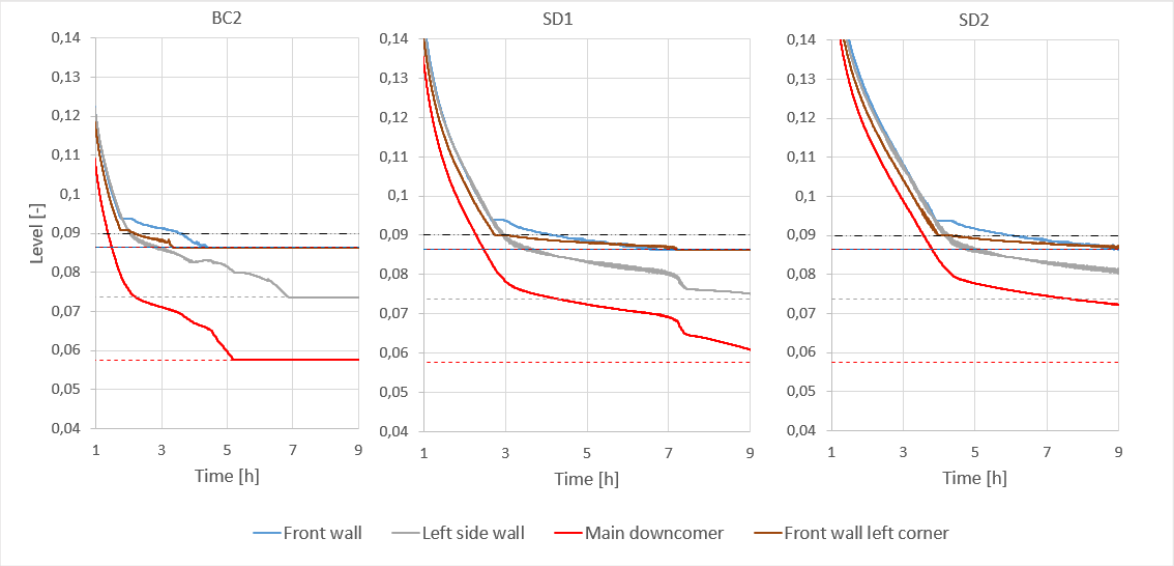

Figure 72. Water level in the furnace walls and the main downcomer.

Examining the line graph shapes it is noticed that less pressure creates smoother water level descend. Highest temperatures are observed on the front wall, which are shown in figure 73.

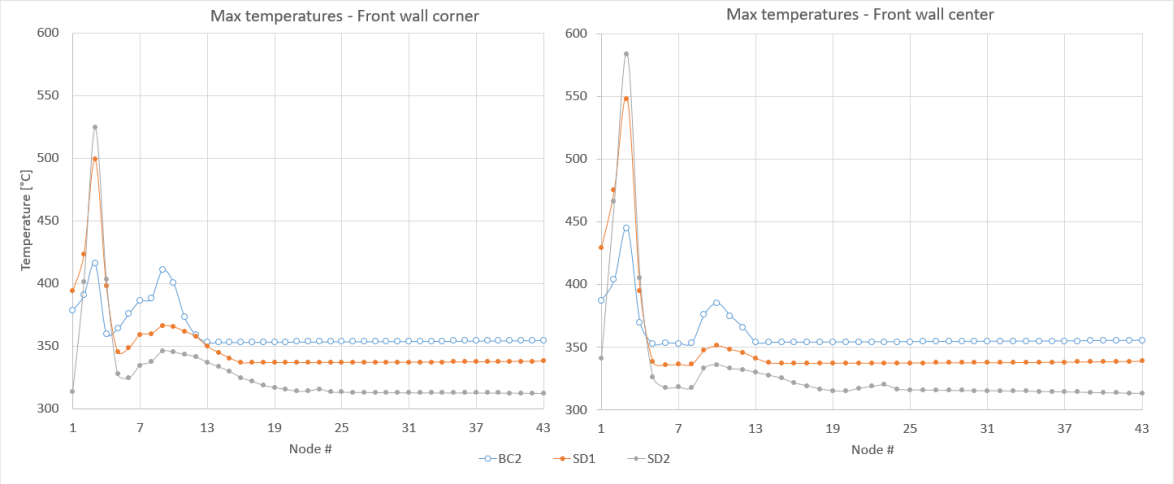

Figure 73. Highest temperatures on front wall nodes. The points display highest observed temperatures in the nodes. Higher node number represents higher elevation.

In case SD2 the floor tube node (node 3) receives the highest temperature of 584°C, because of the water level descending just below the node. There is no steam circulation in case SD2 to cool the tube, and the constant heat flux to the floor tubes rises the temperature. Late start of the steam circulation in case SD1 raises floor tube temperatures also high. In case BC2 the center module dries faster, enabling the steam circulation to cool down the material before huge overheating.

6.5 Floor tube drying

For easy comparison, drying of the floor modules of each case is presented in figure 74.

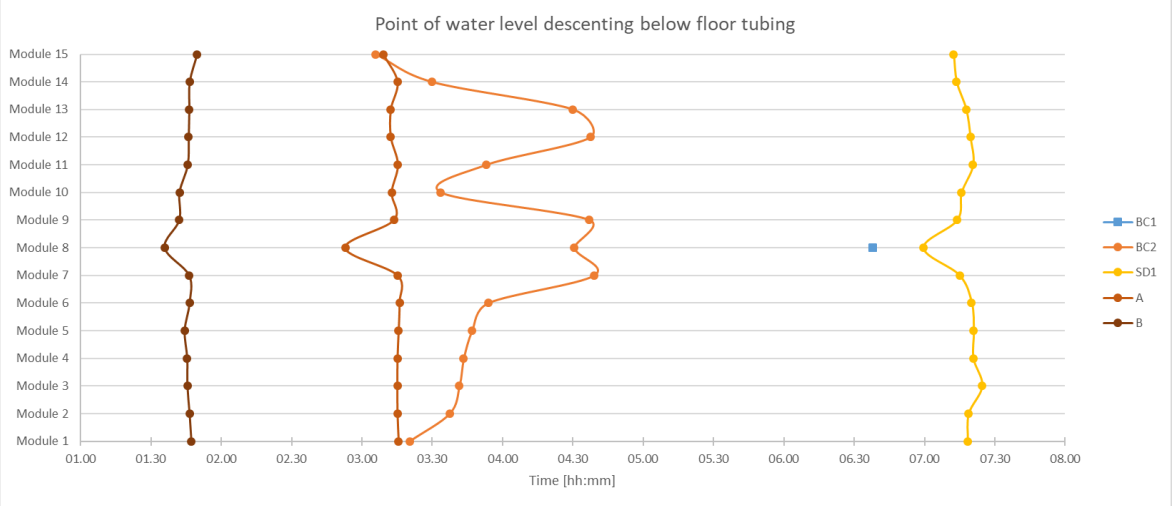

Figure 74. Point of floor drying completely. The points drawn on the graph present time, when the joint lowest elevation of the rear and front floor tubing reaches void fraction of 1. Cases SD2, C and D are not shown, because in each of these cases the floor tubes stay at least partly watered.

We observed no floor tube drying in cases C and D, since the water level does not descend to the floor tube level. Cases A, B and SD1 share similar profiles. In case SD1, the lower boiling temperature causes the floor to dry much later, but produces similar profile to cases A and B. In case BC2, drying of the total floor area is distributed on the span of 1 and half hours. The profile shape is different from cases A and B, because the amount of heat in the deposits closes in on the energy needed to boil the water in the furnace walls. Corners dry first because of the hotter lower deposit temperature in the corners compared to the center. Table 15 compares the energy bound to deposits compared to energy required for boiling water in the furnace walls.

Table 15. Rough estimation of energy in deposits compared to energy required to boil the water in the furnace walls, assuming water density of 640 $kg\ m^{-3}$ and heat of vaporization of 1125 $kJ\ kg^{-1}$.

Energy in deposits / energy required for boiling	
BC1	4,21
BC2	3,34
A	4,20
B	5,11
C	2,55
D	1,82

All of the deposit heat is not used to boil water; some of the energy heats up steam. Also, some water is drained from the ash hopper and boiler bank, which is not taken into account here.

7 DISCUSSION

The most significant observations that were found are presented next. The reality and effect of highest observed temperatures is discussed. The main findings of both sensitivity analyses are presented. The base case results are compared to results of previous black out studies done at Andritz. Lastly, the current deposit model is analyzed, and some methods are presented to better approximate the deposit thickness on furnace walls.

7.1 Lower furnace deposit

The lower front wall contains 2,64 times more deposit in case BC1 compared to case BC2. Comparing the water level change of both base cases we see that in BC1 only the center module on the front wall dries completely. In BC2 all components dry completely. The deposit sensitivity study shows that increasing the furnace wall deposits evenly advances the drying of floor tubes. However, uneven addition of deposit on the walls does not advance floor drying, but rather causes most of the floor to stay wetted. The physical phenomena behind this behavior is not clear. Some kind of sensitivity analysis could provide more information on the subject.

7.2 High tube temperatures

The highest temperatures are presented in figures 49, 50, 61 and 62. Comparatively, BC2 has a big difference against results from BC1. In BC2 the temperatures barely reach over 400°C, while in BC1 we observe the front wall corner to reach temperatures of 524°C. If we consider the yield strength of tubes of the lower furnace to be somewhere between 400-580°C, there is potential of tube cracking in case BC1. However, the wall deposit accumulation is larger in the model, compared to reality. Looking at figure 76, the real deposit mass in the furnace is most likely less than 50% compared to the current deposit model, closing in on the deposit mass modeled in case C. Also, furnace side cooling was not taken into account in this study, which could contribute to faster cooling of the deposit.

Large differences are observed partly because of difference in the deposit mass in the furnace and partly because of the cooling effect of the steam circulation. High temperatures originate where the deposit temperature and thickness are the highest and also on the floor tubes,

which are exposed to a constant heat flux. The lowest wall modules (0,09 – 0,26), which have the thickest deposit accumulation conduct heat vertically to adjacent modules (0,26 – 0,64), rising temperatures on modules with thinner deposits.

7.3 Sensitivity analysis

Increasing the deposit thickness equally on all walls makes the water level in the furnace descend faster, meaning that water evaporates faster. The floor will dry evenly when there is enough heat in the wall deposits to boil the water. When the heat in the wall deposits closes in on the heat needed to boil the water in the walls, the drying order of the floor tubes becomes uneven and ominous. In cases C and D the screen water level is decreasing during the simulation, while the water level in the furnace walls keeps rising. Water evaporates in the hotter screen while condensing in the cooler furnace walls. The temperature profiles are similar between cases, excluding the floor tubes and the lowest wall parts. Even addition of deposit results in higher material temperatures.

Lowering the steam drum pressure lowers the boiling point of water, reducing water evaporation in the boiler during the simulation. Water level descends also smoother in case SD2 with lowest pressure, compared to the other cases. Lower pressure leads to lower temperatures on the furnace walls.

7.4 Model results comparison

The model in this study (5) is validated by comparing the results of the current model with the results of four previous models (1-4) with similar boundary conditions. However, there are some important differences which should be mentioned first. The previous models are different in size and were not subjected to the boundary condition of 850°C limit temperature for the deposit. The resulting high temperatures are observed in the initial deposit temperature profiles in appendixes 2 to 5. Model 4 doesn’t use the same boundary conditions for deposit thickness as the other cases. Also, the heat flux profile was not acquired via the use of CFD-sampling in models 1-4. It is realized that comparing the old and new results between each other doesn’t necessarily prove that correct boiler behavior is exhibited. We can nonetheless examine the differences between results and discuss why they exist.

7.4.1 Initial deposit temperature profile

The deposit temperature profiles at steady-state operation should have similar shape. The profiles are shown in figure 43 and 44 (model 5) and in appendixes 2 to 5 (models 1-4). The profiles seem to agree well above the nose tip. With model 5, the temperatures are low at the liquor gun level compared to results of models 1-4. The center of the front wall contains a port, which reduces incoming heat flux to the water circulation in that location, causing the low initial temperature profile. A noticeable difference is in the boiler bank profile. While the results of models 1-4 have a similar curved shape, resulting profile from model 5 is flat. This is most likely because of flat heat flux profile used in the cases of model 5.

7.4.2 Water level

The water level didn't descend to floor tube level in any of the previous modelling cases. Larger wall area in the furnace doesn't necessarily mean that the water level will descend lower, since the mass of deposit on the wall increases at the same rate (if we don't take into account differences between lower and upper furnace deposit layer sizes). The steam drum contributes also to the water volume. In this study, the steam drum contains roughly 17% of the water with furnace walls. Relatively, the steam drum volume gets lower, the higher the wall area is. Because the steam drum volume doesn't scale as well as the water volume in furnace wall tubes, there must be a point where all of the deposit heat can evaporate all of the boiler water.

7.5 Deposit model development

As the deposit accumulation has a strong effect on the behavior of the model, the best available knowledge has to be used to determine correct deposit layer thickness and distribution on the evaporative tubing. Apros model deposits are thicker than in reality (shown in Figure 41) and the amount of heat released during blackout simulation is therefore larger. The relative difference in stored heat can be calculated as the relation of cross-section areas:

$$\frac{Q_1}{Q_2} = \frac{c_p \rho V_1 T}{c_p \rho V_2 T} = \frac{V_1}{V_2} = \frac{A_1 L}{A_2 L} = \frac{A_1}{A_2} \tag{28}$$

, where Q refers to stored heat in the deposit, c_p to specific heat capacity, V to deposit volume, L to tube length, T to temperature and A to cross-sectional area of the deposit. Number 1 denotes parameters in reality, while number 2 denotes parameters in Apros. A_2 is easily determined, but A_1 requires deeper analysis. Let us assume a radially even thickness of deposit on each tube. With small thickness and long fins, this approximation would work. However, when the deposit thickness is large, and fin width small (which is exactly the case on the furnace lower walls) the situation is more complicated. Figure 75 elaborates the case further.

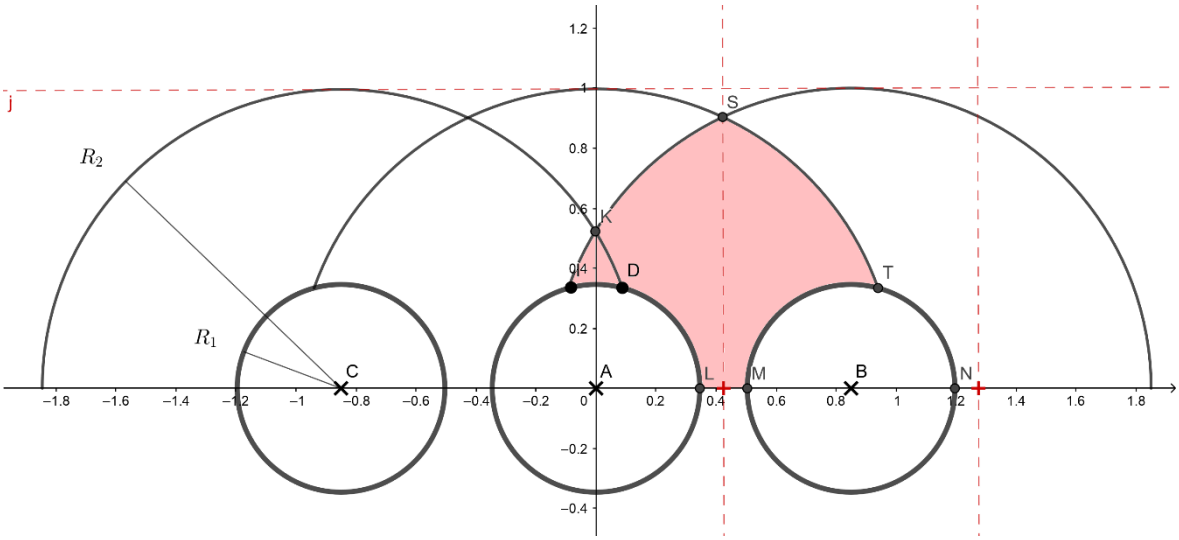

Figure 75. Deposit layer overlapping on furnace wall. The red area contains overlapping of three adjacent deposits. Area S-K-D-L-M-T-S is overlapped by two tube deposits, while area K-I-D is overlapped by three. Steel tube radius R_1 and deposit surface radius R_2 are presented in relation to the deposit radius, hence $R_2 = 1$. The red dashed lines present a discretized amount of deposit allocated to each tube.

An analytical solution for deposit allocation is hard to determine when there are overlapping of multiple deposit layers. For example, area K-I-D geometrically belongs to all three tubes. When considering heat diffusion, the most heat flows towards the middle tube, which is clearly the closest heat sink in the system. Taking into account heat diffusion the area K-I-D would belong mostly, if not totally, to the middle tube. Let's only take into account overlapping of two adjacent tubes, and divide the area vertically to each side. This way, the overlapping area can be divided to each tube geometrically and thermodynamically plausible way. Line S-L divides the overlapping area in Figure 75.

Now the allocated deposit volume can be calculated as follows:

$$A_{deposit} = \int_{-\frac{l}{2}}^{\frac{l}{2}} \sqrt{r_{deposit}^2 - x^2}\,dx - \int_{-r_{pipe}}^{r_{pipe}} \sqrt{r_{pipe}^2 - x^2}\,dx \qquad (29)$$

, where A stands for the cross-section area of deposit on tube wall, l for distance between tube center points (and the red dashed lines), r for radius and x for horizontal coordinate. This area can be approximated with a box shape when the deposit accumulation is high enough. Let's compare the analytical solution, box solution and the deposit used in Apros.

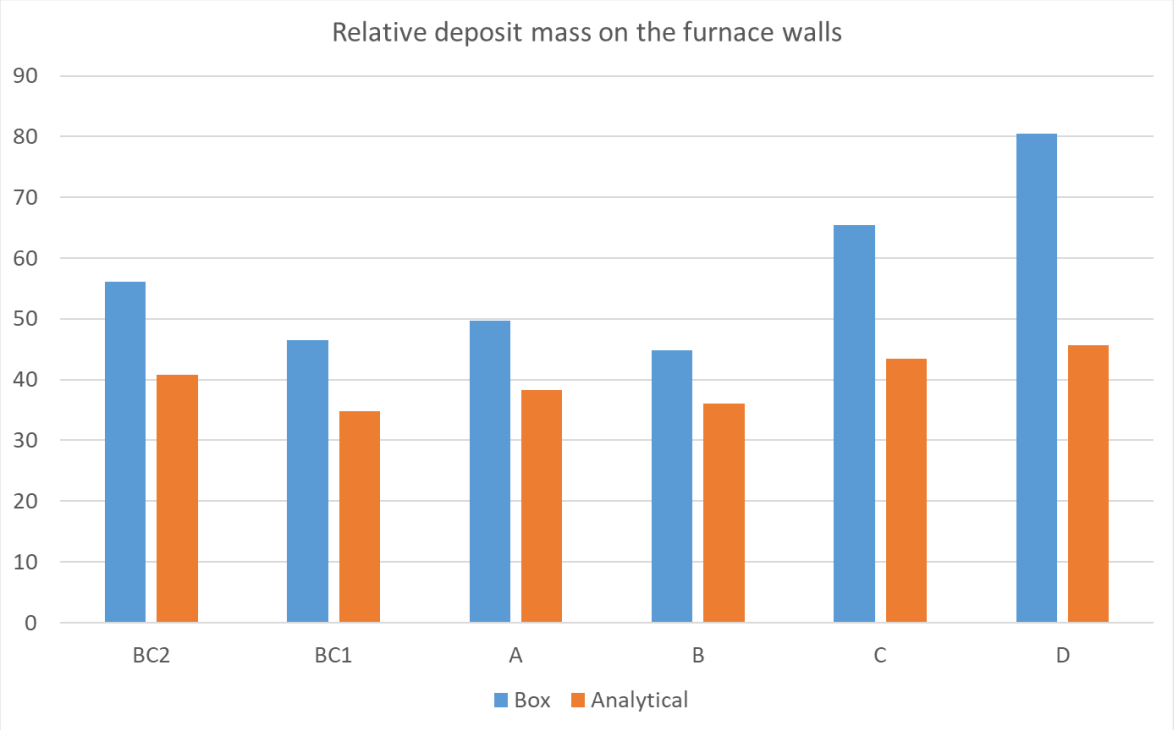

Figure 76. The deposit thicknesses calculated with the box and analytical methods are compared to the deposit thickness used in the Apros model.

Greatest difference is found in case BC1, where the analytical solution provides ~34% of the deposit mass compared to the Apros model. Box approximation works best with case B, where the deposit thickness is high.

8 CONCLUSIONS

A standard method to simulate power blackout in a kraft recovery boiler is successfully presented in this work. The model is presented so that it is possible to replicate for different sized boilers. Since no validation data was available for this study, it is hard to confirm how well the model performs. Much accuracy would be gained with an improved deposit model, which should be the first target of development. A constant or a time dependent outer surface temperature could be used as the floor boundary condition instead of a constant heat flux to model the temperature changes of the floor more accurately in higher temperatures.

In case BC1 the tube material temperatures rise critically high on the lower furnace. In case BC2 the material temperatures rise also quite high, but remain noticeably lower compared to case BC1. In both base cases, the corner floor tubes overheat more compared to the center because of the higher initial deposit temperature on the lower walls. Steam circulation inside the boiler has a cooling effect, which prevents most overheating of the lower furnace in case BC2. We observed, that a steam circulation efficiently distributes the heat of the deposits around the boiler, keeping the material temperatures low.

The sensitivity study reveals, that even addition of deposit on the furnace walls causes the floor tubes to dry uniformly at the same time. Instead, when the deposit mass is decreased to a certain limit, the heat in the deposits isn’t enough to dry the floor tubes evenly, making the drying order of the floor tubes uneven and ominous. It is also shown in the deposit sensitivity analysis that addition of deposit mass increases material temperatures quite evenly. Lowering the steam drum pressure lowers the boiling point of water and therefore reduces evaporation of boiler water.

REFERENCE

Adams, T.N., Frederick, W.J., Grace, T.M., Hupa, M., Iisa, K., Jones, A.K. and Tran, H. (1997). *Kraft recovery boilers.* Atlanta: TAPPI PRESS.

Albrecht, M.J. (2002). *Enhancing the circulation analysis of a recovery boiler through the incorporation of 3-D furnace heat transfer results from COMO.* September 8-12, 2002. San Diego, California, U.S.A: TAPPI.

Andritz Oy (2018). *Process design manual: Combustion air distribution.* Internal material: Andritz Oy.

Andritz Oy (2017). *Process design manual: Boiler Water Circulation.* Internal material: Andritz Oy.

Andritz Oy (2016a). *Recovery Boiler References.* Internal materials: Andritz Oy.

Andritz Oy (2016b). *Iggesund kraft recovery boiler plant.* Internal material: Andritz Oy.

Baehr, H.D. and Stephan, K. (2006). *Heat and Mass Transfer.* 2nd edn. Verlag, Berlin, Heidelberg, New York: Springer.

Baxter, L.L., Lind, T., Kauppinen, E. and Robinson, A. (2001). *Thermal properties of recovery boiler deposits*. June 11-14, 2001. TAPPI.

Finnish recovery boiler committee (2013). *Ohje soodakattilalaitosten varmennetun jännitejakelun periaatteeksi.* Suomen Soodakattilayhdistys ry.

Finnish recovery boiler committee (2009). *Soodakattilan turvallisuussuositus.* Suomen Soodakattilayhdistys ry.

Forberg, U. (2015). *The evolution of advanced corrosion-resistant composite tube for recovery boilers*. PPI, 57(9), pp. 53-56.

Gullichsen, J. and Fogelholm, C. (1999). *Papermaking science and technology. Book 6, B, Chemical pulping.* Helsinki: Fapet.

Haribhakti, P., Joshi, P.B. and Kumar, R. (2018). *Failure investigation of boiler tubes - a comprehensive approach.* ASM International. ISBN 978-1-5231-2041-3.

IEA (2018). *World Energy Outlook - Executive Summary, 2018.* Available at: https://www.emis.com/php/search/doc?pc=AC&dcid=635318741&primo=1 (Accessed: 8.4.2019).

Incropera, F.P., Dewitt, D.P., Bergman, T.L. and Lavine, A.S. (2003). *Principles of heat and mass transfer.* ISV. 7th edn. Ansari Road, Daryaganj, New Delhi: Wiley India.

Kitto, J.B. and Stultz, S.C. (2005). *Steam/its generation and use.* 41st edn. Barberton, Ohio, USA: The Babcock & Wilcox Company.

KnowPulp (2016). *Recausticising.* Available at: http://www.knowpulp.com/extranet/english/pulping/causticizing/0_general/frame.htm (Accessed: 19.11.2018).

Lemmon, E.W., McLinden, M.O. and Friend, D.G. (2018). *Thermophysical Properties of Fluid Systems.* Gaithersburg MD: National Institute of Standards and Technology.

Li, B., Engblom, M., Lindberg, D., Brink, A., Hupa, M., Koschask, R. and Mueller, C. (2012). *Numerical investigation of Kraft recovery furnace wall temperature*. Journal of Science and Technology for Forest Products and Processes, 2(5), pp. 41-48.

Linzer, W. and Walter, H. (2003). *Flow reversal in natural circulation systems*. Applied thermal engineering, 23, pp. 2363-2372.

Maakala, V. (2013) *Multi-objective optimization of recovery boiler dimensions using computational fluid dynamics.* Aalto University Shcool of Engineering.

Ozawa, M., Umekawa, H., Mishima, K., Hibiki, T. and Saito, Y. (2001). *CHF in oscillatory flow boiling channels*. Trans IChemE, 79(Part A).

Padki, M.M., Palmer, K., Kakaç, S. and Veziroğlu, T.N. (1992). *Bifurcation analysis of pressure-drop oscillations and the Ledinegg instability*, International Journal of Heat and Mass Transfer, 35(2), pp. 525-532.

Pöyry (2015). *World Fibre Outlook up to 2030 market report.*

Ruspini, L.C., Marcel, C.P. and Clausse, A. (2014). *Two-phase flow instabilities: A review*, International journal of heat and mass transfer, 71, pp. 521-548.

Sirainen, A., Röppänen, J., Maakala, V., Lappalainen, J. and Vakkilainen, E. (2017) *Improved evaluation of recovery boiler water circulation design with the help of state-of-the-art CFD-based heat flux data.* 24-26 May 2017.

The black liquor recovery boiler advisory committee (2018). *Recommended good practice for design, operation, and testing of the emergency shutdown system for black liquor recovery boilers.* Available at: http://www.blrbac.org/sites/default/files/BLRBAC%20Emergency%20Shutdown%20Procedure%20Rev%209%20R1.pdf (Accessed: 19 Jan 2019).

Tran, H. (2015). *Recovery boiler fireside deposits and plugging prevention.* Available at: https://www.researchgate.net/publication/268268846_RECOVERY_BOILER_FIRESIDE_DEPOSITS_AND_PLUGGING_PREVENTION (Accessed: 10.1.2019).

Tran, H. and Vakkilainen, E. (n. d.). *The kraft chemical recovery process.* Available at: https://www.tappi.org/content/events/08kros/manuscripts/1-1.pdf (Accessed: 26.11.2018).

Vakkilainen, E. (2017). *Steam generation from biomass: construction and design of large boilers.* Amsterdam: Butterworth-Heinemann.

Vakkilainen, E. (2005). *Kraft recovery boilers - Principles and practice.* Suomen Soodakattilayhdistys ry.

Vakkilainen, E., Nieminen, M. and Lampinen, P. (2014). *Continuous development of recovery boiler technology – 50 years of cooperation in Finland.* Suomen soodakattilayhdistys, pp. 237.

VTT (2017). *Apros 6 Help - Apros Overview.* Available at: (Accessed: 7.1.2019).

Ylijoki, J., Karppinen, I., Puska, E., Silde, A., Kontio, H. and Porkholm, K. (2015). *Apros validation: Selected validation cases related to nuclear safety analyses and training simulators.* Apros. Available at: www.apros.fi/en/product_information_2/quality_validation (Accessed: 5.7.2019)

APPENDIX I: INITIAL DEPOSIT TEMPERATURE PROFILE OF A PREVIOUS BLACKOUT SIMULATION (CASE 1)

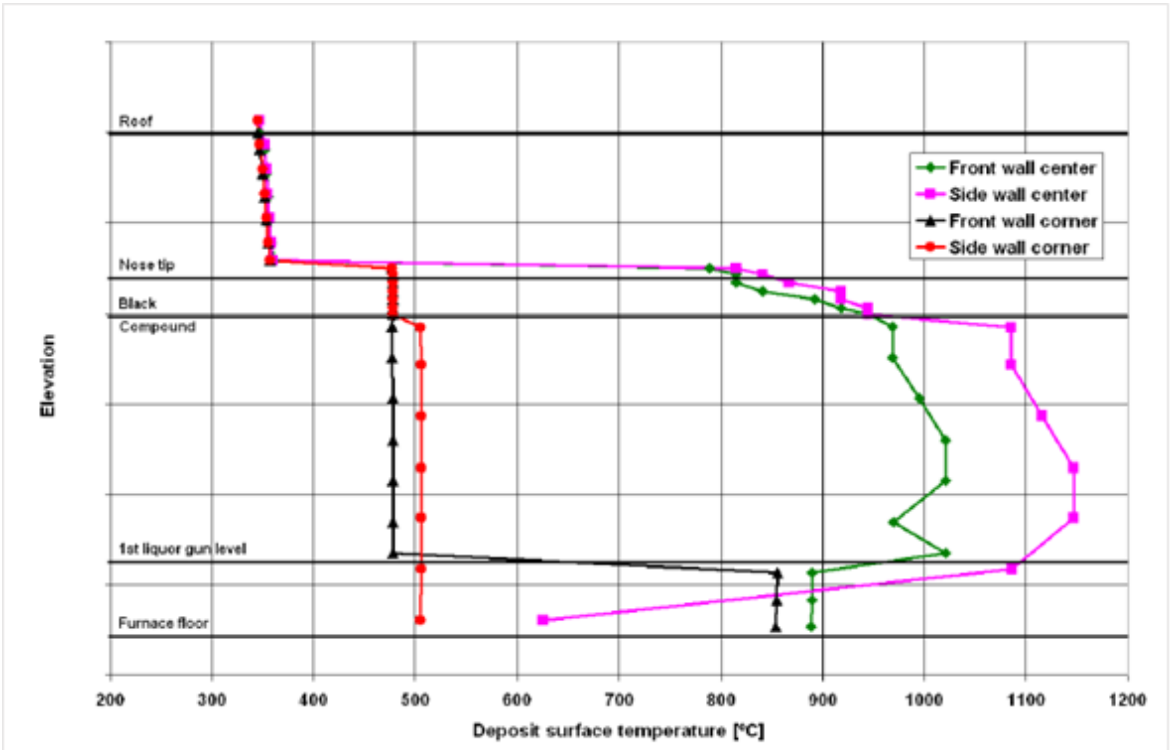

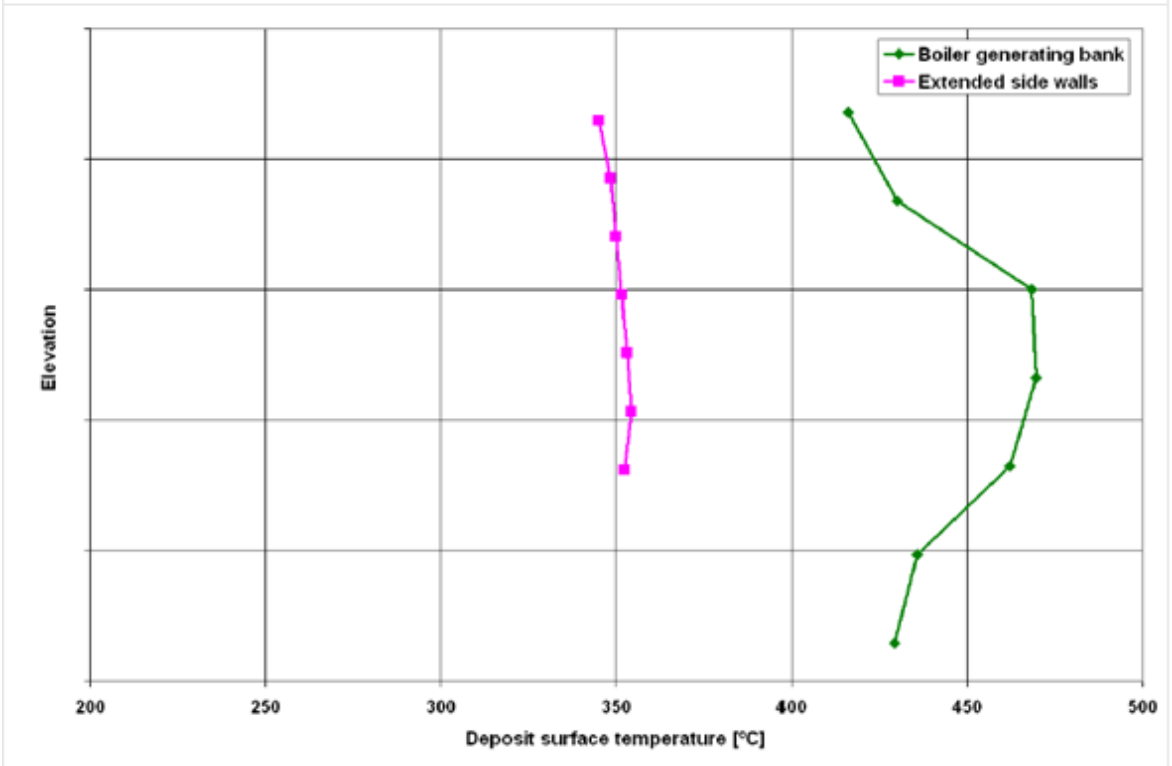

APPENDIX II: INITIAL DEPOSIT TEMPERATURE PROFILE OF A PREVIOUS BLACKOUT SIMULATION (CASE 2)

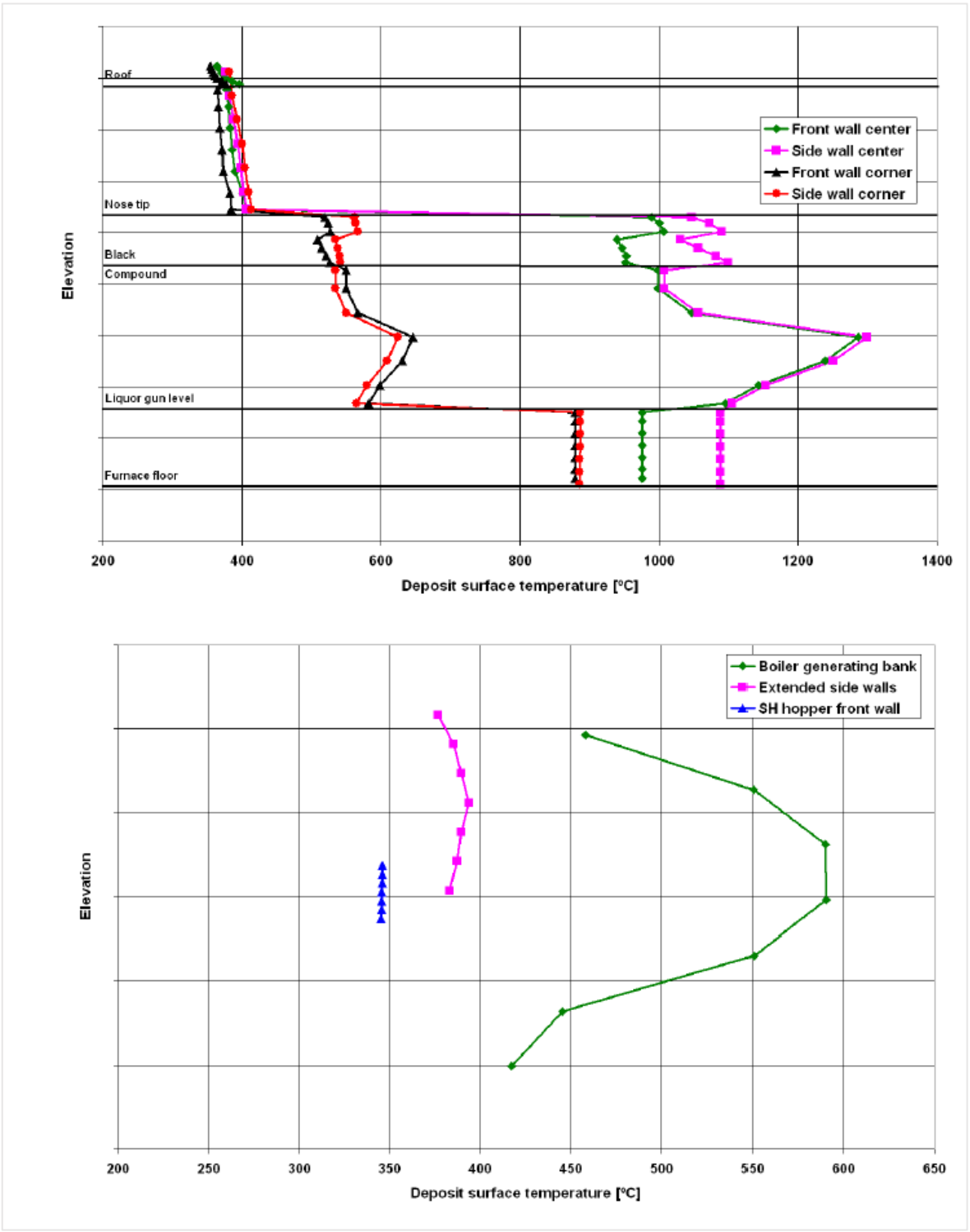

APPENDIX III: INITIAL DEPOSIT TEMPERATURE PROFILE OF A PREVIOUS BLACKOUT SIMULATION (CASE 3)

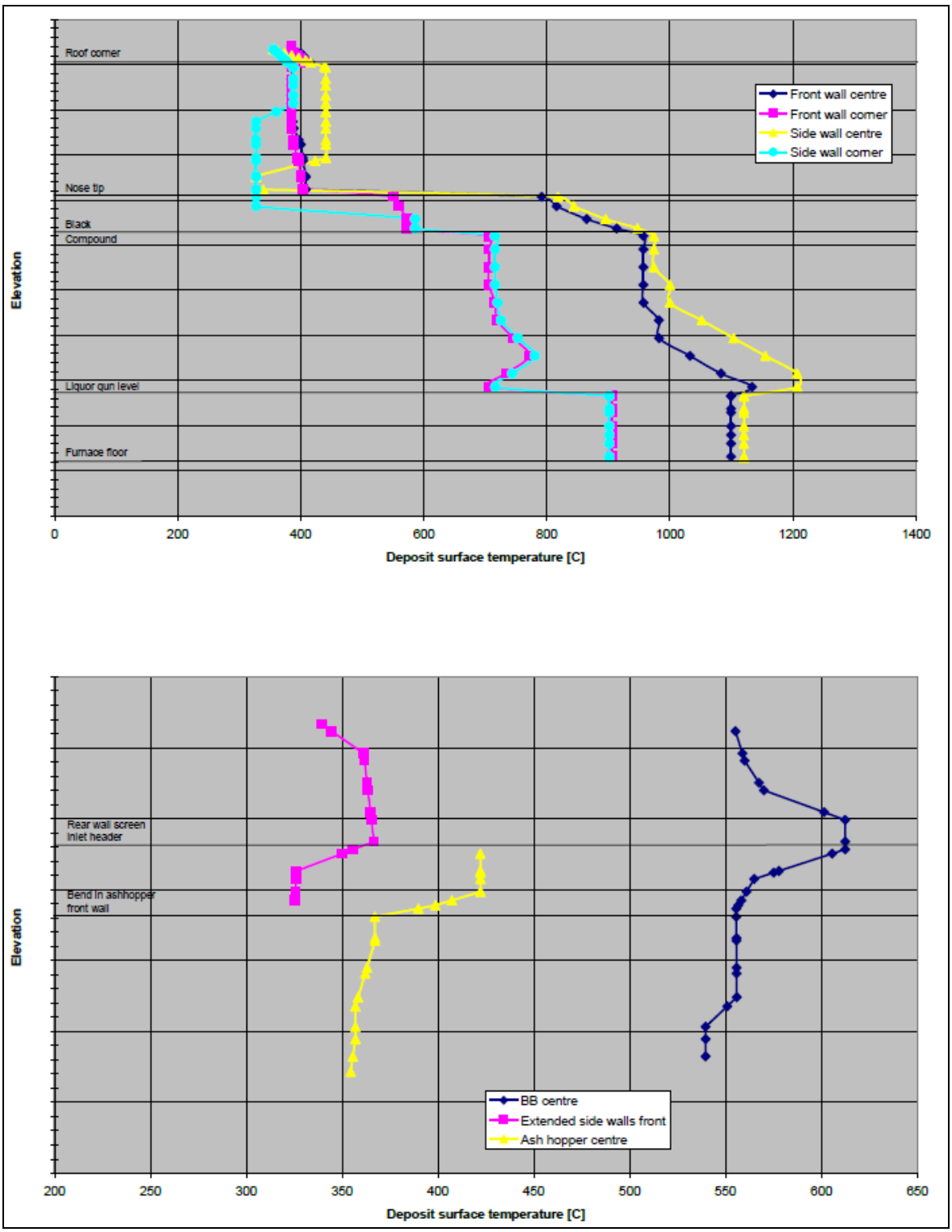

APPENDIX IV: INITIAL DEPOSIT TEMPERATURE PROFILE OF A PREVIOUS BLACKOUT SIMULATION (CASE 4)

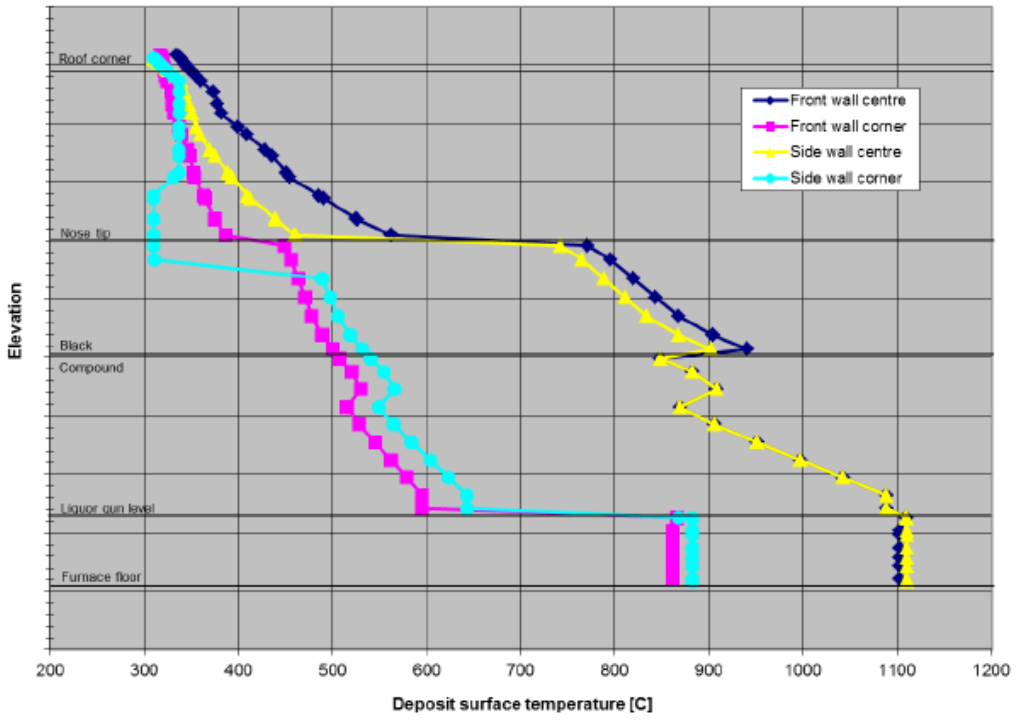

Figure 2. Surface temperatures of the deposits on the furnace walls before blackout.